UNIVERSIDADE DE LISBOA
FACULDADE DE CIÊNCIAS
DEPARTAMENTO DE FÍSICA

Extensions of the scalar sector of the Standard Model

Rodrigo Capucha

Mestrado em Física
Especialização em Física Nuclear e Partículas

Dissertação orientada por:
Doutor Rui Santos
Doutor António Onofre

2020

Acknowledgements

I would like to thank everyone that helped and supported me throughout this amazing journey. First and foremost, to my supervisor, Doutor Rui Santos, for all the guidance, helpful discussions, for motivating and pushing me, and for all the incredible experiences that were provided to me throughout this year and a half. To Duarte, thank you for the never-ending patience, for always being available, and for the countless times that you have helped me when I was stuck during this project. To Doutor António Onofre, my second supervisor, I want to express my immense gratitude for the incredible amount of time that was spent teaching me about the most varied subjects, and the overall good mood, excitement and dedication, and fun and interesting conversations. To all three, a sincere thank you for all your mentorship, and friendship.

I would also like to thank my friends for all the endless support throughout the years, and for the helpful inputs that you gave me in order to complete this work. To Daniel, for being kind enough to correct more than 200 latex errors, and for the beautiful Mathematica plots. To João, for all the fun discussions, and for reading and reviewing my entire work during the holidays, when you could be doing more interesting things. To José, for the help given in countless situations, for cheering me up when I was tired and for all the patience and kindness. To another João, for all the moral support and good times that we spent together, and for always showing me the positive side of things. To all my friends in CFTC, for all the fun moments, and to all my other friends, a heartfelt thank you.

Last but not least, I want to thank my family for your unconditional love, support, patience and belief in me. Even though you do not understand at all what my work is about, you always try to help in any way you can. In particular, I want to thank my parents, for supporting my choices and providing me with the opportunities to accomplish my dreams. To the rest of the family - brother, sister, cousins, uncles and aunts, and so on - thanks for everything.

Abstract

The matter-antimatter asymmetry observed in the Universe cannot be explained by the amount of violation of Charge Conjugation and Parity (CP) in the Standard Model (SM). This shortcoming of the SM is one of the main motivations that led to the proposal of several extensions of the SM with new sources of CP-violation, a necessary requirement to explain the baryon asymmetry, according to the Sakharov conditions for baryogenesis. In this thesis, we will look at some of the main features of a particular type of models where the SM Higgs potential is changed by the addition of a second scalar doublet to the SM field content. These models are known as Two-Higgs-Doublet Models (2HDMs). They provide a very rich phenomenology at the Large Hadron Collider (LHC) and future colliders because of the introduction of new scalar states, and may answer many unsolved problems that are not addressed in the SM, such as the insufficiency of CP-violation and the existence of Dark Matter (DM).

The CP-nature of the discovered Higgs is still an open issue. While it has been established by the ATLAS (A Toroidal LHC Apparatus) and CMS (Compact Muon Solenoid) collaborations that the discovered scalar cannot be a pure pseudoscalar, a mixed state with a large CP-odd component is still possible. This would be an indication of CP-violation in the scalar sector. The search for new sources of CP-violation and Beyond the Standard Model (BSM) physics is one of the main goals of the LHC. This can be achieved by a precise measurement of the Yukawa couplings since the CP-nature of the Higgs can be directly probed in its production alongside fermions. In this dissertation, we explore the sensitivity of CP-discrimination in the Higgs (h) couplings to bottom (b) and top quarks (t), for $b\bar{b}h$, bh and in dilepton final states of $t\bar{t}h$ events (with $h \to b\bar{b}$) produced at the LHC and generated with MadGraph5_aMC@NLO. These Higgs bosons are generic, i.e., they may not correspond to the discovered one with a mass of 125 GeV, and are either pure CP-even or pure CP-odd. Several observables introduced in previous works are evaluated for a varying scalar boson mass, m_h, in order to probe the CP-sensitivity in the different processes. We show that for $b\bar{b}h$ and bh final states, CP-discrimination is not possible for the observables considered, even for very light Higgs masses of 10 GeV. For $t\bar{t}h$, we found that distinguishing different CP states becomes increasingly difficult for larger masses, and seemingly impossible for masses above 450 GeV, at parton level. For the tops, we additionally apply an algorithm to reconstruct, for the first time, $t\bar{t}h$ events with a Higgs mass different from 125 GeV. Confidence Levels (CLs) for exclusion are computed for this process, as a function of the LHC luminosity, for different scenarios. We found that exclusion scenarios at the LHC require more luminosity for a fixed CL as we increase the scalar boson mass. CP-odd exclusion also requires more luminosity, relative to CP-even exclusion, for $m_h < 160$ GeV. With the current LHC luminosity of 150 fb^{-1}, exclusion of a pure CP-even Higgs with a mass below 80 GeV, assuming SM-like couplings, is already possible. Also, the information that we may learn in these exclusion scenarios still leaves a large allowed parameter space for the Complex Two-Higgs-Doublet Model (C2HDM).

Keywords: Higgs boson, CP-violation, 2HDM, top and bottom Yukawa couplings, LHC.

Resumo

A quantidade de violação de CP no SM não é suficiente para explicar a assimetria matéria-antimatéria observada no Universo. Este é um dos principais motivos que levou ao desenvolvimento de extensões do SM com fontes adicionais de violação de CP, que é uma das condições necessárias para explicar a assimetria bariónica, de acordo com as condições de Sakharov para a bariogénese. Nesta tese, abordam-se os principais aspectos de um tipo de modelos onde se adiciona ao potencial do Higgs do SM um segundo dubleto escalar, designados como 2HDMs. Estes modelos caracterizam-se por uma fenomenologia muita rica ao nível do LHC e de futuros aceleradores, devido à existência de novos escalares, e poderão dar resposta a vários problemas não abordados pelo SM, como por exemplo a quantidade insuficiente de violação de CP e a existência de matéria escura.

A natureza CP do Higgs descoberto no LHC ainda não foi determinada. Embora as colaborações ATLAS e CMS tenham estabelecido que esse Higgs não pode ser um pseudoescalar puro, uma mistura de estados CP com uma componente CP-ímpar diferente de zero ainda é possível, o que seria uma indicação de violação de CP no sector escalar. O principal objectivo do LHC actualmente consiste na procura de novas fontes de violação de CP e de física para além do SM. Para isso é importante medir de forma precisa os acoplamentos de Yukawa, já que a natureza CP do Higgs pode ser directamente investigada na sua produção juntamente com fermiões. Nesta dissertação, explora-se a possibilidade de discriminar diferentes estados de CP nos acoplamentos do Higgs com os quarks bottom e top, para eventos do tipo $b\bar{b}h$, bh e para o canal dileptónico em eventos $t\bar{t}h$ ($h \to b\bar{b}$) produzidos no LHC, e gerados pelo MadGraph5_aMC@NLO. Os Higgs gerados nem sempre correspondem ao descoberto com uma massa de 125 GeV, e são CP-pares ou CP-ímpares. Várias distribuições existentes na literatura foram calculadas para diferentes massas do Higgs, de modo a investigar a sensibilidade para diferentes componentes de CP nos vários processos. Mostra-se que para $b\bar{b}h$ e bh, não é possível distinguir diferentes estados CP para as variáveis consideradas, mesmo para Higgs muito leves com massas de 10 GeV. Para $t\bar{t}h$, viu-se que essa distinção se torna mais díficil para massas do Higgs maiores, e praticamente impossível para massas acima de 450 GeV. Para os tops, aplicou-se ainda um algoritmo que permitiu reconstruir, pela primeira vez para massas do Higgs diferentes de 125 GeV, os eventos $t\bar{t}h$. Calcularam-se também níveis de confiança para a exclusão de diferentes cenários e massas, em função da luminosidade integrada do LHC. Descobrimos que é necessária mais luminosidade para excluir a existência de Higgs mais pesados, para um certo CL. Também é necessária mais luminosidade para excluir um Higgs CP-ímpar relativamente a um que é CP-par, para $m_h < 160$ GeV. Tendo em conta a actual luminosidade do LHC de 150 fb^{-1}, já é possível excluir um Higgs CP-par com massa abaixo de 80 GeV, assumindo os acoplamentos padrão do SM. Além disso, a informação retirada destas exclusões ainda deixa um espaço de parâmetros grande para o C2HDM.

Palavras-chave: bosão de Higgs, violação de CP, 2HDM, acoplamentos de Yukawa do top e bottom, LHC.

Contents

List of Tables

List of Figures

Nomenclature

Physics Constants

$\hbar$	Reduced Plank constant.
c	Speed of light.

Greek Symbols

δ_{jk}	Dirac delta function.
Δ_{kj}	Yukawa couplings for the down-quarks.
ϵ_{ijk}	Fully antisymmetric tensor.
η	Pseudo-rapidity.
γ_5	Gamma five matrix.
γ_μ	Gamma matrices.
Γ_t	Decay width of the top.
Γ_{kj}	Yukawa couplings for the up-quarks.
$\kappa_{hf\bar{f}}$	Total coupling strength relative to the SM for $f\bar{f}h$.
λ_a	Gell-Mann matrices.
ρ	Rho parameter.
τ_k	Pauli matrices.
θ_Y^X	Angle between the direction of Y, in the CM of X, and the direction of X, in the CM of its mother.
θ_w	Weinberg angle.

Particles and fields

ℓ	Lepton.
$\hat{d}^{phy}$	Physical fields for the down-quarks.
$\hat{u}^{phy}$	Physical fields for the up-quarks.
$\mathcal{H}_i$	Higgs doublets in the Higgs basis.

ν_ℓ	Lepton neutrino.
ν_μ	Muon neutrino.
ν_τ	Tau neutrino.
ν_e	Electron neutrino.
Φ, φ	Scalar field.
ψ	Spinor.
A^μ	Vector field for the photon.
$f\bar{f}h$	Higgs and fermion pair production.
$F_j^{\mu\nu}$	Field strength tensor for the weak isospin fields.
$F_Y^{\mu\nu}$	Field strength tensor for the weak hypercharge field.
f_L	Left-handed fermion.
f_R	Right-handed fermion.
$F_{\mu\nu}$	Electromagnetic field strength tensor.
fh	Higgs and fermion production.
$G^\pm$	Charged Goldstone bosons.
G_μ^a	Gluon field.
$G_{\mu\nu}^a$	Gluon field strength tensor.
$H^\pm$	Charged Higgs bosons.
h^{phy}	Physical field for the Higgs.
H^{SM}	SM Higgs.
h_{125}	125 GeV Higgs boson.
hVV	Higgs and vector boson pair interaction.
p	Proton.
$W^\pm$	W bosons.
Z^0	Z boson.
A	CP-odd Higgs boson.
b	Bottom.
B$^\mu$	U(1)$_Y$ gauge field.
c	Charm.

d Down.

H, h Higgs boson.

s Strange.

t Top.

u Up.

W_i^μ SU(2) gauge fields.

$W_\mu^\pm$ Vector field for the $W^\pm$ bosons.

Z^μ Vector field for the Z boson.

Roman Symbols

$\hat{k}_z$ Unitary vector along the z-direction.

$\not{E}^{x/y}$ Missing transverse energy components.

$\vec{p}_f$ Three-momentum of particle f.

A_{FB} Forward-backward asymmetry.

D_μ Covariant derivative.

f_{abc} Structure constants.

g_s Strong coupling constant.

$g_{\mu\nu}$ Metric tensor.

$g_{Hf\bar{f}}$ Couplings between the Higgs and a pair of fermions.

g_{HVV} Couplings between the Higgs and a pair of vector bosons.

$M_{l_{kj}}$ Yukawa couplings for the leptons.

p^μ Four-vector momentum.

p_f^x X component of the three-momentum of particle f.

p_f^y Y component of the three-momentum of particle f.

p_f^z Z component of the three-momentum of particle f.

p_T Transverse momentum.

R_α Rotation matrix for an angle α.

S Action.

v Vacuum expectation value of the scalar field.

V_{CKM} CKM matrix.

x^μ	Four-vector position.
g'	$U(1)_Y$ coupling constant.
M	Mass dimension.
m	Mass.
P_L	Left-handed projector operator.
P_R	Right-handed projector operator.
q	Quark flavour.
T	Weak isospin.
$T^\pm$	Raising and lowering operator of SU(2).
T_i	Generator of SU(2).

Superscripts and Math Symbols

†	Transpose conjugate.
$\mathcal{CP}$	CP operator.
$\mathcal{C}$	Charge conjugation operator.
$\mathcal{P}$	Parity operator.
$\otimes$	Kronecker product.
∂_μ	Partial derivative.
$I, \mathbb{1}$	Identity matrix.
*	Complex conjugate.
Im	Imaginary part.
Re	Real part.
T	Transpose.
U	Unitary matrix.

Glossary

2D Two-Dimensional. Pages: xiii, 53, 54, 56–58

2HDM Two-Higgs-Doublet Model. Pages: v, vii, ix, xi, xix, 25–28, 30–32

A2HDM Aligned Two-Higgs-Doublet Model. Page: 32

ATLAS A Toroidal LHC Apparatus. Pages: v, vii, 1, 36, 48

BDT Boosted Decision Tree with an adaptative boost. Pages: xiii, 51–53

BDTG Boosted Decision Tree with a Gradient boost. Pages: xiii, 51–53

BR Branching Ratio. Page: 46

BSM Beyond the Standard Model. Pages: v, ix, 2, 25, 33

C2HDM Complex Two-Higgs-Doublet Model. Pages: v, vii, ix–xi, xiv, 32–34, 75, 76

CKM Cabibbo-Kobayashi-Maskawa. Pages: x, 20, 23, 89

CL Confidence Level. Pages: v, xiv, 3, 35, 65–73

CM Center of Mass. Pages: xiii, xiv, 26, 36–39, 47, 59, 63, 64, 67, 91, 92

CMS Compact Muon Solenoid. Pages: v, vii, 1, 36

CP Charge Conjugation and Parity. Pages: v, vii, ix–xi, xiii, xiv, 2, 3, 21–23, 25, 27–35, 37, 38, 42–46, 51, 53, 59, 65, 68–73, 75–77, 89

DM Dark Matter. Pages: v, 2, 5, 25

DoF Degrees of Freedom. Pages: 15–17, 28, 87, 89

FCCC Flavour Changing Charged Current. Page: 12

FCNC Flavour Changing Neutral Current. Pages: 12, 25, 26, 31, 32

GGF Gluon Fusion. Pages: 35, 36

GR General Relativity. Page: 1

GUT Grand Unified Theory. Page: 1

IDM Inert Doublet Model. Page: 25

KG Klein-Gordon. Page: 15

LAB Laboratory. Pages: xiii, 38, 59, 60, 62, 64, 66

LHC Large Hadron Collider. Pages: v, vii, x, xix, 1–3, 32, 33, 35, 37, 45, 47–49, 65, 68, 75, 91

LO Leading Order. Pages: xiii, 36, 43, 44, 46–48, 91

MC Monte Carlo. Page: 37

NFC Natural Flavour Conservation. Page: 32

NHDM N-Higgs-Doublet Model. Page: 25

NLO Next-to-Leading Order. Pages: xiii, 37, 39, 46, 48, 49, 51, 56–59

NNLL Next-to-Next-to Leading Logarithmic. Page: 47

NNLO Next-to-Next-to Leading Order. Page: 47

PDF Probability Density Function. Pages: xiii, 53–55

QCD Quantum Chromodynamics. Pages: 8, 9, 37, 47, 53

QED Quantum Electrodynamics. Pages: 7–10

QFT Quantum Field Theory. Page: 1

ROC Receiver Operating Characteristic. Pages: xiii, 51

SM Standard Model. Pages: v, vii, ix, xi, xiii, xiv, 1, 2, 5–9, 11, 12, 15, 18, 22, 23, 25–33, 35–37, 39, 46, 65, 68, 70–73, 89

SSB Spontaneous Symmetry Breaking. Pages: 2, 14, 15, 17

SUSY Supersymmetry. Page: 25

TM Truth Match. Pages: xiii, xiv, 50–53, 56–59, 62, 65–67

TMVA Toolkit for Multivariate Analysis. Pages: xiii, 50–52

ToE Theory of Everything. Page: 1

VBF Vector-Boson Fusion. Pages: 35, 36

VEV Vacuum Expectation Value. Pages: 14–16, 26, 27, 30

Chapter 1

Introduction

The Holy Grail of modern physics is to find a theory that fully explains all physical aspects of the Universe, sometimes called a Theory of Everything (ToE) [1]. Any viable candidate must at least describe all known interactions in a common theoretical framework and hopefully unify them into a single fundamental theory.

Historically, the first ideas of unification go back to classical antiquity, but the first major development came in the 17th century, when Isaac Newton showed that all celestial objects obey the same fundamental law of universal gravitation [2]. In the nineteenth century, Hans Christian Ørsted discovered a connection between electricity and magnetism and later Maxwell provided a description of both interactions as different aspects of a unified electromagnetic theory [3], thanks to the contribution of other scientists such as Ampère, Ohm, Faraday, Gauss, amongst others.

In the 20th century, two major revolutions took place that lay the foundations of what today we call modern physics. The first one happened in 1915, when Albert Einstein published his General Theory of Relativity (GR) [4], and the second one in the mid-1920s, with the establishment of quantum mechanics. Later, two new interactions, the strong and weak nuclear forces, were discovered. In the years that followed, the development of Quantum Field Theory (QFT) played a major part in the understanding of electromagnetism and the weak and strong nuclear forces under a quantum framework, and in the 1960s, Glashow, Salam and Weinberg developed a unified picture of these three interactions which was able to unify the first two in the electroweak interaction. This theory is called the Standard Model (SM) of particle physics[1] [6–8].

The SM is the expression of our current understanding of particle physics, where forces between particles are described by the exchange of particles. It explains the mechanism through which elementary particles acquire mass and introduces a large number of particles which have already been discovered. The last one was found in 2012, when a new scalar particle with a mass close to 125 GeV, later identified as the Higgs boson, was discovered by the ATLAS (A Toroidal LHC Apparatus) [9] and CMS (Compact Muon Solenoid) [10] collaborations at the Large Hadron Collider (LHC), thus confirming the prediction of the electroweak symmetry breaking mechanism of the SM [11]. The SM provides a successful description of (almost[2]) all current experimental data from colliders, and represents one of the triumphs of modern

[1]The unification attempts did not stop with the SM. For instance, several attempts were made to unify the electroweak and strong interactions under a Grand Unified Theory (GUT) [5]. Although these models are puzzling and definitely interesting, none of them have achieved experimental validation, so the SM and simple extensions of it will be the main focus of this work.

[2]There are very few exceptions where this is not true, like for instance the measured value for the anomalous magnetic moment of the muon, which shows a 3.5 σ deviation from the SM prediction [12], and B meson decays such as $\bar{B}^0 \to D^+\tau^-\bar{\nu}_\tau$, in which the measured decay rates differ from the theoretical predictions calculated in the SM [13].

physics [14–16].

Whilst the SM is undoubtedly very successful in describing a wide range of precise experimental measurements, it is an incomplete theory with many unanswered questions, possibly being the low-energy limit of a more fundamental theory. For example, it cannot explain the observed matter-antimatter asymmetry in the Universe [17], it does not contain a viable Dark Matter (DM) candidate [18] nor massive neutrinos (although they can be included) [12], and it does not include gravity at all. Furthermore, it is not clear whether the observed Higgs boson corresponds to the scalar predicted by the SM. Other questions that we may pose are: why are there three generations of fermions, can we unify the strong and electroweak interactions, why are the weak interactions left-handed, why do the fermion masses have the values that they have, and so forth. Therefore, it is necessary to explore new physics in order to give an answer to the problems not addressed by the SM.

In the SM, the use of a single Higgs doublet is the simplest choice, but it is not the only possibility. Since the SM is incomplete, a few of its problems can be solved by keeping the entirety of its structure, and simply adding new pieces to it, such as more scalar doublets. These extensions of the SM are the type of models that will be studied in this thesis. While none of the models considered in this thesis provide solutions to all of the aforementioned problems simultaneously, they solve at least some of the experimental and theoretical shortcomings of the SM.

Models with non-minimal Higgs sectors lead to a rich spectrum of characteristic collider signatures and astroparticle consequences which is why the main task of the LHC experiments at the moment is the search and probe of the fundamental properties of the discovered Higgs and physics beyond the Standard Model (BSM). In particular, a primary goal is the determination of the Higgs Charge Conjugation and Parity (CP) quantum numbers as that may give clues to the baryogenesis problem [19], and to measure more accurately its couplings to the fermions.

The structure of this thesis is the following. In chapter 2, the mathematical formulation of the sectors of the SM - the strong, the electroweak and the Higgs sectors[3] - is presented, highlighting the importance of symmetries, the local gauge principle, Spontaneous Symmetry Breaking (SSB) and the Higgs mechanism. Also, the origin of CP-violation in the SM is discussed.

In chapter 3, extensions of the scalar sector of the SM with two doublets are discussed. We start by presenting the main reasons why these models are necessary, followed by the most important constraints that one must consider when dealing with this type of BSM models. Then, to illustrate some of the features of Two-Higgs-Doublet Models (2HDMs), two of its several versions will be looked into: the first one is CP-conserving and the second one explicitly violates CP and is called Complex Two-Higgs-Doublet Model (C2HDM).

In chapter 4, we study the possibility of determining the CP nature of a scalar produced at the LHC in association with a bottom quark pair ($b\bar{b}h$), in single bottom and Higgs associated production (bh), and in the dileptonic channel of the associated production with a top pair ($t\bar{t}h$), with the Higgs, h, decaying to a bottom pair ($h \to b\bar{b}$). A generic CP-violating Yukawa coupling for the bottom and top quarks is used to study these interactions, which are simulated in MadGraph5_aMC@NLO. We consider a scalar which is either CP-even, like in the SM, or CP-odd, and we look for the possibility of distinguishing these two states from each other at parton level by using CP-sensitive observables introduced in previous works. This study is performed for a wide range of scalar boson masses, between 10-125 GeV for $b\bar{b}h$, and 40-500 GeV for $t\bar{t}h$. Afterwards, a full reconstruction is applied in $t\bar{t}h$ samples with a Higgs boson whose mass varies between 40 GeV and 300 GeV, but also to the expected Standard Model backgrounds at the

[3]The Higgs sector is actually a part of the electroweak sector. The distinction made here is just to separate the parts of the electroweak sector with or without the Higgs in them.

LHC for those processes. We present the main aspects of event generation, selection, and reconstruction for all the samples that go through reconstruction. Also, in order to estimate the experimental sensitivity for a search, expected Confidence Levels (CLs) for the exclusion of several scenarios are presented as a function of the luminosity, for different distributions and Higgs masses. Some of the questions that we answer are: are we sensitive to the CP-components of an hypothetical new scalar that may be found at the LHC? Does that sensitivity change with the scalar boson mass? Also, does the CP nature of said scalar affects the possibility of excluding (or discover) its existence? And what can we conclude in the context of the C2HDM with this type of exclusion scenarios?

Finally, we conclude in chapter 5 by summarizing the main results obtained in the previous chapters.

Chapter 2

The Standard Model

2.1 The elements of the SM

The world around us is composed mostly of protons, neutrons, electrons (the three constituents of atoms) and electron neutrinos, interacting with each other via the electromagnetic, strong and weak forces[1]. However, at higher energy scales, a much richer structure is observed. For example, the protons and neutrons are actually bound states of fundamental particles called quarks, with both the protons and the neutrons being composed of different numbers of up and down-quarks. The electron, the electron neutrino, the up-quark and the down-quark are known as the first generation of fermions [20].

The fermions are particles with half-integer spin. They obey the Fermi-Dirac statistics and the Pauli exclusion principle and are described by antisymmetric wave functions. In the SM there are two types of spin-1/2 fermions: the leptons, which do not interact via the strong force, and the quarks, which have all types of interactions. In total there are six leptons and six quarks, organized in three families or generations, and each fermion has a corresponding antiparticle. They are thought to be elementary particles, and are the constituents of matter (apart from the neutrinos). Each generation is actually a copy of the others with a different mass. This can be seen in Table 2.1 and Table 2.2. As for the neutrinos, while it is known that they are not massless, their masses have yet to be determined [12].

Interactions in the SM are mediated by spin-1 particles, known as gauge or vector bosons. The photon is the gauge boson of the electromagnetic force. In the case of the strong interaction, that role is played by the gluon which, like the photon, is massless. The weak interaction is mediated by the charged W^+ and W^- bosons, responsible for β-decay, and the neutral Z boson. All three of them are massive particles.

The final element of the Standard Model is the Higgs boson. Unlike the previous particles, the Higgs boson has zero spin, and is the only fundamental scalar discovered to date. It plays a very special role in the SM since it provides the mechanism by which all other elementary particles acquire mass. The properties of the bosons of the SM are shown in Table 2.3.

[1] Not considering Dark Matter.

Table 2.1: Leptons of the SM. They interact via the electromagnetic and weak interactions, apart from the neutrinos who only interact via the weak force. Each member of a generation has greater mass than the corresponding particles of lower generations. Uncertainties and further details about the mass values presented here and in the tables below can be found in [12].

Leptons (spin = 1/2)			
Generation	Flavour	Charge (e)	Mass
I	Electron - e	-1	$\approx$ 511 keV
	Electron neutrino - ν_e	0	$<$ 2 eV
II	Muon - μ	-1	$\approx$ 105.7 MeV
	Muon neutrino - ν_μ	0	$<$ 2 eV
III	Tau - τ	-1	$\approx$ 1.78 GeV
	Tau neutrino - ν_τ	0	$<$ 2 eV

Table 2.2: Quarks of the SM. They interact via all forces: electromagnetic, weak and strong.

Quarks (spin = 1/2)			
Generation	Flavour	Charge (e)	Mass
I	Up - u	2/3	2.16 MeV
	Down - d	-1/3	4.67 MeV
II	Charm - c	2/3	1.27 GeV
	Strange - s	-1/3	93 MeV
III	Top - t	2/3	172.9 GeV
	Bottom - b	-1/3	4.18 GeV

Table 2.3: Bosons of the SM. The photon mediates the electromagnetic force, the $W^\pm$ and Z^0 the weak force and the gluons the strong force.

Bosons			
Type	Name	Charge (e)	Mass
Gauge Bosons (spin = 1)	Photon - γ	0	0
	W bosons - $W^\pm$	$\pm$1	80.379 GeV
	Z boson - Z^0	0	91.1876 GeV
	Gluon - g	0	0
Scalar Bosons (spin = 0)	Higgs boson - H	0	125.10 GeV

2.2 Symmetries and gauge principle

The mathematical framework of the SM is based on quantum field theory. The dynamics and kinematics of the theory are dictated by a Lorentz invariant quantity which is called Lagrangian density[2] (although people usually refer to it just as Lagrangian), and the particles are described by quantum fields that depend on space-time coordinates.

In order to construct the Lagrangian in terms of the fields, certain guidelines should be followed. The first one is that the Lagrangian should preserve the symmetries of the system under consideration, and the second one is that the Lagrangian should be renormalizable - if the Lagragian is non-renormalizable, infinities would appear when calculating amplitudes and other quantities that we cannot cancel out. The first thing to do is to postulate what are those symmetries, after which we write the most general renormalizable Lagrangian that respects them. It is at this point that we use the gauge principle [21], which is a way to derive interactions between the objects that appear in the Lagrangian from continuous symmetries. The method consists in demanding that a theory invariant under some global continuous symmetry remains invariant if the symmetry is local, i.e. if its parameters depend on the space-time points, which leads to the introduction of extra vector fields called gauge fields[3].

To see how this works, we will use the gauge principle to derive the Lagrangian of Quantum Electrodynamics (QED). For a Dirac field ψ with mass m, the Lagrangian can be written as

$$\mathcal{L} = \frac{i}{2}[\bar{\psi}\gamma^{\mu}(\partial_{\mu}\psi) - (\partial_{\mu}\bar{\psi})\gamma^{\mu}\psi] - m\bar{\psi}\psi\,, \tag{2.1}$$

where $\bar{\psi} = \psi^{\dagger}\gamma^{0}$ and $\partial_{\mu} \equiv \frac{\partial}{\partial x^{\mu}}$ is the partial derivative with respect to one of the four space-time components. ψ is a 4×1 column field called a spinor, and γ_{μ} and γ^{0} are 4×4 matrices[4] which obey

$$\{\gamma_{\mu}, \gamma_{\nu}\} = \gamma_{\mu}\gamma_{\nu} + \gamma_{\nu}\gamma_{\mu} = 2g_{\mu\nu}\,, \tag{2.2}$$

$$\gamma^{0}\gamma_{\mu}(\gamma^{0})^{-1} = \gamma_{\mu}^{\dagger}\,, \quad (\gamma^{0})^{\dagger} = \gamma^{0}. \tag{2.3}$$

Since ∂_{μ} and m have mass (M) dimension, the dimension of ψ must be $M^{3/2}$ and the matrices γ_{μ} and γ^{0} are both dimensionless, as every term in a Lagrangian must have dimension M^{4} (see appendix A). Now consider a $U(1)$ gauge transformation of the Dirac fields of the form

$$\psi \to e^{-iQ\alpha}\psi, \quad \bar{\psi} \to e^{iQ\alpha}\bar{\psi}, \tag{2.4}$$

where Q is the generator of the $U(1)$ group and also, in this case, the electric-charge operator, and α is an arbitrary phase independent from the space-time coordinates. The Lagrangian in Equation 2.1 is invariant under the transformation in Equation 2.4. But if we make the parameter α dependent on x^{μ} then it no

[2] It plays a role similar to that of the Schrödinger equation in non-relativistic quantum mechanics, but a Lagrangian is not an equation of motion - it is a polynomial function of the fields and their derivatives which may be used to derive an equation of motion according to the Hamilton principle.

[3] Theories resulting from the application of this principle are called gauge theories. The SM is an example of a gauge theory with a $SU(3)_{col} \times SU(2) \times U(1)_{Y}$ group symmetry.

[4] In the Dirac representation, $\gamma^{0} = \tau_{3} \otimes I_{2\times 2}$ and $\gamma^{k} = (-i\tau_{2}) \otimes \tau_{k}$ ($k = 1, 2, 3$) where τ_{k} are the Pauli matrices (see appendix B) and $\otimes$ the Kronecker product.

longer remains that way since the kinetic term changes into

$$\frac{i}{2}[\bar{\psi}\gamma^\mu(\partial_\mu\psi) - (\partial_\mu\bar{\psi})\gamma^\mu\psi] \to \frac{i}{2}[\bar{\psi}\gamma^\mu(\partial_\mu\psi) - (\partial_\mu\bar{\psi})\gamma^\mu\psi] + Q(\partial_\mu\alpha)\bar{\psi}\gamma^\mu\psi. \tag{2.5}$$

In order to restore the gauge invariance we introduce a real vector field A^μ which transforms under the local gauge transformation as

$$A^\mu \to A^\mu + \frac{\partial^\mu\alpha}{e}, \tag{2.6}$$

where e is the electric charge of the proton and in particular the coupling constant of electromagnetism, and we add to the Lagrangian the term

$$-eQ\,\bar{\psi}\gamma^\mu\psi\,A_\mu. \tag{2.7}$$

Notice that this is the same as making $p_\mu \to p_\mu - eQA_\mu$ and $p_\mu \to p_\mu + eQA_\mu$ for the momentum $p_\mu = i\partial_\mu$ of the fields ψ and $\bar{\psi}$, respectively, since

$$\begin{aligned}\mathcal{L}' &= \frac{i}{2}[\bar{\psi}\gamma^\mu(\partial_\mu\psi) - (\partial_\mu\bar{\psi})\gamma^\mu\psi] - m\bar{\psi}\psi - eQ\,\bar{\psi}\gamma^\mu\psi\,A_\mu \\ &= \frac{1}{2}[\bar{\psi}\gamma^\mu(i\partial_\mu - eQA_\mu)\psi - \{(i\partial_\mu + eQA_\mu)\bar{\psi}\}\gamma^\mu\psi] - m\bar{\psi}\psi.\end{aligned} \tag{2.8}$$

To complete the Lagrangian of this interaction, we need to introduce a kinetic-energy term for the new field A_μ (representing the photon) which must be invariant under this field transformation. After that we obtain the Lagrangian of QED

$$\begin{aligned}\mathcal{L}_{QED} &= \bar{\psi}(i\gamma^\mu\partial_\mu - m - eQ\gamma^\mu A_\mu)\psi - \frac{1}{4}F_{\mu\nu}F^{\mu\nu} \\ &= \bar{\psi}(i\gamma^\mu D_\mu - m)\psi - \frac{1}{4}F_{\mu\nu}F^{\mu\nu},\end{aligned} \tag{2.9}$$

where $F_{\mu\nu} = \partial_\mu A_\nu - \partial_\nu A_\mu$ and $D_\mu = \partial_\mu + ieQA_\mu$ [5]. Hence, from a simple symmetry we were able to fully derive the Lagrangian of the electromagnetic interaction - this is the usefulness of the gauge principle that is used everywhere in the SM to construct interactions out of symmetries. Notice how we cannot add to the Lagrangian in Equation 2.9 a mass term for the gauge field A_μ, i.e. a term proportional to $A_\mu A^\mu$ as that would break the gauge invariance. A_μ must then be massless.

2.3 The strong sector

The strong interaction is described by Quantum Chromodynamics (QCD), which is a non-abelian gauge theory with gauge group $SU(3)$ [22]. QCD describes the interactions between coloured particles, where colour is a quantum number like the electric charge of electromagnetism. There are two types of fundamental coloured particles: the quarks (anti-quarks), which can have three distinct colours (anti-colours), and the gluons, which may carry one of eight colours. The gluons are the gauge bosons of QCD. Due to a phenomenon called colour confinement, colour charged particles cannot be isolated indefinitely, and therefore their direct observation is not possible [12]. Their existence is known through the observation of colourless particles called hadrons, which are formed out of quarks and gluons through the process of hadronization as a consequence of the aforementioned phenomenon of colour confinement.

[5] The generalized momentum operator D_μ is called a covariant derivative.

There are two types of hadrons: the baryons, formed by three quarks, and the mesons, formed by a quark anti-quark pair.

Besides colour, the quarks and the anti-quarks carry a flavour. In total there are six flavours, as we have seen in Table 2.2. Since the quarks are particles with spin-1/2 and for each flavour q there are three quarks with different colours q_1, q_2 and q_3, the QCD Lagrangian is given by

$$\mathcal{L}_{strong} = \sum_{q=u,d,s,c,b,t} \sum_{j,k=1}^{3} \bar{q}_j i\gamma^\mu (D_\mu)_{jk} q_k - \frac{1}{4} \sum_{a=1}^{8} G^a_{\mu\nu} G^{\mu\nu}_a, \tag{2.10}$$

where $(D_\mu)_{jk} = \partial_\mu \delta_{jk} + i g_s \sum_{a=1}^{8} G^a_\mu [\frac{\lambda_a}{2}]_{jk}$ and $G^a_{\mu\nu} = \partial_\mu G^a_\nu - \partial_\nu G^a_\mu - g_s \sum_{b,c=1}^{8} f_{abc} G^b_\mu G^c_\nu$. In these expressions, g_s is the strong coupling constant , λ_a are the Gell-Mann matrices (see appendix B), f_{abc} are the structure constants of $SU(3)$ and G^μ_a are the fields of the 8 gluons. Notice that the matrices in Equation 2.10 act in different spaces: γ_μ acts on the Dirac space and λ_a is a 3×3 matrix acting on colour space.

The structure of QCD is very similar to that of QED: both are mediated by massless gauge bosons that only couple to particles (anti-particles) with non-zero colour charge or non-zero electric charge, respectively. Nevertheless, since the former arises from a non-abelian group, i.e. a group whose generators do not commute, to keep the gauge invariance there is an extra term in the kinetic components of the gluon fields, proportional to the structure constants of $SU(3)$, giving rise to gluon self-interactions[6].

2.4 The electroweak sector

In the Standard Model the electromagnetic and the weak nuclear forces are unified through the electroweak interaction, despite them being very different from each other. While the weak interaction violates parity and only acts on left-handed fermions, electromagnetism conserves parity and acts on both left- and right-handed fermions. Parity violation by the weak interaction was demonstrated in the Wu experiment [23].

The electroweak interaction in the SM is a gauge theory with gauge group $SU(2) \times U(1)_Y$. The $SU(2)$ group has coupling constant $-g$ and three generators T_1, T_2 and T_3 which obey $[T_j, T_k] = i \sum_{l=1}^{3} \epsilon_{jkl} T_l$. It is the group of the weak isospin (T). The gauge group $U(1)_Y$ has coupling constant $-g'$ and only one generator, Y, which plays the same role as the electric charge of QED. It is called the weak hypercharge.

The covariant derivative is given by

$$D^\mu = \partial^\mu - ig \left(W^\mu_1 T_1 + W^\mu_2 T_2 + W^\mu_3 T_3 \right) - ig' B^\mu Y, \tag{2.11}$$

where W^μ_i ($i = 1, 2, 3$) and B^μ are the gauge fields of the $SU(2)$ and $U(1)_Y$ gauge groups, respectively. These fields mix in order to create the states that are physically observable. Also, since we must recover the covariant derivative of QED, instead of g and g' we will use the electric charge e and the Weinberg

[6] Since the structure constants are zero for abelian groups like U(1), there are no such terms in QED.

angle θ_w which have the following definitions:

$$g = \frac{e}{\sin\theta_w}, \tag{2.12}$$

$$g' = \frac{-e}{\cos\theta_w}. \tag{2.13}$$

The gauge fields A^μ and Z^μ are defined as

$$\begin{pmatrix} B^\mu \\ W_3^\mu \end{pmatrix} = \begin{pmatrix} \cos\theta_w & \sin\theta_w \\ -\sin\theta_w & \cos\theta_w \end{pmatrix} \begin{pmatrix} A^\mu \\ Z^\mu \end{pmatrix}. \tag{2.14}$$

As we can see in the Equation 2.14 the Weinberg angle is a mixing angle that allows to rotate between the fields of the unphysical gauge bosons (B^μ and W_3^μ) and the fields A^μ and Z^μ. Notice that this transformation is unitary so that the kinetic-energy terms remain well normalized, i.e.

$$\left(\partial^\mu B^\nu\right)\left(\partial_\mu B_\nu\right) + \left(\partial^\mu W_3^\nu\right)\left(\partial_\mu W_{3\nu}\right) = \left(\partial^\mu A^\nu\right)\left(\partial_\mu A_\nu\right) + \left(\partial^\mu Z^\nu\right)\left(\partial_\mu Z_\nu\right), \tag{2.15}$$

and orthogonal since the fields A^μ and Z^μ are real. We also define

$$Q = T_3 + Y \tag{2.16}$$

to be the electric charge operator. Since

$$\begin{aligned} gW_3^\mu T_3 + g'B^\mu Y =& \frac{e}{\sin\theta_w}\left(-A^\mu\sin\theta_w + Z^\mu\cos\theta_w\right)T_3 \\ &- \frac{e}{\cos\theta_w}\left(A^\mu\cos\theta_w + Z^\mu\sin\theta_w\right)Y \\ =& -eA^\mu\left(T_3 + Y\right) \\ &+ eZ^\mu\left(T_3\cot\theta_w - Y\tan\theta_w\right), \end{aligned} \tag{2.17}$$

the definition in Equation 2.16 comes naturally as we want to recover QED. Using Equations 2.12, 2.13, 2.14 and 2.16 in the derivative in Equation 2.11 yields

$$\begin{aligned} D^\mu =& \partial^\mu + ieQA^\mu - i\frac{g}{\cos\theta_w}\left(T_3 - Q\sin^2\theta_w\right)Z^\mu \\ &- ig\left(W_1^\mu T_1 + W_2^\mu T_2\right). \end{aligned} \tag{2.18}$$

If we further define

$$W_\mu^\pm = \frac{W_1^\mu \mp iW_2^\mu}{\sqrt{2}}, \tag{2.19}$$

which again is a unitary transformation, then we finally have the covariant derivative written in a way where we can see the dependence on the physical gauge fields

$$\begin{aligned} D^\mu =& \partial^\mu + ieQA^\mu \\ &- i\frac{g}{\cos\theta_w}\left(T_3 - Q\sin^2\theta_w\right)Z^\mu \\ &- ig\left(W^{\mu+}T_+ + W^{\mu-}T_-\right), \end{aligned} \tag{2.20}$$

and we retrieve the covariant derivative of electromagnetism. The $T_\pm$ are the raising and lowering operators of $SU(2)$ given by

$$T_\pm = \frac{T_1 \pm iT_2}{\sqrt{2}}. \tag{2.21}$$

2.4.1 The Fermions

Fermions can be classified according to their chirality, which is a relativistic invariant corresponding to the eigenvalue of a 4×4 matrix which we call γ_5 and define as $\gamma_5 = i\gamma^0\gamma^1\gamma^2\gamma^3$. The eigenvalues of γ_5 are ± 1. Fermions with chirality +1 are called right-handed (R), while L is used for left-handed fermions (chirality -1). In the limit of zero mass, chirality and helicity, the latter being the projection of the spin of the fermion relative to its momentum direction, are the same thing[7], which is related to the right/left-handed naming. Chirality is important because weak interactions are chiral, that is, fermions with distinct chiralities interact in a different way.

In the SM we have both R and L fermions, which have different values of T_3 and Y, but the same electric charge, i.e., an electron has always electric charge -1, regardless of being left-handed or right-handed. The left-handed components of the leptons are put in $SU(2)$ doublets with $Y = -1/2$,

$$\begin{pmatrix} \nu_{eL} \\ e_L \end{pmatrix}, \quad \begin{pmatrix} \nu_{\mu L} \\ \mu_L \end{pmatrix}, \quad \begin{pmatrix} \nu_{\tau L} \\ \tau_L \end{pmatrix}, \tag{2.22}$$

while for the quarks we have $Y = 1/6$

$$\begin{pmatrix} u_L \\ d_L \end{pmatrix}, \quad \begin{pmatrix} c_L \\ s_L \end{pmatrix}, \quad \begin{pmatrix} t_L \\ b_L \end{pmatrix}. \tag{2.23}$$

In this way, the upper components (T_3 [8] $= +1/2$) have zero charge for the neutrinos and + 2/3 for the up quarks, and the lower components ($T_3 = -1/2$) have charge -1 for the charged leptons and - 1/3 for the down quarks.

The right-handed components are singlets of $SU(2)$, i.e., the weak isospin T is zero (hence $T_3 = 0$). Therefore, the charged leptons e_R, μ_R and τ_R have hypercharge $Y = -1$, the up quarks u_R, c_R and t_R have $Y = +2/3$ and the down quarks d_R, s_R and b_R have $Y = -1/3$. There are no right-handed neutrinos in the SM, since neutrino oscillations were not known at the time and therefore they were though to be massless [24]. Then, the kinetic terms for the leptons are given by

$$\begin{aligned} \mathcal{L}_{leptons} = \sum_{j=1}^{3} \overline{L}_{Lj}\gamma^\mu \Bigg[i\partial_\mu + \begin{pmatrix} 0 & 0 \\ 0 & eA_\mu \end{pmatrix} + \frac{g}{c_w}\begin{pmatrix} 1/2 & 0 \\ 0 & s_w^2 - 1/2 \end{pmatrix} Z_\mu \\ + \frac{g}{\sqrt{2}}\begin{pmatrix} 0 & W_\mu^+ \\ W_\mu^- & 0 \end{pmatrix} \Bigg] L_{Lj} + \sum_{j=1}^{3} \overline{l_{Rj}}\gamma^\mu \left(i\partial_\mu + eA_\mu + \frac{gs_w^2}{c_w} Z_\mu \right) l_{Rj}, \end{aligned} \tag{2.24}$$

where in this notation $L_L = \{(\nu_{eL},\ e_L)^T, (\nu_{\mu L},\ \mu_L)^T, (\nu_{\tau L},\ \tau_L)^T\}$ and $l_R = \{e_R,\ \mu_R,\ \tau_R\}$. The index

[7] Outside of this limit, chirality and helicity are very different things. Helicity has physical interpretation and changes depending on the reference frame. Chirality is an intrinsic property and a purely mathematical concept that defines the transformation law of a given field.

[8] Here T_3 refers to the third component of the weak isospin.

j refers to the generation, so we have $L_{L1} = (\nu_{eL},\ e_L)^T$, $l_{R1} = e_R$, and so on. We are also using the notation where $s_w = \sin\theta_w$ and $c_w = \cos\theta_w$.

For the quarks[9], we have

$$\begin{aligned}\mathcal{L}_{quarks} = \sum_{j=1}^{3} \overline{Q}_{Lj}\gamma^\mu \Bigg[i\partial_\mu + -e \begin{pmatrix} 2/3 & 0 \\ 0 & -1/3 \end{pmatrix} A_\mu + \frac{g}{\sqrt{2}} \begin{pmatrix} 0 & W_\mu^+ \\ W_\mu^- & 0 \end{pmatrix} \\ + \frac{g}{c_w} \begin{pmatrix} 1/2 - 2s_w^2/3 & 0 \\ 0 & s_w^2/3 - 1/2 \end{pmatrix} Z_\mu \Bigg] Q_{Lj} \\ + \sum_{j=1}^{3} \overline{U_{Rj}}\gamma^\mu \left(i\partial_\mu - \frac{2}{3}\left[eA_\mu + \frac{gs_w^2}{c_w} Z_\mu \right] \right) U_{Rj} \\ + \sum_{j=1}^{3} \overline{D_{Rj}}\gamma^\mu \left(i\partial_\mu + \frac{1}{3}\left[eA_\mu + \frac{gs_w^2}{c_w} Z_\mu \right] \right) D_{Rj},\end{aligned} \tag{2.25}$$

with $Q_L = \{(u_L,\ d_L)^T, (c_L,\ s_L)^T, (t_L,\ b_L)^T\}$, $U_R = \{u_R,\, c_R,\, t_R\}$ and $D_R = \{d_R,\, s_R,\, b_R\}$.

There is a couple of aspects worth mentioning from Equation 2.24 and Equation 2.25. Looking at the vertices which involve a $W_\mu^\pm$, we see that they only couple to left-handed fermions of different flavours. For that reason, these interactions are sometimes called Flavour Changing Charged Currents (FCCCs). On the contrary, A_μ and Z_μ couple to both left- and right-handed fermions of equal flavour, therefore there are no Flavour Changing Neutral Currents (FCNCs) at tree level in this sector[10]. Also, notice the absence of mass terms in both Equation 2.24 and Equation 2.25. This is because those break the electroweak symmetry. To see that, we introduce the projector operators

$$P_R = \frac{1+\gamma_5}{2}, \quad P_L = \frac{1-\gamma_5}{2}, \tag{2.26}$$

which obey the usual relations for projector operators:

$$P_R + P_L = 1, \quad (P_R)^2 = P_R, \quad (P_L)^2 = P_L, \quad P_R P_L = P_L P_R = 0. \tag{2.27}$$

One may write $\psi = (P_L + P_R)\psi = \psi_L + \psi_R$. Since $\gamma_5^\dagger = -\gamma^0\gamma_5(\gamma^0)^{-1}$, then

$$\overline{\psi}P_L = \psi^\dagger\gamma^0 P_L = \psi^\dagger P_R^\dagger \gamma^0 = \overline{P_R\psi} = \overline{\psi_R}, \tag{2.28}$$

and $\overline{\psi}P_R = \overline{\psi_L}$. Thus,

$$\begin{aligned} m\overline{\psi}\psi &= m\overline{\psi}\left(P_L + P_R\right)\psi \\ &= m\overline{\psi}\left(P_L^2 + P_R^2\right)\psi \\ &= m\left(\overline{\psi_R}\psi_L + \overline{\psi_L}\psi_R\right). \end{aligned} \tag{2.29}$$

From Equation 2.29 we conclude that a Dirac mass terms breaks chirality, and since in the SM ψ_L and ψ_R have different quantum numbers, it also breaks the $SU(2) \times U(1)_Y$ gauge invariance. On the

[9] As it was said before, each quark has three different colours, but that is only relevant for the strong interaction. In the electroweak sector we sum over the colours, i.e., whenever we have something like $\overline{q}q$ that is the same as $\overline{q}_1 q_1 + \overline{q}_2 q_2 + \overline{q}_3 q_3$.

[10] There is not FCNCs at tree level in the SM, since the gluons and the Higgs also preserve flavour [25, 26].

contrary, terms like $\overline{\psi}\gamma^\mu D_\mu\psi$ conserve chirality, since $\{\gamma^\mu, \gamma_5\} = 0$ and therefore

$$\begin{aligned}\overline{\psi}\gamma^\mu D_\mu\psi &= \overline{\psi}\left(P_L + P_R\right)\gamma^\mu D_\mu\psi \\ &= \overline{\psi}\left(P_L^2 + P_R^2\right)\gamma^\mu D_\mu\psi \\ &= \overline{\psi}(P_L\gamma^\mu D_\mu P_R + P_R\gamma^\mu D_\mu P_L)\psi \\ &= \overline{\psi}_R\gamma^\mu D_\mu\psi_R + \overline{\psi}_L\gamma^\mu D_\mu\psi_L,\end{aligned} \tag{2.30}$$

hence the kinetic terms for the fermions keep the electroweak symmetry unbroken. As a side note, notice how the couplings between the fermions and A_μ and $W_\mu^\pm$, apart from constants, are $Q_f\gamma_\mu$ and $\gamma_\mu P_L$, respectively. Since A_μ comes multiplied by γ_μ but $W_\mu^\pm$ has terms like $\gamma_\mu - \gamma_\mu\gamma_5$, electromagnetism is sometimes called a vector interaction, while the weak interaction is called a vector minus axial vector interaction.

2.4.2 Electroweak gauge sector

Once again we must write the kinetic terms for the gauge fields. Since we now have in $SU(2)$ a non-Abelian gauge group plus an Abelian group $U(1)$, these terms will be equal to

$$\mathcal{L}_{\text{EWgauge}} = -\frac{1}{4}\left(F_Y^{\mu\nu}F_{\mu\nu Y} + \sum_{j=1}^{3} F_j^{\mu\nu}F_{\mu\nu}^j\right), \tag{2.31}$$

where $F_Y^{\mu\nu} = \partial^\mu B^\nu - \partial^\nu B^\mu$ and $F_j^{\mu\nu} = \partial^\mu W_j^\nu - \partial^\nu W_j^\mu + g\sum_{k,l=1}^{3}\epsilon_{jkl}W_k^\mu W_l^\nu$. To check that the kinetic-energy terms are adequately normalized, we must look into the terms that are quadratic in the fields, denoted as $\mathcal{L}^{(2)}$. They are given in Equation 2.32, and we see that fields with zero electric charge are multiplied by a factor of $1/2$, while charged fields do not have the same factor, because of their definitions in Equation 2.19.

$$\begin{aligned}\mathcal{L}^{(2)}_{\text{EWgauge}} = &-\left(\partial^\mu W^{+\nu}\right)\left(\partial_\mu W_\nu^-\right) + \left(\partial^\mu W^{+\nu}\right)\left(\partial_\nu W_\mu^-\right) \\ &-\frac{1}{2}\left(\partial^\mu Z^\nu\right)\left(\partial_\mu Z_\nu\right) + \frac{1}{2}\left(\partial^\mu Z^\nu\right)\left(\partial_\nu Z_\mu\right) \\ &-\frac{1}{2}\left(\partial^\mu A^\nu\right)\left(\partial_\mu A_\nu\right) + \frac{1}{2}\left(\partial^\mu A^\nu\right)\left(\partial_\nu A_\mu\right).\end{aligned} \tag{2.32}$$

Putting all pieces together, the Lagrangian of the electroweak sector is equal to

$$\mathcal{L}_{EW} = \mathcal{L}_{leptons} + \mathcal{L}_{quarks} + \mathcal{L}_{\text{EWgauge}}. \tag{2.33}$$

2.5 The Higgs sector

2.5.1 Spontaneous symmetry breaking

Spontaneous Symmetry Breaking (SSB) is a process that causes the ground state of a system to be less symmetric than the Lagrangian of the system itself. In nature, an example of SSB happens when a thin cylindrical metal bar is under pressure along the direction of its axis. The bar has symmetry under rotations around the axis, but if the pressure on the bar becomes strong enough, it will bend towards one arbitrary side, breaking the original rotational symmetry when in the state of minimum energy [27]. Although the system has lost symmetry, stability is gained in a process that resembles a phase transition.

In field theory, SSB occurs when a field acquires a Vacuum Expectation Value (VEV), i.e. a nonzero value in the vaccum[11]. This is done by giving a VEV to a scalar field, so that the Lorentz symmetry is not spontaneously broken[12]. To illustrate what happens when we spontaneously break a continuous symmetry in the vaccum, consider the Lagrangian for a complex scalar field with a $|\phi|^4$ interaction

$$\mathcal{L} = (\partial_\mu \phi)(\partial^\mu \phi^*) - m^2 \phi \phi^* - \lambda \phi^2 \phi^{*2}. \tag{2.34}$$

This Lagrangian has a global $U(1)$ symmetry under random phase changes of ϕ. We assume $\lambda > 0$ in order for the potential to be bounded from below, preventing its energy to become infinitely negative as ϕ grows. The state of minimum energy is achieved when $\partial V/\partial\phi = 0$, which has two solutions: $|\phi|^2 = 0$ and $|\phi|^2 = -m^2/2\lambda \equiv v^2$. Replacing the first solution in Equation 2.34 gives $V = 0$. For the second one, we get $V = -m^4/4\lambda < 0$. Then, the minimum is not at $V = 0$, since there is a solution which has less energy. However, this is only true for $m^2 < 0$, because we must have $|\phi|^2 > 0$, hence in this case the term with m^2 cannot be interpreted as a mass term. More so, m^2 actually has a similar role to that of pressure in the case of the bending cylindrical bar: when m^2 goes from positive to negative, it triggers SSB.

Suppose that $m^2 < 0$. Since the phase of ϕ at the minimum is arbitrary, there is a continuum of values of ϕ with an identical minimum energy. Without loss of generality, we choose the vacuum to be at $\phi = v$. Since the field ϕ can still oscillate around its VEV, we can write it as $\phi = v + \phi_{osc}$, and its oscillations as

$$\phi_{osc} = \frac{a + ib}{\sqrt{2}}, \tag{2.35}$$

where a and b are real fields with zero VEV. Hence, we have

$$\begin{aligned}\mathcal{L} = &-\frac{m^2 v^2}{2} + \frac{1}{2}(\partial_\mu a)(\partial^\mu a) + m^2 a^2 + \frac{1}{2}(\partial_\mu b)(\partial^\mu b) \\ &+ \frac{m^2 a\left(a^2 + b^2\right)}{\sqrt{2} v} + \frac{m^2\left(a^2 + b^2\right)^2}{8 v^2}.\end{aligned} \tag{2.36}$$

The first term in Equation 2.36 is just a constant (irrelevant for dynamics). Notice that the linear terms in a and b have vanished, as they should, because we are at the minimum of those fields. Also, we see that while a has a positive squared mass $-2m^2$, b is massless. This massless field is called a Goldstone boson

[11] In particle physics we call vacuum to the state of minimum energy of a physical system.

[12] This is not a problem with scalar fields since they are invariant under the Lorentz symmetry.

and its existence is predicted by the Goldstone theorem [28, 29] which states that there is an unphysical massless scalar corresponding to each generator of a continuous global symmetry of the Lagrangian that is not a symmetry of the vacuum[13]. This is what happens in SSB - the number of broken symmetries result in an equal number of unphysical bosons, while the remaining Degrees of Freedom (DoF) give rise to massive scalar particles.

2.5.2 The Higgs mechanism

The SM is a theory with many particles, and the majority of them have mass. But if we add mass terms to the Lagrangian, its gauge symmetries are broken. Thus, we need an alternative way to give mass to the particles of the SM while keeping its gauge invariance.

The alternative is the Higgs mechanism [11], which is a way of generating mass by adding a field with a VEV that causes Spontaneous Symmetry Breaking. To see how this works, we will look at the scalar sector of the SM. In this sector, we start with a $SU(2) \times U(1)_Y$ gauge symmetry which is broken down to a $U(1)_Q$ symmetry in the vacuum, the actual observed symmetry in nature, and we introduce a scalar field with a VEV. This field cannot be a singlet of weak isospin, otherwise we would not break $SU(2)$, and it must have zero electric charge, so that $U(1)_Q$ remains unbroken and the photon remains massless. The simplest solution is to add a single doublet of isospin: this is the choice made in the SM, sometimes referred to as the minimal Higgs structure [30]. The doublet scalar field is denoted by ϕ and is composed of complex Klein-Gordon (KG) fields. It is equal to

$$\phi = \begin{pmatrix} \varphi^+ \\ \varphi^0 \end{pmatrix}. \tag{2.37}$$

Given the definition in Equation 2.16 of electric charge, we must have $Y = 1/2$ for this field. To write the potential, we can only have terms that are invariant under $SU(2) \times U(1)_Y$ and with dimension M^4 at most. To meet the first condition, we must know that under an $SU(2)$ transformation, $\phi \to U\phi$, where U is an $SU(2)$ matrix. Since U is unitary, i.e., $U^\dagger U = \mathbb{1}$, then only terms like $\phi^\dagger\phi$ are invariant, and because a scalar field has mass dimension one, both conditions are met if the potential takes the very simple form given by

$$V = \mu^2\phi^\dagger\phi + \lambda\left(\phi^\dagger\phi\right)^2, \tag{2.38}$$

where μ^2 has dimension M^2 and λ is dimensionless. Assuming $\lambda > 0$ and $\mu^2 < 0$ the minimum is at $\phi^\dagger\phi = -\mu^2/2\lambda = v^2$. We also choose the VEV of φ^+ to be zero. Since we can always put all VEVs in the lower component of the isospin doublet by a gauge transformation in the fields, or change the definition of Q to make sure the vacuum remains invariant under $U(1)_Q$, this choice is not an assumption. Also, this choice is what really determines the expression of the electric charge, which by definition must be such that the VEV has zero charge [31].

To check the remaining symmetries of the vacuum state, we must determine the value of $G\langle\phi\rangle_0$, where G are the generators of a symmetry group and $\langle\phi\rangle_0$ [14] is the value of the field ϕ at the state of minimum energy. If it is zero, the vaccuum is still invariant under that symmetry. Otherwise, the symmetry

[13] These scalars correspond to vibrations around the vacuum along a direction that offers no resistance because the potential is constant.

[14] $\langle\phi\rangle_0 = \langle 0|\phi|0\rangle$, where $|0\rangle$ is the ground state.

is said to be broken because it does not preserve the ground state. With $\langle\phi\rangle_0 = (0, v)^T$, we have

$$2T_1 \langle\phi\rangle_0 = \tau_1 \langle\phi\rangle_0 = \begin{pmatrix} v \\ 0 \end{pmatrix}, \tag{2.39}$$

$$2T_2 \langle\phi\rangle_0 = \tau_2 \langle\phi\rangle_0 = -i \begin{pmatrix} v \\ 0 \end{pmatrix}, \tag{2.40}$$

$$2T_3 \langle\phi\rangle_0 = \tau_3 \langle\phi\rangle_0 = - \begin{pmatrix} 0 \\ v \end{pmatrix}, \tag{2.41}$$

$$Y \langle\phi\rangle_0 = \frac{1}{2} \begin{pmatrix} 0 \\ v \end{pmatrix}, \tag{2.42}$$

$$Q \langle\phi\rangle_0 = \begin{pmatrix} 0 \\ 0 \end{pmatrix}. \tag{2.43}$$

Then, according to the Goldstone theorem, we will have 3 Goldstone bosons corresponding to the breaking of $SU(2) \times U(1)_Y$ to $U(1)_Q$, and one massive scalar particle (the Higgs), as we have 4 Degrees of Freedom in the doublet. To see that this is indeed the case we write

$$\varphi^0 = v + \frac{H + i\chi}{\sqrt{2}}, \tag{2.44}$$

where H and χ are real fields with zero VEV and expand the potential in Equation 2.38 which gives

$$\begin{aligned} V = \mu^2 \Bigg[& \tfrac{v^2}{2} - H^2 - \tfrac{H}{\sqrt{2}v} \left(H^2 + \chi^2 + 2\varphi^- \varphi^+\right) \\ & - \tfrac{1}{2v^2} \Bigg(\tfrac{H^4 + \chi^4}{4} + \tfrac{H^2 \chi^2}{2} \\ & + \varphi^- \varphi^+ \left(H^2 + \chi^2\right) + \varphi^{-2} \varphi^{+2} \Bigg) \Bigg]. \end{aligned} \tag{2.45}$$

Since both χ and $\varphi^\pm$ are massless, while H is a massive particle with mass $m_H^2 = -2\mu^2$, we do have three Goldstone bosons and one Higgs boson.

Finally, let us look at the kinetic-energy terms. Expanding the Lagrangian we have

$$\begin{aligned}
\mathcal{L}_{kin} &= (D_\mu\phi)^\dagger D^\mu\phi = \left(D_\mu\varphi^-\right)\left(D^\mu\varphi^+\right) + \left(D_\mu\varphi^{0^*}\right)\left(D^\mu\varphi^0\right) \\
&= \Bigg[\partial_\mu\varphi^- + i\frac{gv}{\sqrt{2}}W_\mu^- - ieA_\mu\varphi^- + i\frac{g}{2c_w}\left(c_w^2 - s_w^2\right)Z_\mu\varphi^- \\
&+ i\frac{g}{2}W_\mu^-(H - i\chi)\Bigg] \times \Bigg[\partial^\mu\varphi^+ - i\frac{gv}{\sqrt{2}}W^{+\mu} + ieA^\mu\varphi^+ \\
&- i\frac{g}{2c_w}\left(c_w^2 - s_w^2\right)Z^\mu\varphi^+ - i\frac{g}{2}W^{+\mu}(H + i\chi)\Bigg] \\
&+ \Bigg[\frac{\partial_\mu H}{\sqrt{2}} - i\frac{\partial_\mu\chi}{\sqrt{2}} - i\frac{gv}{2c_w}Z_\mu - i\frac{g}{2\sqrt{2}c_w}Z_\mu(H - i\chi) \\
&+ i\frac{g}{\sqrt{2}}W_\mu^+\varphi^-\Bigg] \times \Bigg[\frac{\partial^\mu H}{\sqrt{2}} + i\frac{\partial^\mu\chi}{\sqrt{2}} + i\frac{gv}{2c_w}Z^\mu \\
&+ i\frac{g}{2\sqrt{2}c_w}Z^\mu(H + i\chi) - i\frac{g}{\sqrt{2}}W^{-\mu}\varphi^+\Bigg].
\end{aligned} \tag{2.46}$$

Considering only the quadratic terms that come from the relation in Equation 2.46,

$$\begin{aligned}
\mathcal{L}_{kin}^{(2)} = &\left(\partial_\mu\varphi^-\right)\left(\partial^\mu\varphi^+\right) \\
&+ \frac{1}{2}\left[\left(\partial_\mu H\right)\left(\partial^\mu H\right) + \left(\partial_\mu\chi\right)\left(\partial^\mu\chi\right)\right] \\
&+ \frac{g^2v^2}{2}W_\mu^-W^{+\mu} + \frac{g^2v^2}{4c_w^2}Z_\mu Z^\mu \\
&+ i\frac{gv}{\sqrt{2}}\left(W_\mu^-\partial^\mu\varphi^+ - W_\mu^+\partial^\mu\varphi^-\right) + \frac{gv}{\sqrt{2}c_w}Z_\mu\partial^\mu\chi,
\end{aligned} \tag{2.47}$$

we see that three of the four gauge bosons are now massive. This is how the Higgs mechanism works - the Golstone bosons that came from SSB are swallowed by the gauge bosons, becoming their longitudinal components, which makes them massive (massless gauge bosons only have two DoF, while gauge bosons with mass have three).

Looking at the masses of the gauge bosons, they are $m_W = gv/\sqrt{2}$ and $m_Z = gv/\sqrt{2}c_w$, which leads to the correct relation $m_W = m_Z c_w$. Finally, to deal with terms such as $W_\mu^-\partial^\mu\varphi^+$, in order to define a propagator for the fields, a gauge must be chosen. A possibility is to choose the unitary gauge [32], which removes the unphysical bosons from the Lagrangian by an appropriate transformation of the scalar field. Another possibility is to use the Feynman–'t Hooft gauge, which adds to the Lagrangian a term $W_\mu^-\partial^\mu\varphi^+$ with opposite sign from the one in Equation 2.47, so that they cancel each other out. Even though the calculations that follow still include Goldstone bosons, these particles can be removed and we do not end up with more Degrees of Freedom than what we had at the beginning.

2.5.3 The Yukawa sector

Similarly to the gauge bosons, we know experimentally that the leptons and the quarks have mass. Since a Dirac mass term cannot be included in the initial Lagrangian as it breaks the gauge invariance of the SM, we need an alternative way to give mass to the fermions. Once again we will use the Higgs for that. The couplings between the fermions and the Higgs are called the Yukawa couplings. For the leptons, we can write

$$\mathcal{L}_{\text{lepton Yukawa}} = -\sum_{j,k=1}^{3} M_{l_{kj}} \overline{L_{Lj}} \begin{pmatrix} \varphi^+ \\ \varphi^0 \end{pmatrix} l_{Rk} + \text{H.c.}, \tag{2.48}$$

where M_l is a diagonal matrix with real elements and H.c. is the Hermitian conjugate. Since the fields in L_{Lj} have $Y = -1/2$, ϕ has $Y = 1/2$ and l_{Rk} has $Y = -1$, the Lagrangian in Equation 2.48 is gauge invariant. If we write Equation 2.48 explicitly for the electron, we have

$$\begin{aligned} \mathcal{L}_{\text{lepton Yukawa}} = \cdots - m_e \Bigg[& \overline{\nu_{eL}} e_R \frac{\varphi^+}{v} + \overline{e_R} \nu_{eL} \frac{\varphi^-}{v} \\ & + \overline{e}e \left(1 + \frac{H}{\sqrt{2}v}\right) + \frac{i\chi}{\sqrt{2}v} \overline{e}\gamma_5 e \Bigg], \end{aligned} \tag{2.49}$$

where we find a mass term for the electron equal to $-m_e\overline{e}e$. We also have a Yukawa coupling between the electron and the Higgs, which shows an important aspect about these couplings: they are proportional to the fermion mass. Then, for smaller masses, they are smaller too ($m_e/\sqrt{2}v \approx 511$ keV$/246$ GeV $\approx 10^{-6}$ [12]; for the top, $m_t/\sqrt{2}v \approx 173$ GeV$/246$ GeV ≈ 0.7, so the Yukawa coupling of the top is about 5 orders of magnitude larger than the Yukawa coupling of the electron). Notice as well how there is not any mass term for the neutrinos, since the SM does not consider right-handed neutrinos. There is another way to give them mass [33], but that is outside the scope of this work.

The main difference between the leptons and the quarks in the Yukawa sector is that for each left-handed quark there is also a right-handed one. To give mass to the up-quarks, we use $\tilde{\phi} = X\phi^* = i\tau_2\phi^*$, which also transforms as an $SU(2)$ doublet (see appendix B). Hence, the Yukawa Lagrangian for the quarks is:

$$\begin{aligned} \mathcal{L}_{\text{ quark Yukawa}} = & -\sum_{j=1}^{3}\sum_{k=1}^{3} \Gamma_{jk} \overline{Q_{Lj}} D_{Rk} \begin{pmatrix} \varphi^+ \\ \varphi^0 \end{pmatrix} \\ & -\sum_{j=1}^{3}\sum_{k=1}^{3} \Delta_{jk} \overline{Q_{Lj}} U_{Rk} \begin{pmatrix} \varphi^{0^*} \\ -\varphi^- \end{pmatrix} \\ & + \text{H.c.}, \end{aligned} \tag{2.50}$$

where Γ and Δ are 3×3 complex and arbitrary matrices with the Yukawa couplings of the quarks. Since these matrices are not diagonal, the quark fields that we have used so far are actually unphysical states (weak eigenstates). In order to write the Lagrangian as a function of the physical states (or mass eigenstates) only, we will need to perform a basis transformation which rotates the matrices and the fields simultaneously so that in the end we have diagonal matrices. To do this, we define $M_u = v\Delta$ and $M_d = v\Gamma$, plus four 3×3 unitary matrices $V_{L,R}^{u,d}$ such that

$$V_L^{u\dagger} M_u V_R^u = \hat{M}_u \equiv \text{diag}\left(m_u, m_c, m_t\right), \tag{2.51}$$

$$V_L^{d\dagger} M_d V_R^d = \hat{M}_d \equiv \text{diag}\left(m_d, m_s, m_b\right). \tag{2.52}$$

As for the physical fields, they are

$$\hat{u}_L^{phy} \equiv \begin{pmatrix} \hat{u}_L \\ \hat{c}_L \\ \hat{t}_L \end{pmatrix} = V_L^{u\dagger} \begin{pmatrix} u_L \\ c_L \\ t_L \end{pmatrix}, \tag{2.53}$$

$$\hat{d}_L^{phy} \equiv \begin{pmatrix} \hat{d}_L \\ \hat{s}_L \\ \hat{b}_L \end{pmatrix} = V_L^{d\dagger} \begin{pmatrix} d_L \\ s_L \\ b_L \end{pmatrix}, \tag{2.54}$$

$$\hat{u}_R^{phy} \equiv \begin{pmatrix} \hat{u_R} \\ \hat{c_R} \\ \hat{t_R} \end{pmatrix} = V_R^{u\dagger} \begin{pmatrix} u_R \\ c_R \\ t_R \end{pmatrix}, \tag{2.55}$$

$$\hat{d}_R^{phy} \equiv \begin{pmatrix} \hat{d_R} \\ \hat{s_R} \\ \hat{b_R} \end{pmatrix} = V_R^{d\dagger} \begin{pmatrix} d_R \\ s_R \\ b_R \end{pmatrix}. \tag{2.56}$$

Expanding in Equation 2.50 and rotating into the physical fields the quark Yukawa Lagrangian becomes

$$\begin{aligned}
\mathcal{L}_{\text{quark Yukawa}} &= -\overline{\hat{d}_L^{phy}} V_L^{d\dagger} M_d V_R^d \hat{d}_R^{phy} \left(1 + \frac{H + i\chi}{\sqrt{2}v}\right) \\
&\quad - \overline{\hat{u}_L^{phy}} V_L^{u\dagger} M_u V_R^u \hat{u}_R^{phy} \left(1 + \frac{H - i\chi}{\sqrt{2}v}\right) \\
&\quad - \overline{\hat{u}_L^{phy}} V_L^{u\dagger} M_d V_R^d \hat{d}_R^{phy} \frac{\varphi^+}{v} \\
&\quad + \overline{\hat{d}_L^{phy}} V_L^{d\dagger} M_u V_R^u \hat{u}_R^{phy} \frac{\varphi^-}{v} + \text{H.c.} \\
&= -\overline{\hat{d}_L^{phy}} \hat{M}_d \hat{d}_R^{phy} \left(1 + \frac{H + i\chi}{\sqrt{2}v}\right) \\
&\quad - \overline{\hat{u}_L^{phy}} \hat{M}_u \hat{u}_R^{phy} \left(1 + \frac{H - i\chi}{\sqrt{2}v}\right) \\
&\quad - \overline{\hat{u}_L^{phy}} V_{CKM} \hat{M}_d \hat{d}_R^{phy} \frac{\varphi^+}{v} \\
&\quad + \overline{\hat{d}_L^{phy}} V_{CKM}^\dagger \hat{M}_u \hat{u}_R^{phy} \frac{\varphi^-}{v} + \text{H.c.},
\end{aligned} \tag{2.57}$$

where $V_{CKM} = V_L^{u\dagger} V_L^d$ is the Cabibbo-Kobayashi-Maskawa (CKM) matrix (see appendix C). Finally, with $\hat{u}^{phy} = \hat{u}_L^{phy} + \hat{u}_R^{phy}$ and $\hat{d}^{phy} = \hat{d}_L^{phy} + \hat{d}_R^{phy}$,

$$\begin{aligned}
&\mathcal{L}_{\text{quark Yukawa}} = -\overline{\hat{d}^{phy}} \hat{M}_d \hat{d}^{phy} \left(1 + \tfrac{H}{\sqrt{2}v}\right) - \overline{\hat{d}^{phy}} \hat{M}_d \gamma_5 \hat{d}^{phy} \tfrac{i\chi}{\sqrt{2}v} \\
&- \overline{\hat{u}^{phy}} \hat{M}_u \hat{u}^{phy} \left(1 + \tfrac{H}{\sqrt{2}v}\right) + \overline{\hat{u}^{phy}} \hat{M}_u \gamma_5 \hat{u}^{phy} \tfrac{i\chi}{\sqrt{2}v} \\
&+ \overline{\hat{u}^{phy}} \left(\hat{M}_u V_{CKM} P_L - \hat{M}_d V_{CKM} P_R\right) \hat{d}^{phy} \tfrac{\varphi^+}{v} \\
&+ \overline{\hat{d}^{phy}} \left(\hat{M}_u V_{CKM}^\dagger P_R - \hat{M}_d V_{CKM}^\dagger P_L\right) \hat{u}^{phy} \tfrac{\varphi^-}{v}.
\end{aligned} \tag{2.58}$$

Notice that the kinetic-terms for the quarks in Equation 2.25 remain unchanged by this basis transformation since we are using unitary matrices, except for the vertices containing $W^\pm$ bosons. For instance,

$$
\begin{aligned}
&\left(\overline{u_L}, \overline{c_L}, \overline{t_L}\right) \gamma^\mu \left(u_L, c_L, t_L\right)^T \\
&= \overline{\hat{u}_L^{phy}} V_L^{u\dagger} \gamma^\mu V_L^u \hat{u}_L^{phy} \\
&= \overline{\hat{u}_L^{phy}} \gamma^\mu \hat{u}_L^{phy} \\
&= \overline{\hat{u}^{phy}} \gamma^\mu P_L \hat{u}^{phy},
\end{aligned}
\tag{2.59}
$$

but

$$
\begin{aligned}
&\left(\overline{u_L}, \overline{c_L}, \overline{t_L}\right) \gamma^\mu \left(d_L, s_L, b_L\right)^T \\
&= \overline{\hat{u}_L^{phy}} V_L^{u\dagger} \gamma^\mu V_L^d \hat{u}_L^{phy} \\
&= \overline{\hat{u}_L^{phy}} V_{CKM} \gamma^\mu \hat{u}_L^{phy} \\
&= \overline{\hat{u}^{phy}} V_{CKM} \gamma^\mu P_L \hat{u}^{phy}.
\end{aligned}
\tag{2.60}
$$

In summary, the Higgs sector describes the interactions betweens the Higgs with itself, the gauge bosons and the fermions, and the Higgs mechanism is responsible for giving mass to all these particles. The full Lagrangian of the Higgs sector is

$$
\mathcal{L}_{\text{Higgs}} = \mathcal{L}_{kin} - V + \mathcal{L}_{\text{ lepton Yukawa}} + \mathcal{L}_{\text{ quark Yukawa}} \,. \tag{2.61}
$$

2.6 The CP symmetry

In particle physics, the CP symmetry is the product of two symmetries: parity (P) and charge conjugation (C). Parity is a classical physics symmetry that changes left to right and vice-versa, just like a mirror. For example, under parity the position vector $\vec{r} = (x, y, z)$ changes sign. In relativistic notation, $x^\mu \to x_\mu, \partial^\mu \to \partial_\mu$, $A^\mu \to A_\mu$, and so on. The transformation of a scalar field and a Dirac field under parity is [34]

$$\mathcal{P}\phi(t, \vec{r})\mathcal{P}^\dagger = e^{i\beta_p}\phi(t, -\vec{r}), \tag{2.62}$$
$$\mathcal{P}\phi^*(t, \vec{r})\mathcal{P}^\dagger = e^{-i\beta_p}\phi^*(t, -\vec{r}), \tag{2.63}$$
$$\mathcal{P}\psi(t, \vec{r})\mathcal{P}^\dagger = e^{i\beta_p}\gamma_0\psi(t, -\vec{r}), \tag{2.64}$$
$$\mathcal{P}\overline{\psi}(t, \vec{r})\mathcal{P}^\dagger = e^{-i\beta_p}\overline{\psi}(t, -\vec{r})\gamma_0, \tag{2.65}$$

where $\mathcal{P}$ is the parity operator and β_p an arbitrary phase.

Unlike parity, charge conjugation is not a symmetry of classical physics. It changes a particle into its

antiparticle. Under this transformation[15] [34],

$$\mathcal{C}\phi\mathcal{C}^\dagger = e^{i\beta_c}\phi^*, \tag{2.66}$$
$$\mathcal{C}\phi^*\mathcal{C}^\dagger = e^{-i\beta_c}\phi, \tag{2.67}$$
$$\mathcal{C}A_\mu\mathcal{C}^\dagger = -A_\mu, \tag{2.68}$$
$$\mathcal{C}\psi\mathcal{C}^\dagger = e^{i\beta_c}\psi^c = e^{i\beta_c}C\overline{\psi}^T, \tag{2.69}$$
$$\mathcal{C}\overline{\psi}\mathcal{C}^\dagger = e^{-i\beta_c}\overline{\psi^c} = -e^{-i\beta_c}\psi^T C^{-1}, \tag{2.70}$$

and a weak interaction current of the type $\overline{\psi}\gamma^\mu P_L\psi$ transforms as

$$\begin{aligned}\mathcal{C}\overline{\psi}\gamma^\mu P_L\psi\mathcal{C}^\dagger &= -\psi^T C^{-1}\gamma^\mu\frac{\mathbb{1}-\gamma_5}{2}C\overline{\psi}^T \\ &= \psi^T\gamma^{\mu T}\frac{\mathbb{1}-\gamma_5^T}{2}\overline{\psi}^T \\ &= -\overline{\psi}\ \frac{\mathbb{1}-\gamma_5}{2}\gamma^\mu\psi \\ &= -\overline{\psi}\gamma^\mu\frac{\mathbb{1}+\gamma_5}{2}\psi \\ &= -\overline{\psi}\gamma^\mu P_R\psi.\end{aligned} \tag{2.71}$$

Similarly,

$$\mathcal{P}\overline{\psi}\gamma^\mu P_L\psi\mathcal{P}^\dagger = \overline{\psi}\gamma_\mu P_R\psi. \tag{2.72}$$

As we can see, both P and C change the chirality of weak interactions. Since in the SM the $W^\pm$ bosons do not couple to right-handed fermions, the SM is neither C- nor P-invariant. However, if we apply both C and P a left-handed (right-handed) current is transformed back to itself, then CP can be a symmetry of the weak interaction. To see the effect of this symmetry in the various SM fields, we will assume that all the Lagrangian components are CP-invariant, and check if there are any terms where CP is violated. The CP transformation for the gauge bosons is [34]

$$(\mathcal{CP})A^\mu(t,\vec{r})(\mathcal{CP})^\dagger = -A_\mu(t,-\vec{r}), \tag{2.73}$$
$$(\mathcal{CP})W^{+\mu}(t,\vec{r})(\mathcal{CP})^\dagger = -e^{i\xi_W}W^-_\mu(t,-\vec{r}), \tag{2.74}$$
$$(\mathcal{CP})W^{-\mu}(t,\vec{r})(\mathcal{CP})^\dagger = -e^{-i\xi_W}W^+_\mu(t,-\vec{r}), \tag{2.75}$$
$$(\mathcal{CP})Z^\mu(t,\vec{r})(\mathcal{CP})^\dagger = -Z_\mu(t,-\vec{r}), \tag{2.76}$$

and for the Higgs and the Goldstone bosons we have [34]

$$(\mathcal{CP})\varphi^+(t,\vec{r})(\mathcal{CP})^\dagger = e^{i\xi_W}\varphi^-(t,-\vec{r}), \tag{2.77}$$
$$(\mathcal{CP})\varphi^-(t,\vec{r})(\mathcal{CP})^\dagger = e^{-i\xi W}\varphi^+(t,-\vec{r}), \tag{2.78}$$
$$(\mathcal{CP})H(t,\vec{r})(\mathcal{CP})^\dagger = H(t,-\vec{r}), \tag{2.79}$$
$$(\mathcal{CP})\chi(t,\vec{r})(\mathcal{CP})^\dagger = -\chi(t,-\vec{r}). \tag{2.80}$$

With these transformations, all the terms that only involve scalar and gauge bosons are indeed invariant under CP. Also, notice the relative minus sign between the Higgs and the Goldstone χ. Since the CP

[15] In Equation 2.69 and Equation 2.70, C is a 4×4 matrix such that $-\gamma_\mu^T = C^{-1}\gamma_\mu C$ and $\gamma_5^T = C^{-1}\gamma_5 C$, and β_c another arbitrary phase. In the Dirac representation, $C = i\,\gamma^2\gamma^0$.

eigenvalue of H and χ is $+1$ and -1, respectively, the first one is said to be CP-even (or scalar) and the second one CP-odd (or pseudoscalar[16]).

Now if we look at terms like $\varphi^+\overline{\hat{u}_j^{phy}}P_L\hat{d}_k^{phy}$,

$$(\mathcal{CP})\varphi^+\overline{\hat{u}_j^{phy}}P_L\hat{d}_k^{phy}(\mathcal{CP})^\dagger = e^{i(\beta_k-\beta_j+\xi_W)}\varphi^-\overline{\hat{d}_k^{phy}}P_R\hat{u}_j^{phy}, \tag{2.81}$$

and therefore CP-invariance implies $V_{jk}e^{i(\beta_k-\beta_j+\xi_W)} = V_{jk}^*$ (see Equation 2.58) for all possible flavours, which is equivalent to say that $V_{jk}V_{\gamma\alpha}V_{j\alpha}^*V_{\gamma k}^* = V_{jk}^*V_{\gamma\alpha}^*V_{j\alpha}V_{\gamma k}$. The quantity $Q_{j\gamma k\alpha} = V_{jk}V_{\gamma\alpha}V_{j\alpha}^*V_{\gamma k}^*$ is called a quartet. Hence, CP-invariance can only be achieved if the quartets of the CKM matrix are real. Since the imaginary part of the quartets (also called Jarlskog invariant, J) depends on a CP-violating phase that cannot be removed for more than two generations[17] (see appendix C), there can be (and there is!) CP violation in the Yukawa sector of the SM[18].

[16] Notice how the Yukawa couplings of a pseudoscalar always have a γ_5 (see for example Equation 2.49).

[17] We can only have CP-violation for more than 2 generations of quarks. The third generation of quarks was first proposed to explain the presence of CP-violation in the quark sector [35].

[18] J is very small, but not zero - measurements show that $J = (3.18 \pm 0.15) \times 10^{-5}$ [12]. The observation of the decay of neutral kaons into two pions lead to the discovery of CP-violation in 1964 [36]. This experiment showed that the kaons have a component with $CP = +1$ and another with $CP = -1$, which allowed them to decay to two pions, a state with $CP = +1$, but also to three pions, with $CP = -1$, therefore violating CP.

Chapter 3

Two-Higgs-Doublet Models

3.1 Motivation

Models with several Higgs doublets are often called N-Higgs-Doublet Models (NHDMs). They are among the simplest extensions of the SM Higgs sector, and they are based on the simple assumption that there can be more than one Higgs doublet, just like there is more than one family of fermions in the SM. The number of doublets must be established experimentally, since in the model there is no limitation to it [31]. Then, it becomes necessary to investigate these models theoretically in order to predict future experimental results that may indicate how many generations of Higgs there are.

Although these extensions of the SM are very conservative, they lead to extremely rich phenomenology. For example, they introduce several new massive scalar particles, and may introduce FCNCs at tree level, viable candidates for Dark Matter, and extra sources of CP-violation in the Higgs sector. Besides, many BSM theories like Supersymmetry (SUSY) also require the presence of several Higgs doublets at the electroweak scale [37]. For these reasons, NHDMs - and particularly 2HDMs - are very popular in phenomenological studies.

Historically, the original motivation to consider models with more than one doublet was due to the possibility of having spontaneous CP-violation in them [38], unlike the SM where CP-violation appears explicitly by forcing the Yukawa matrices to be complex. The need for CP-violation comes from the fact that we observe a dominance of matter over anti-matter in the Universe, which can be explained, according to the Sakharov conditions for baryogenesis, if C and CP were violated during the early moments of the Universe [17]. Even though we have CP-violation in the SM, it is not enough to explain the Universe's matter dominance [39]. The other conditions for baryogenesis are baryon number violation, necessary to produce an excess of baryons over anti-baryons, and the interactions must be out of thermal equilibrium, otherwise any baryon number violating process will be balanced by the inverse process.

Another observation that is not explained in the SM is the fact that ordinary baryonic matter accounts only for roughly 15% of the total matter in the Universe, with the other 85% being called Dark Matter [40]. Amongst 2HDMs, the Inert Doublet Model (IDM) provides a scalar Dark Matter candidate [41].

3.2 BSM Constraints

In physics we always need to consider theoretical and experimental constraints since they determine the rules that we must follow when constructing a new theory. If we want to study an extension of a

certain model, in this case the SM, we must be careful not to violate those constraints.

The first one is that the ρ parameter, defined as

$$\rho = \frac{\sum_{i=1}^{n} v_i \left[T_i \left(T_i + 1\right) - Y_i^2\right]}{\sum_{i=1}^{n} 2Y_i^2 v_i}, \tag{3.1}$$

where T_i, Y_i and v_i are the weak isospins, weak hypercharges, and neutral VEVs of the scalar Higgs doublets Φ_i, respectively, must be close to one at tree level [30], since experimentally $\rho_{\text{exp}} = 1.00039 \pm 0.00019$ [12]. For the SM, Equation 3.1 reduces to

$$\rho_{\text{SM}} = \frac{m_W^2}{m_Z^2 \cos^2\left(\theta_W\right)} = 1, \tag{3.2}$$

so it is automatically fulfilled at tree level. Likewise, it is possible to add an arbitrary number of additional SU(2) singlets or doublets to the Lagrangian[1], and even more complicated SU(2) structures, such as a multiplet of SU(2) with $T = 3$ and $Y = 2$, since in these cases we also have $\rho = 1$. Nevertheless, in this thesis we consider only the simpler case where we add an additional doublet to the Lagrangian.

The second constraint is that processes involving FCNCs must be either prohibited or very suppressed. Experimentally, data puts very strict restrictions on such processes [25, 26]. In the SM, they are completely forbidden at tree level.

The third type of constraints comes from theoretical aspects, as opposed to the previous ones. They are called the unitarity constraints. The amplitude in $2 \to 2$ scattering processes of massive vector bosons ($VV \to VV, V = Z, W$) and fermions to vector bosons ($f\bar{f} \to VV$) depends on the Center of Mass (CM) energy, which violates the unitarity of the S matrix. In the SM, this problem is solved through the Higgs boson, which leads to a set of non-trivial cancellations between Feynman diagrams containing the vector bosons, fermions and the Higgs boson, that regulates the high energy behaviour and preserves the unitarity of the theory. For this to remain true in theories with an extended Higgs sector it is sufficient to fulfill the following sum rules for the couplings between fermions, vector bosons and scalar particles [30]:

$$\sum (g_{h^{phy}VV})^2 = (g_{HVV}^{SM})^2, \tag{3.3}$$

$$\sum g_{h^{phy}VV} g_{h^{phy}f\bar{f}} = g_{HVV}^{SM} g_{Hf\bar{f}}^{SM}, \tag{3.4}$$

where we are summing along the physical neutral Higgs bosons spectrum h^{phy}. $g_{h^{phy}f\bar{f}}$ ($g_{h^{phy}VV}$) and $g_{Hf\bar{f}}^{SM}$ (g_{HVV}^{SM}) represent those couplings in the 2HDM and in the SM, respectively. These sum rules are only valid in models containing doublet and singlet Higgs fields. Higgs sector extensions involving triplet or higher Higgs representations lead to more complicated sum rules [30].

[1] In a model with only Higgs doublets and singlets, the tree level value of $\rho = 1$ is automatic [30].

3.3 The CP-conserving 2HDM

3.3.1 The 2HDM scalar sector

To construct the most general potential with two doublets, we must respect the exact same principles that we have used to derive the SM Higgs potential: all the pieces that we add to the potential must have dimension M^4, and the $SU(2) \times U(1)_Y$ symmetry must be preserved. In total, there are 14 different combinations of the scalar fields that are invariant under the electroweak symmetry, therefore the most general potential has 14 free parameters. Also, this potential can be explicitly CP-violating and have several minima which either preserve or violate CP and the electric-charge [31].

In order to understand some of the common traits of these SM extensions[2] as well as the main differences between them and the SM itself, we start by looking into one of the simplest types of 2HDMs. We will restrict ourselves for now to a CP-conserving potential with an additional $\mathbb{Z}_2$ symmetry of the form $\Phi_1 \to \Phi_1$ and $\Phi_2 \to -\Phi_2$. In this scenario, the 2HDM potential is given by [42]

$$\begin{aligned} V_{\text{2HDM}} = & m_{11}^2 \left(\Phi_1^\dagger \Phi_1\right) + m_{22}^2 \left(\Phi_2^\dagger \Phi_2\right) - m_{12}^2 \left[\left(\Phi_1^\dagger \Phi_2\right) + \left(\Phi_2^\dagger \Phi_1\right)\right] \\ & + \frac{\lambda_1}{2}\left(\Phi_1^\dagger \Phi_1\right)^2 + \frac{\lambda_2}{2}\left(\Phi_2^\dagger \Phi_2\right)^2 + \lambda_3 \left(\Phi_1^\dagger \Phi_1\right)\left(\Phi_2^\dagger \Phi_2\right) \\ & + \lambda_4 \left(\Phi_1^\dagger \Phi_2\right)\left(\Phi_2^\dagger \Phi_1\right) + \frac{\lambda_5}{2}\left[\left(\Phi_1^\dagger \Phi_2\right)^2 + \left(\Phi_2^\dagger \Phi_1\right)^2\right], \end{aligned} \tag{3.5}$$

where Φ_i ($i = 1, 2$) are complex $SU(2)$ doublets with $Y = 1/2$, λ_i ($i = 1, ..., 5$) are real-valued dimensionless parameters and m_{11}, m_{22} and m_{12} are real mass parameters. This reduces the number of total parameters to eight. Notice how Equation 3.5 still contains a term that explicitly breaks the $\mathbb{Z}_2$ symmetry - since m_{12} is non-vanishing, the potential is not invariant under the transformation $\Phi_2 \to -\Phi_2$. But as the coefficient in that term has squared mass dimension, this symmetry breaking is only soft, i.e., it does not introduce new divergences in the theory, and therefore, the theory remains renormalizable.

The potential must also be bounded from below to ensure the existence of a global minimum which means that its parameters must obey certain conditions. For the potential in Equation 3.5, we must have [43]

$$\lambda_1 > 0, \quad \lambda_2 > 0, \quad \sqrt{\lambda_1 \lambda_2} + \lambda_3 > 0, \quad \sqrt{\lambda_1 \lambda_2} + \lambda_3 + \lambda_4 - |\lambda_5| > 0. \tag{3.6}$$

The CP-conserving neutral minima are of the form

$$\langle \Phi_1 \rangle_0 = \begin{pmatrix} 0 \\ \frac{v_1}{\sqrt{2}} \end{pmatrix}, \quad \langle \Phi_2 \rangle_0 = \begin{pmatrix} 0 \\ \frac{v_2}{\sqrt{2}} \end{pmatrix}, \tag{3.7}$$

where v_1 and v_2 are real numbers representing the VEVs of the doublets Φ_1 and Φ_2, respectively. If for example we decided to add a phase to v_2, then we could have spontaneous CP-violation, despite the fact that we have started with a CP-conserving potential. Also, if the upper component of the first doublet in Equation 3.7 was non-zero, we would have a charge-breaking minimum that would result in a massive photon, which is another exotic possibility absent in the SM. The minimum in Equation 3.7 is stable. This comes from a result which states that in a generic 2HDM, if at tree level there is a minimum that preserves

[2] To be clear, the only thing that we are changing relative to the SM is the Higgs sector. Everything else remains the same.

the $U(1)_Q$ and CP symmetries, then that minimum is the global one, and any stationary points that break charge conservation or CP are saddle points with more energy [44, 45].

As before, these fields may be expanded around the vacuum state that was chosen. By introducing the fields $\varphi_i^{\pm}$, h_i and a_i ($i = 1, 2$), we write

$$\Phi_1 = \begin{pmatrix} \varphi_1^+ \\ \frac{v_1+h_1+ia_1}{\sqrt{2}} \end{pmatrix}, \quad \Phi_2 = \begin{pmatrix} \varphi_2^+ \\ \frac{v_2+h_2+ia_2}{\sqrt{2}} \end{pmatrix}. \tag{3.8}$$

Once again, the vacuum in Equation 3.7 breaks $SU(2) \times U(1)_Y$ down to $U(1)_Q$, hence, according to the Goldstone theorem, we have three Goldstone bosons and three massive gauge bosons plus a massless one. Since now we have two scalar field doublets instead of just one, there are eight DoF in total thus we will have five massive scalar particles, four more than in the SM. This is the first major consequence of having a second doublet.

Inserting Equation 3.8 in the 2HDM potential of Equation 3.5 and expanding, we find for instance terms that are linear in h_i. There are no terms linear in the fields $\varphi_i^{\pm}$ or a_i, because of charge and CP-conservation. To minimize the potential, we must fulfill the conditions

$$\left.\frac{\partial V_{\text{2HDM}}}{\partial \Phi_1^\dagger}\right|_{\langle\Phi_1\rangle_0,\langle\Phi_2\rangle_0} = 0, \quad \left.\frac{\partial V_{\text{2HDM}}}{\partial \Phi_2^\dagger}\right|_{\langle\Phi_1\rangle_0,\langle\Phi_2\rangle_0} = 0, \tag{3.9}$$

which is equivalent to saying that the linear terms in h_i must vanish. These equations give two minimum conditions:

$$m_{11}^2 = m_{12}^2 \frac{v_2}{v_1} - \frac{1}{2}\lambda_1 v_1^2 - \frac{1}{2}\lambda_{345} v_2^2, \tag{3.10}$$

$$m_{22}^2 = m_{12}^2 \frac{v_1}{v_2} - \frac{1}{2}\lambda_2 v_2^2 - \frac{1}{2}\lambda_{345} v_1^2, \tag{3.11}$$

where $\lambda_{345} = \lambda_3 + \lambda_4 + \lambda_5$.

Looking now at the bilinear terms in the fields, the 2HDM potential containing those terms can be written as

$$\begin{aligned} V_{\text{2HDM}}^{(2)} = &\frac{1}{2}\begin{pmatrix} h_1 & h_2 \end{pmatrix} M_h^2 \begin{pmatrix} h_1 \\ h_2 \end{pmatrix} + \frac{1}{2}\begin{pmatrix} a_1 & a_2 \end{pmatrix} M_a^2 \begin{pmatrix} a_1 \\ a_2 \end{pmatrix} \\ &+ \begin{pmatrix} \varphi_1^+ & \varphi_2^+ \end{pmatrix} M_\varphi^2 \begin{pmatrix} \varphi_1^- \\ \varphi_2^- \end{pmatrix}, \end{aligned} \tag{3.12}$$

where M_h^2, M_a^2 and M_φ^2 are 2×2 squared-mass matrices given by

$$M_h^2 = 2\begin{pmatrix} m_{12}^2 \frac{v_2}{v_1} + \lambda_1 v_1^2 & -m_{12}^2 + \lambda_{345} v_1 v_2 \\ -m_{12}^2 + \lambda_{345} v_1 v_2 & m_{12}^2 \frac{v_1}{v_2} + \lambda_2 v_2^2 \end{pmatrix}, \tag{3.13}$$

$$M_a^2 = 2\left(\frac{m_{12}^2}{v_1 v_2} - \lambda_5\right)\begin{pmatrix} v_2^2 & -v_1 v_2 \\ -v_1 v_2 & v_1^2, \end{pmatrix}, \tag{3.14}$$

$$M_\varphi^2 = \left(\frac{m_{12}^2}{v_1 v_2} - \frac{\lambda_4 + \lambda_5}{2}\right)\begin{pmatrix} v_2^2 & -v_1 v_2 \\ -v_1 v_2 & v_1^2 \end{pmatrix}. \tag{3.15}$$

These matrices are non-diagonal, hence we are not in the basis of the mass eigenstates. To rotate into that basis we will use once again orthogonal matrices. Since we have three different matrices but two of them are proportional to each other, we only need two mixing angles which we will call α and β. The

explicit form of the transformation matrices is

$$R_\alpha = \begin{pmatrix} c_\alpha & -s_\alpha \\ s_\alpha & c_\alpha \end{pmatrix}, \quad R_\beta = \begin{pmatrix} c_\beta & -s_\beta \\ s_\beta & c_\beta \end{pmatrix}, \tag{3.16}$$

where we are using the notation $s_x = \sin x$, $c_x = \cos x$ and $t_x = \tan x$. The diagonal squared-mass matrices are given by

$$D_h^2 = R_\alpha^{\mathrm{T}} M_h^2 R_\alpha, \tag{3.17}$$

$$D_a^2 = R_\beta^{\mathrm{T}} M_a^2 R_\beta, \tag{3.18}$$

$$D_\varphi^2 = R_\beta^{\mathrm{T}} M_\varphi^2 R_\beta, \tag{3.19}$$

and the physical fields are

$$\begin{pmatrix} H \\ h \end{pmatrix} = R_\alpha^T \begin{pmatrix} h_1 \\ h_2 \end{pmatrix}, \tag{3.20}$$

$$\begin{pmatrix} G \\ A \end{pmatrix} = R_\beta^T \begin{pmatrix} a_1 \\ a_2 \end{pmatrix}, \tag{3.21}$$

$$\begin{pmatrix} G^\pm \\ H^\pm \end{pmatrix} = R_\beta^T \begin{pmatrix} \varphi_1^\pm \\ \varphi_2^\pm \end{pmatrix}. \tag{3.22}$$

Then, Equation 3.12 may be rewritten as

$$\begin{aligned} V_{\mathrm{2HDM}}^{(2)} =& \frac{1}{2} \begin{pmatrix} H & h \end{pmatrix} D_h^2 \begin{pmatrix} H \\ h \end{pmatrix} + \frac{1}{2} \begin{pmatrix} G & A \end{pmatrix} D_a^2 \begin{pmatrix} G \\ A \end{pmatrix} \\ &+ \begin{pmatrix} G^+ & H^+ \end{pmatrix} D_\varphi^2 \begin{pmatrix} G^- \\ H^- \end{pmatrix}. \end{aligned} \tag{3.23}$$

The entries of the mass matrices D_h^2, D_a^2 and D_φ^2, which are the squared masses of these physical fields, are given explicitly by

$$m_H^2 = \left[\left(M_h^2\right)_{11} + \left(M_h^2\right)_{22} + \sqrt{\left(\left(M_h^2\right)_{11} - \left(M_h^2\right)_{22}\right)^2 + 4\left(M_h^2\right)_{12}^2} \right], \tag{3.24}$$

$$m_h^2 = \left[\left(M_h^2\right)_{11} + \left(M_h^2\right)_{22} - \sqrt{\left(\left(M_h^2\right)_{11} - \left(M_h^2\right)_{22}\right)^2 + 4\left(M_h^2\right)_{12}^2} \right], \tag{3.25}$$

$$m_G^2 = 0, \tag{3.26}$$

$$m_A^2 = 2v^2 \left(\frac{m_{12}^2}{v_1 v_2} - \lambda_5 \right), \tag{3.27}$$

$$m_{G^\pm}^2 = 0, \tag{3.28}$$

$$m_{H^\pm}^2 = v^2 \left(\frac{m_{12}^2}{v_1 v_2} - \frac{\lambda_4 + \lambda_5}{2} \right), \tag{3.29}$$

where $v^2 = v_1^2 + v_2^2$ with $v_1 = v\cos\beta$ and $v_2 = v\sin\beta$, and $(M_h^2)_{ij}$ $(i,j = 1,2)$ are the entries of the mass matrix M_h^2. As we can see, we have indeed three Goldstone bosons like in the SM, G and $G^\pm$, and five massive scalars. Two of them ($H^\pm$) are charged Higgs bosons, and the remaining three are all neutral, with H and h forming a CP-even pair and A being a CP-odd Higgs. Furthermore, the two angles α and β

are related to the 2HDM potential parameters after the diagonalization through the following expressions

$$\mathrm{t}_\beta = \frac{v_2}{v_1}, \tag{3.30}$$

$$\mathrm{t}_{2\alpha} = \frac{\mathrm{s}_{2\beta}\left(M^2 - \lambda_{345}v^2\right)}{\mathrm{c}_\beta^2\left(M^2 - \lambda_1 v^2\right) - \mathrm{s}_\beta^2\left(M^2 - \lambda_2 v^2\right)}, \tag{3.31}$$

where $M^2 = m_{12}^2/s_\beta c_\beta$ [46].

As for the kinetic-energy terms, since the symmetry of this extended Higgs sector is the same, the covariant derivative in these terms is the one from Equation 2.20. Then, the masses of the gauge bosons are also the same as long as the VEV v is interpreted as the measured value of $v \approx 246$ GeV [12]. The difference from the SM comes from the fact that we now have several massive scalars that couple with the gauge bosons of the SM, giving rise to a richer phenomenology in this sector.

To study the interactions between the Higgs and the gauge bosons it is easier to write the Lagrangian in a different basis called the Higgs basis [47]. The doublets in this basis are obtained if we perform an orthogonal transformation on them parametrized by the angle β introduced before. Denoting $\mathcal{H}_i$ as the Higgs doublets in this basis and with

$$\begin{pmatrix} \mathcal{H}_1 \\ \mathcal{H}_2 \end{pmatrix} = R_\beta^T \begin{pmatrix} \Phi_1 \\ \Phi_2 \end{pmatrix} = \begin{pmatrix} c_\beta & s_\beta \\ -s_\beta & c_\beta \end{pmatrix} \begin{pmatrix} \Phi_1 \\ \Phi_2 \end{pmatrix}, \tag{3.32}$$

we have

$$\mathcal{H}_1 = \begin{pmatrix} G^\pm \\ \frac{1}{\sqrt{2}}\left(v + h_1' + iG\right) \end{pmatrix} \quad \text{and} \quad \mathcal{H}_2 = \begin{pmatrix} H^\pm \\ \frac{1}{\sqrt{2}}\left(h_2' + iA\right) \end{pmatrix}. \tag{3.33}$$

This rotation in the doublets space puts all the Goldstone bosons in the first doublet, just like in the SM, while the physical Higgses are in both doublets, in a way that the separation between them is more evident. Also, it brings all the VEVs to the first doublet.

Looking at the Higgs couplings to gauge bosons relative to the SM, they are

$$g_{hVV} = g_{HVV}^{SM}\sin(\beta - \alpha), \tag{3.34}$$

$$g_{HVV} = g_{HVV}^{SM}\cos(\beta - \alpha), \tag{3.35}$$

$$g_{AVV} = 0, \tag{3.36}$$

where $g_{HZZ}^{SM} = gm_Z/\cos\theta_w$ and $g_{HWW}^{SM} = gm_W$. These trilinear couplings only exist if the doublet has a VEV, which is why g_{AVV} is zero[3]. For the same reason, the CP-even fields interact with gauge bosons only via the unphysical field h_1'. The factors of $\sin(\beta-\alpha)$ and $\cos(\beta-\alpha)$ come from the fact that $h_1' = \cos(\beta-\alpha)H + \sin(\beta-\alpha)h$ (see Figure 3.1). Therefore, Equation 3.3 is verified since $\sum\left(g_{h^{phy}VV}\right)^2 = \left(g_{HVV}^{SM}\right)^2$, where $h^{phy} = \{h, H, A\}$.

In this model (and also in other 2HDMs), it can happen that there is a scalar which resides almost entirely in the first doublet and is very SM-lile, while the remaining neutral Higgs interacts very weakly with gauge boson pairs. This is called alignment in the scalar sector [31]. In this case, there are two

[3] g_{AVV} being zero is actually a consequence of having a CP-conserving potential where A is CP-odd.

limits that can lead to alignment: if $\beta - \alpha \to \pi/2$, then the lightest neutral Higgs[4] corresponds to the experimentally observed 125 GeV Higgs h_{125}, while H decouples from the gauge bosons; if $\beta \approx \alpha$, the heavier scalar H is SM-like, and h does not couple to gauge bosons. Both limits may explain why we still have not observed extra massive scalars, assuming that they exist.

For completeness, the Lagrangian of this sector is given by

$$\mathcal{L}_{\text{scalar2HDM}} = (D_\mu \mathcal{H}_1)^\dagger (D^\mu \mathcal{H}_1) + (D_\mu \mathcal{H}_2)^\dagger (D^\mu \mathcal{H}_2) - V_{\text{2HDM}}. \tag{3.37}$$

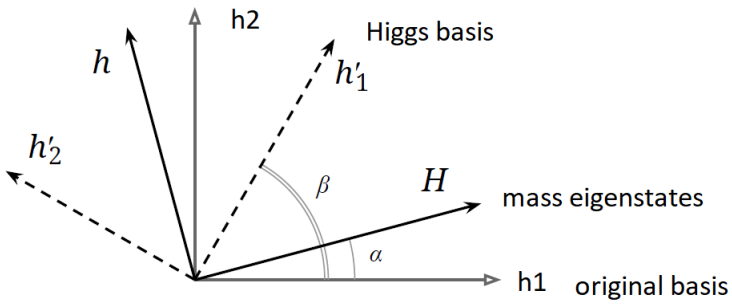

Figure 3.1: Relation between the three bases in the space of CP-even neutral scalar fields. Adapted from [31].

3.3.2 The 2HDM Yukawa sector

The most general Yukawa Lagrangian where both doublets are used is equal to

$$\begin{aligned}\mathcal{L}_{\text{2HDM Yukawa}} = -\sum_{j,k=1}^{3} \Bigg(& \overline{Q_{Lj}} \left[\Phi_1 \Gamma_{1jk} + \Phi_2 \Gamma_{2jk}\right] D_{Rk} \\ & - \overline{Q_{Lj}} \left[\tilde{\Phi}_1 \Delta_{1jk} + \tilde{\Phi}_2 \Delta_{2jk}\right] U_{Rk} \\ & - \overline{L_{Lj}} \left[\Phi_1 M_{l1_{kj}} + \Phi_2 M_{l2_{kj}}\right] l_{Rk} \Bigg) + \text{H.c.}.\end{aligned} \tag{3.38}$$

In the SM, the Yukawa matrices can be diagonalized individually, giving rise to the fermion masses and ruling out FCNCs at tree level. But in a general 2HDM, when we rotate into the basis of the mass eigenstates, we cannot always guarantee that those matrices are simultaneously diagonalizable [31, 42]. For instance, if $\tilde{\Gamma_1}$ and $\tilde{\Gamma_2}$ represent the Γ matrices in the new basis, since we cannot be sure that both of them are diagonal, there is now the possibility of having flavour-changing neutral currents due to terms such as $h_i \, \overline{\hat{d}_L^{phy}} \, \tilde{\Gamma}_i \, \hat{d}_R^{phy}$. This presents a problem because of the very strong experimental constraints on FCNCs. Fortunately, there are mechanisms which suppress FCNCs at tree level - they are allowed but kept under control - and those which completely forbid them, which can be achieved naturally, i.e., without the need of fine-tuning the parameters of the theory, by imposing discrete or continuous symmetries [31]. In fact, the purpose of the $\mathbb{Z}_2$ symmetry imposed in the beginning was precisely to avoid FCNCs in the Yukawa sector.

[4] By convention, h is the lightest of the neutral Higgses.

In this thesis, we restrict ourselves to models which prohibit FCNCs at tree level. This symmetry-protected Natural Flavour Conservation (NFC) can be implemented through four independent types of 2HDM Yukawa sectors [31], where we extend the $\mathbb{Z}_2$ symmetry to the fermionic fields:

- Type I: all fermions couple exclusively to Φ_2.
- Type II: the down-type fermions D_R and l_R couple to Φ_1 while the up-type quarks couple to Φ_2.
- Lepton-specific or Type X: the quarks couple to Φ_2 and the leptons couple to Φ_1.
- Flipped or Type Y: similar to type X but now we have Φ_1 coupling to D_R instead of l_R.

These 4 types are represented schematically in Table 3.1 [5]. In Table 3.2, we show the Yukawa couplings for the neutral Higgs bosons of the CP-conserving 2HDM.

Table 3.1: Four Yukawa types for 2HDMs with Natural Flavour Conservation. The signs shown for the fermionic fields represent how they change under the $\mathbb{Z}_2$ symmetry $\Phi_1 \xrightarrow{\mathbb{Z}_2} \Phi_1$ and $\Phi_2 \xrightarrow{\mathbb{Z}_2} -\Phi_2$.

Model	U_R	D_R	l_R	Q_L	U_R	D_R	L_L	l_R
Type I	Φ_2	Φ_2	Φ_2	+	-	-	+	-
Type II	Φ_2	Φ_1	Φ_1	+	-	+	+	+
Lepton-specific	Φ_2	Φ_2	Φ_1	+	-	-	+	+
Flipped	Φ_2	Φ_1	Φ_2	+	-	+	+	-

Table 3.2: Neutral Higgses couplings to up-type quarks ($g_{h/H/Au\bar{u}}$), down-type quarks ($g_{h/H/Ad\bar{d}}$), and leptons ($g_{h/H/A\ell\bar{\ell}}$), in the different Yukawa types for the CP-conserving 2HDM. The Yukawa Lagrangian with the neutral Higgs bosons is: $\mathcal{L}^{\text{neutrals}}_{\text{2HDM Yukawa}} = -\sum_{f=u,d,\ell} g^{SM}_{Hf\bar{f}} \left(g_{hf\bar{f}} \bar{f} f h + g_{Hf\bar{f}} \bar{f} f H - i g_{Af\bar{f}} \bar{f} \gamma_5 f A \right)$, with $g^{SM}_{Hf\bar{f}} = \frac{m_f}{v}$. These couplings, together with the ones for the gauge bosons, verify Equation 3.4.

Model	$g_{hu\bar{u}}$	$g_{hd\bar{d}}$	$g_{h\ell\bar{\ell}}$	$g_{Hu\bar{u}}$	$g_{Hd\bar{d}}$	$g_{H\ell\bar{\ell}}$	$g_{Au\bar{u}}$	$g_{Ad\bar{d}}$	$g_{A\ell\bar{\ell}}$
Type I	c_α/s_β	c_α/s_β	c_α/s_β	s_α/s_β	s_α/s_β	s_α/s_β	$1/t_\beta$	$-1/t_\beta$	$-1/t_\beta$
Type II	c_α/s_β	$-s_\alpha/c_\beta$	$-s_\alpha/c_\beta$	s_α/s_β	c_α/c_β	c_α/c_β	$1/t_\beta$	t_β	t_β
Lepton-Specific	c_α/s_β	c_α/s_β	$-s_\alpha/c_\beta$	s_α/s_β	s_α/s_β	c_α/c_β	$1/t_\beta$	$-1/t_\beta$	t_β
Flipped	c_α/s_β	$-s_\alpha/c_\beta$	c_α/s_β	s_α/s_β	c_α/c_β	s_α/s_β	$1/t_\beta$	t_β	$-1/t_\beta$

3.4 The C2HDM

The C2HDM is one of the simplest scalar sector extensions of the SM to include new sources of CP-violation. Due to its simplicity, this model has been used as a benchmark to search for CP-violation and to probe the CP quantum numbers of both the discovered Higgs and any other yet undiscovered scalar at the LHC. It has been the subject of many studies [19, 49–52].

To construct this model, we use the potential from Equation 3.5, but now both m^2_{12} and λ_5 are complex parameters - due to the hermiticity of the potential, only these two parameters can be non-real [51]. Then,

[5] There is a class of models where the fermions can couple to both doublets since their Yukawa matrices are proportional to each other. Then, both matrices can be individually diagonalized, preventing FCNCs. They are called the Aligned Two-Higgs-Doublet Models (A2HDMs) [48], and they are non-renormalizable models.

we have

$$\begin{aligned} V =& m_{11}^2 \left|\Phi_1\right|^2 + m_{22}^2 \left|\Phi_2\right|^2 - \left(m_{12}^2 \Phi_1^\dagger \Phi_2 + \text{H.c.}\right) + \frac{\lambda_1}{2}\left(\Phi_1^\dagger \Phi_1\right)^2 + \frac{\lambda_2}{2}\left(\Phi_2^\dagger \Phi_2\right)^2 \\ &+ \lambda_3 \left(\Phi_1^\dagger \Phi_1\right)\left(\Phi_2^\dagger \Phi_2\right) + \lambda_4 \left(\Phi_1^\dagger \Phi_2\right)\left(\Phi_2^\dagger \Phi_1\right) + \left[\frac{\lambda_5}{2}\left(\Phi_1^\dagger \Phi_2\right)^2 + H.c.\right]. \end{aligned} \tag{3.39}$$

In the C2HDM the CP-violation is explicit and there is only one independent CP-violating phase. Expanding the doublets as in Equation 3.8, the minimum conditions are

$$m_{11}^2 v_1 + \frac{\lambda_1}{2} v_1^3 + \frac{\hat{\lambda}_{345}}{2} v_1 v_2^2 = \text{Re}\left(m_{12}^2\right) v_2, \tag{3.40}$$

$$m_{22}^2 v_2 + \frac{\lambda_2}{2} v_2^3 + \frac{\hat{\lambda}_{345}}{2} v_1^2 v_2 = \text{Re}\left(m_{12}^2\right) v_1, \tag{3.41}$$

$$2\,\text{Im}\left(m_{12}^2\right) = v_1 v_2\,\text{Im}\left(\lambda_5\right), \tag{3.42}$$

where $\hat{\lambda}_{345} = \lambda_3 + \lambda_4 + \text{Re}(\lambda_5)$. Parametrizing m_{12}^2 and λ_5 as $m_{12}^2 = |m_{12}^2| e^{i\,\theta(m_{12}^2)}$ and $\lambda_5 = |\lambda_5| e^{i\,\theta(\lambda_5)}$ and choosing the vacuum expectation values to be real, together with the condition $\theta(\lambda_5) \neq 2\theta(m_{12}^2)$, makes it impossible to remove both CP-violating phases simultaneously [19].

As a result of having complex parameters in the potential, the Higgs spectrum will be modified. We still have two charged scalars $H^\pm$, but the neutral Higgses H_i $(i = 1, 2, 3)$ are now a mixture between the fields h_j and a_j $(j = 1, 2)$ with no definite CP quantum numbers given by the rotation

$$\begin{pmatrix} H_1 \\ H_2 \\ H_3 \end{pmatrix} = R \begin{pmatrix} h_1 \\ h_2 \\ a_3 \end{pmatrix}, \tag{3.43}$$

where $a_3 = -s_\beta a_1 + c_\beta a_2$. The squared-mass matrix of the neutral scalar states h_1, h_2 and a_3, M^2_{neutrals}, is diagonalised via

$$R M^2_{\text{neutrals}} R^T = \text{diag}\left(m_{H_1}^2, m_{H_2}^2, m_{H_3}^2\right), \tag{3.44}$$

with R parametrized as [51]

$$R = \begin{pmatrix} c_1 c_2 & s_1 c_2 & s_2 \\ -\left(c_1 s_2 s_3 + s_1 c_3\right) & c_1 c_3 - s_1 s_2 s_3 & c_2 s_3 \\ -c_1 s_2 c_3 + s_1 s_3 & -\left(c_1 s_3 + s_1 s_2 c_3\right) & c_2 c_3 \end{pmatrix}, \tag{3.45}$$

where $s_i = \sin\alpha_i$, $c_i = \cos\alpha_i$, and $-\pi/2 \leq \alpha_i \leq \pi/2$ $(i = 1, 2, 3)$. By convention, $m_{H_1} \leq m_{H_2} \leq m_{H_3}$.

The full set of interactions between the Higgs bosons and the remaining SM fields can be found in [52]. The Yukawa interactions found in Table 3.3 are of particular interest since they differ in structure from the SM. Now, besides the usual CP-even coupling component, there is also a CP-odd component that did not exist in the SM. If this structure is found in the Yukawa couplings, not only would we be in the presence of new physics, but also we would have new sources of CP-violation. The existence of more general Yukawa couplings in BSM theories can be probed directly either in the production or decay of Higgs bosons at the LHC [19]. This will be the main topic considered in the next chapter.

Table 3.3: Neutral Higgses couplings to fermions in the C2HDM. The Yukawa Lagragian has the form $\mathcal{L}^{\text{neutrals}}_{\text{C2HDM Yukawa}} = -\sum_{i=1}^{3}\sum_{f=u,d,\ell} g^{SM}_{Hf\bar{f}}\,\overline{f}\left[a_{H_i f\bar{f}} + i\,b_{H_i f\bar{f}}\,\gamma_5\right] f\,H_i$, where $a_{H_i f\bar{f}}$ and $b_{H_i f\bar{f}}$ are the coefficients of the CP-even and CP-odd parts of the couplings shown in this table, respectively. Table from [19].

	u-type	d-type	leptons
Type I	$\frac{R_{i2}}{s_\beta} - i\frac{R_{i3}}{t_\beta}\gamma_5$	$\frac{R_{i2}}{s_\beta} + i\frac{R_{i3}}{t_\beta}\gamma_5$	$\frac{R_{i2}}{s_\beta} + i\frac{R_{i3}}{t_\beta}\gamma_5$
Type II	$\frac{R_{i2}}{s_\beta} - i\frac{R_{i3}}{t_\beta}\gamma_5$	$\frac{R_{i1}}{c_\beta} - it_\beta R_{i3}\gamma_5$	$\frac{R_{i1}}{c_\beta} - it_\beta R_{i3}\gamma_5$
Lepton-Specific	$\frac{R_{i2}}{s_\beta} - i\frac{R_{i3}}{t_\beta}\gamma_5$	$\frac{R_{i2}}{s_\beta} + i\frac{R_{i3}}{t_\beta}\gamma_5$	$\frac{R_{i1}}{c_\beta} - it_\beta R_{i3}\gamma_5$
Flipped	$\frac{R_{i2}}{s_\beta} - i\frac{R_{i3}}{t_\beta}\gamma_5$	$\frac{R_{i1}}{c_\beta} - it_\beta R_{i3}\gamma_5$	$\frac{R_{i2}}{s_\beta} + i\frac{R_{i3}}{t_\beta}\gamma_5$

Chapter 4

Probing the CP nature of a scalar produced at the LHC

4.1 Introduction

A common strategy to determine the Higgs CP is to look for observables sensitive to its CP that can be measured at the LHC, such as angular correlations in Higgs decays or in Higgs production channels. Since only the CP–even component of the hVV couplings is projected out - the VV couplings with a pure CP-odd state are zero at tree level and higher order corrections are tiny - the couplings to fermions may provide a better way to probe the Higgs CP nature. The reason is that both CP-even and CP-odd components can be non-zero in the case of fermions[1] [53]. Nevertheless, the VV couplings are still useful. The pure pseudoscalar hypothesis for the discovered scalar has already been ruled out at 99.98 $\%$ Confidence Level, which was achieved by an analysis of the γ, Z and W interactions with the Higgs [14, 15]. Even though so far all measurements of the properties of the discovered Higgs are compatible with the SM [14–16], a precise measurement of its Yukawa couplings is still lacking. Therefore, mixing between a CP-even and CP-odd component is still allowed by experimental data [54].

Within the SM, there are four main production modes of the Higgs at the LHC: Gluon Fusion (GGF), Vector-Boson Fusion (VBF), Higgs production in association with a W/Z boson (Vh), and Higgs production in association with a $t\bar{t}$ pair. Representative diagrams for these processes are shown in Figure 4.1. The gluon-fusion production mode has the largest cross-section at the LHC, and the dominant contribution to this process in the SM comes from a top loop [55]. On the contrary, $t\bar{t}h$ production has the smallest cross-section (see Figure 4.2). Also, $t\bar{t}h$ has a complicated final state, with the top decaying mostly into a bottom and a W, which in turn may decay either hadronically or leptonically, as well as large backgrounds that complicate its study. Despite those reasons, this is the only process[2] where we can measure directly the couplings between the top and the Higgs [55]. This measurement may allow the determination of the Higgs CP nature and the observation of CP-violating effects. Besides, since the top and Higgs coupling is the largest of all Higgs to fermion couplings, this channel will have large production rates relative to the other fermions, making it the most direct probe that we can use.

[1] Since we are only sensitive to CP-even components in hVV couplings (apart from constants that may come from CP-odd components), this interaction would only change by a multiplicative factor in the case of a Higgs with both CP components. On the other hand, we are sensitive to both CP-states in the case of fermions. That may allow to determine CP by searching for differences in differential distributions for CP-sensitive variables, instead of just looking for differences in the number of events expected.

[2] Apart from the single top and Higgs associated production, which will not be discussed in this work.

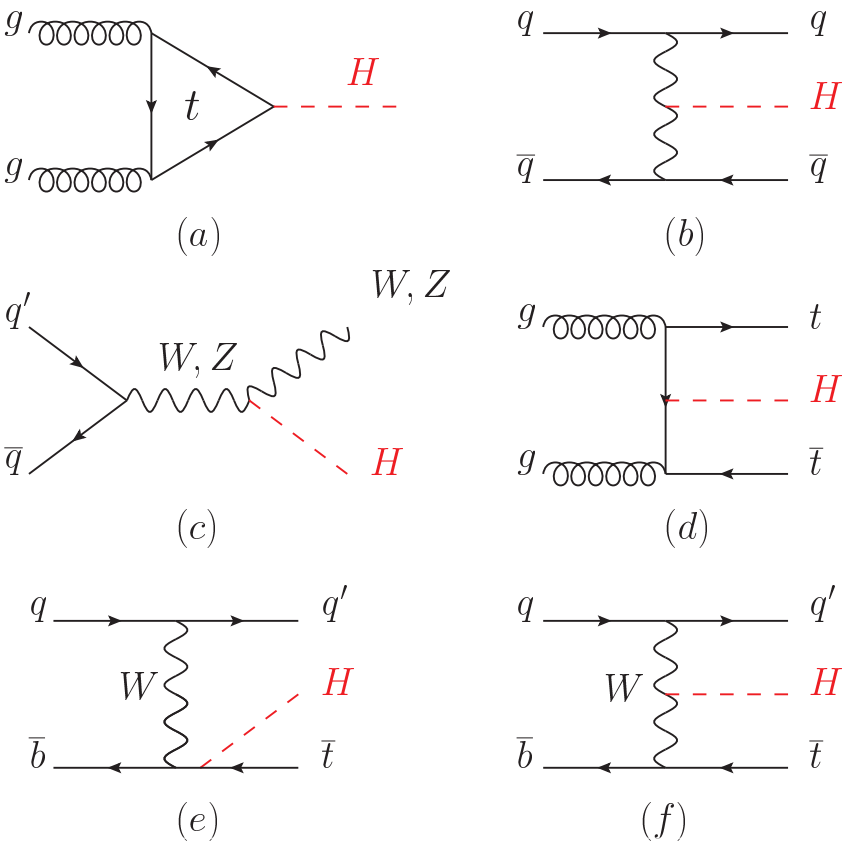

Figure 4.1: Main Leading Order (LO) Feynman diagrams in Higgs production. (a) GGF; (b) VBF; (c) Vh; (d) $t\bar{t}h$; (e-f) single top and Higgs associated production. Image from [12].

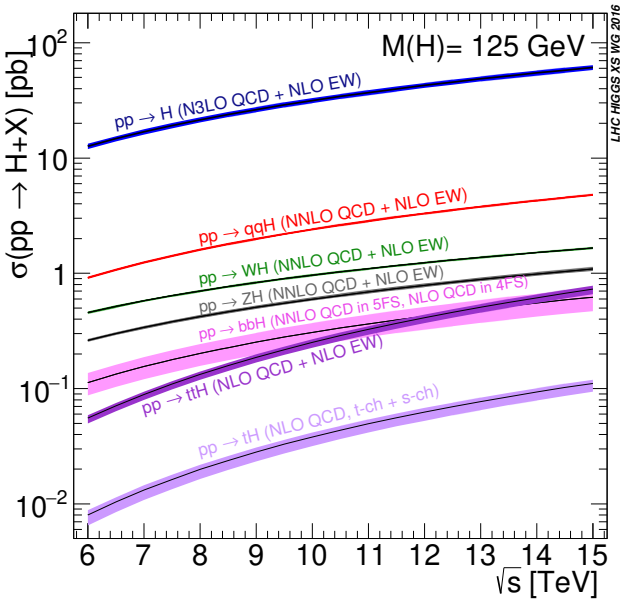

Figure 4.2: SM Higgs boson production cross-sections as a function of the Center of Mass energy, for proton-proton (pp) collisions. The VBF process is represented as qqH. Image from [12].

In spite of its rarity, the observation of the $t\bar{t}h$ process was recently announced independently by the CMS and the ATLAS collaborations [56, 57]. Several discriminating observables to probe the vertex

of this interaction have been suggested throughout the years by many authors [55, 58–61], including kinematic quantities of the $t\bar{t}h$ system and angular distributions between the decay products of the top and anti-top.

Fewer studies exist for the bottom quark, since its production rate relative to the top's is expected to be smaller in the SM. The studies that exist have shown that it is difficult to measure anomalous couplings in the $b\bar{b}h$ process [58, 62, 63]. Nevertheless, in the hope of reaching different conclusions or, in a worst case scenario, confirm the ones already stated, we will examine the possibility of determining the structure of the bottom quark Yukawa couplings. Afterwards, we will consider the situation of an hypothetical scalar of arbitrary mass produced at the LHC with a $t\bar{t}$ pair and see how that affects the sensitivity to its CP nature.

4.2 Simulations of $b\bar{b}h$ events at parton level

The Higgs couplings to fermions are parametrized in a model-independent way through the effective Lagrangian

$$\mathcal{L}_{hf\bar{f}} = -\sum_f g^{SM}_{Hf\bar{f}}\,\kappa_{hf\bar{f}}\,\bar{f}\,(\cos\alpha + i\,\sin\alpha\,\gamma_5)\,fh, \tag{4.1}$$

where $g^{SM}_{Hf\bar{f}} = m_f/v$ is the SM Yukawa coupling and $\kappa_{hf\bar{f}}$ represents the total coupling strength relative to the SM. In this work we set $\kappa_{hf\bar{f}} = 1$, unless otherwise stated. The CP phase is determined by α: if $\cos\alpha = 1$, we have a pure CP-even Higgs boson ($h = H$); if $\cos\alpha = 0$, the interaction is purely CP-odd ($h = A$). The interaction with the SM Higgs is recovered by setting $\kappa_{hf\bar{f}} = 1$, $\cos\alpha = 1$ and the mass of h, m_h, to 125 GeV. In our analysis, only the CP-even and CP-odd cases are considered.

The simulations of proton-proton collisions at the LHC with a Center of Mass energy of 13 TeV were performed at parton level[3] using the Monte Carlo (MC) event generator MadGraph5_aMC@NLO [64] with Next-to-Leading Order (NLO) corrections in QCD, for $b\bar{b}h$ production. To account both CP-even and CP-odd coupling components the HC_NLO_X0 model [65] was used. The masses of the bottom and top quarks were set to 4.7 GeV and 173 GeV, respectively. The mass of the scalar h is indicated in the text or in the figures[4]. Other details that depend on the topology that we chose will be discussed further on. Every result related to $b\bar{b}h$ production is shown at parton level only, and no background events were generated for this case. Since for $t\bar{t}h$ production we perform an event reconstruction and we generate background processes as well, that production process will be discussed separately further on.

[3]Parton or generator level refers to the hard-scattering part of a collision process and its first subsequent decay products, before any showering/hadronization occurs. By showering we are refering to effects that lead to the emission of additional QCD radiation before hadronization.

[4]Throughout our analysis, h will represent different particles which may have a different mass and CP, but h is always a scalar boson.

4.3 CP-violation in $b\bar{b}h$ production

We begin our discussion of $pp \to b\bar{b}h$ by choosing the variables that best suit our goal. We have decided to use the observables introduced in the literature [58, 59], with the prospect that these may also show sensitivity to the bottom Yukawa interactions.

In particular, we have considered the Gunion-He variable b_4, defined in Equation 4.2

$$b_4 = \frac{p_b^z p_{\bar{b}}^z}{|\vec{p}_b||\vec{p}_{\bar{b}}|}, \tag{4.2}$$

where $\vec{p}_b$ ($\vec{p}_{\bar{b}}$) is the b ($\bar{b}$) three-momentum and p_b^z ($p_{\bar{b}}^z$) its z component. The z-direction corresponds to the beam line. Also, we used several angular observables denoted as θ_Y^X, which are defined as the angle between the direction of flight of the Y system, measured in the rest frame of X, with respect to the direction of X in the rest frame of its mother. Essentially, these are three-dimensional angles between the momenta of the decay products of $b\bar{b}h$ final states. To visualize them we can imagine $b\bar{b}h$ events from the point of view of a decay chain of successive one-to-two processes. The first decay starts from the $b\bar{b}h$ Center of Mass system, labeled 123, and its decay products will then follow successive decays until all intermediate particles have decayed. The successive two-body decays that 123 goes through are: 123 $\to$ 1 + 23, 23 $\to$ 2 + 3 and 3 $\to$ 4 + 5. Figure 4.3 shows the angles that we can measure. Three families of further observables can be constructed: $f(\theta_1^{123})g(\theta_4^3)$, $f(\theta_1^{123})g(\theta_3^{23})$ and $f(\theta_3^{23})g(\theta_4^3)$, where f, g are simple trigonometric functions. The 123 system momentum direction is measured with respect to the Laboratory (LAB) frame. Particles 1 to 3 can be the b, $\bar{b}$ or h, without repetition. Particle 4 can be any of the products of the decay of the b-quarks and the Higgs boson.

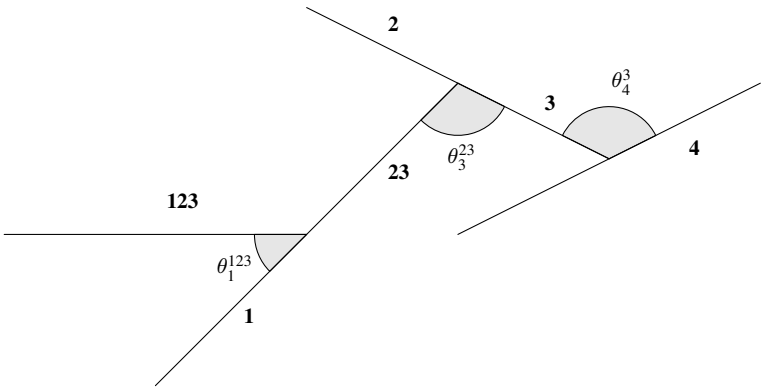

Figure 4.3: Schematic representation of the $b\bar{b}h$ decay chain and angles between the different systems and decay products. Image from [66].

The computation of these angles requires several Lorentz boosts in order to change between reference frames. Since the generators of the Lorentz group do not commute, the result of boosting particle 4 directly from the Laboratory frame into the CM frame of particle 3 or sequentially through all intermediate CM systems is different, thus both approaches need to be considered. To give some examples for the sake of clarity, $\theta_b^{b\bar{b}h}$ would be the angle between the momentum direction of the b-quark, in the $b\bar{b}h$ CM system, and the $b\bar{b}h$ direction, in the LAB frame. $\theta_{\tau^-}^h$ is the angle between the momentum of the τ^-, in the Higgs boson CM frame (with a direct boost from the τ^- momentum in the LAB frame into the Higgs

CM frame), and the Higgs momentum in the bh (or $\bar{b}h$) CM frame. $\theta^h_{\tau^-}$ (sequential boost, labeled seq) is the angle defined as the previous one but now the τ^- momentum is boosted through all intermediate CM systems ($b\bar{b}h$, bh or $\bar{b}h$ and h). Finally, θ^{bh}_h would be the angle between the momentum of the Higgs, in the bh CM system, and the bh direction in the $b\bar{b}h$ CM frame. Since angles are defined by reference systems we can permute the different particles through the positions of those systems. This increases even more the number of angles that we can calculate.

In Figure 4.4, we show a few normalized distributions of the observables that were considered, each of them at generator level with the cuts described previously. We see no significant difference between the $\cos\alpha = 1$ (blue solid line) and $\cos\alpha = 0$ (red solid line) cases, suggesting that it is not possible to distinguish between these two situations. We have verified this for other kinematic distributions, and the results are the same.

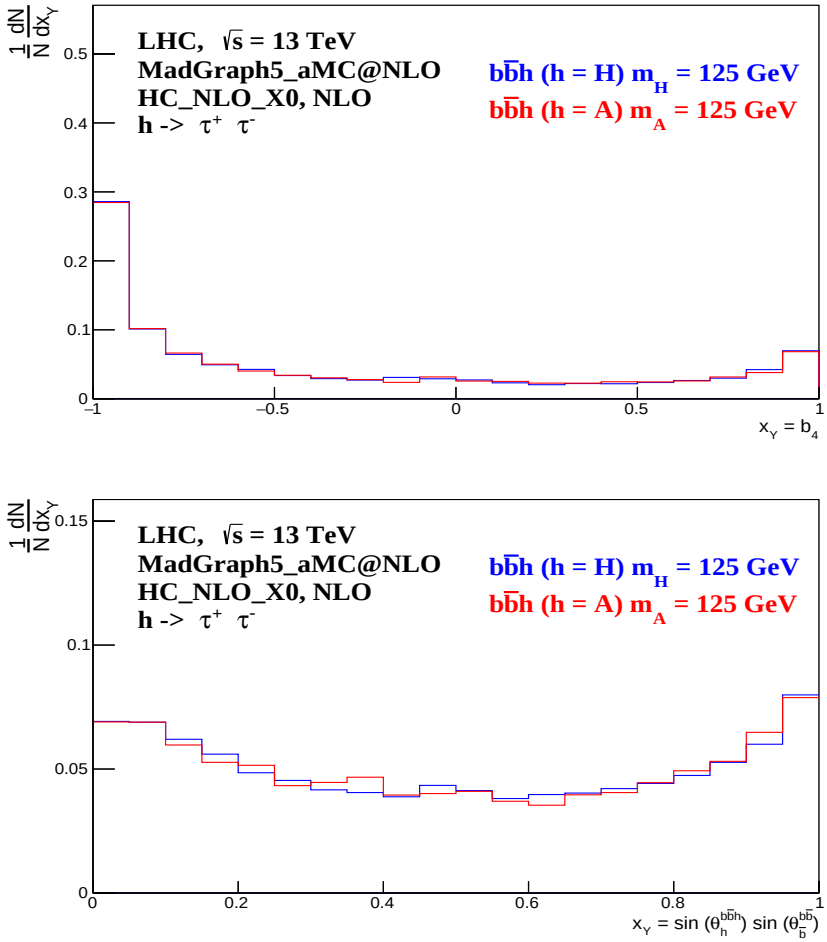

Figure 4.4: Parton level b_4 and θ^X_Y distributions at NLO, normalized to unity. The red lines correspond to the pseudoscalar signal and the blue lines to the scalar SM-like signal. Spin correlation effects were preserved by using MadSpin [67] to perform the decay of the Higgs bosons to taus ($h \to \tau^+\tau^-$).

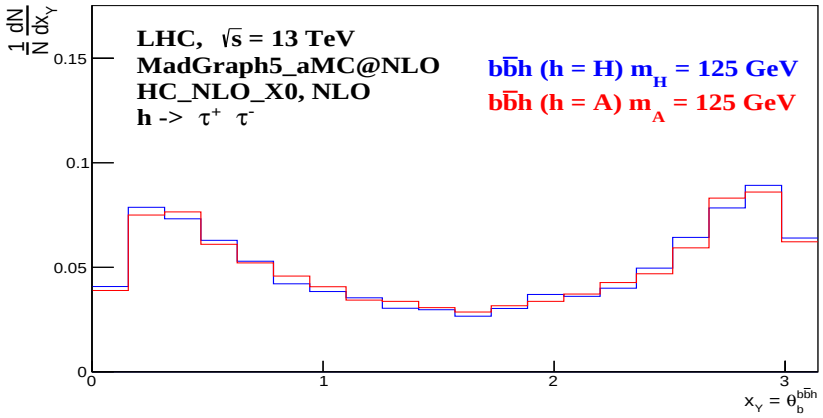

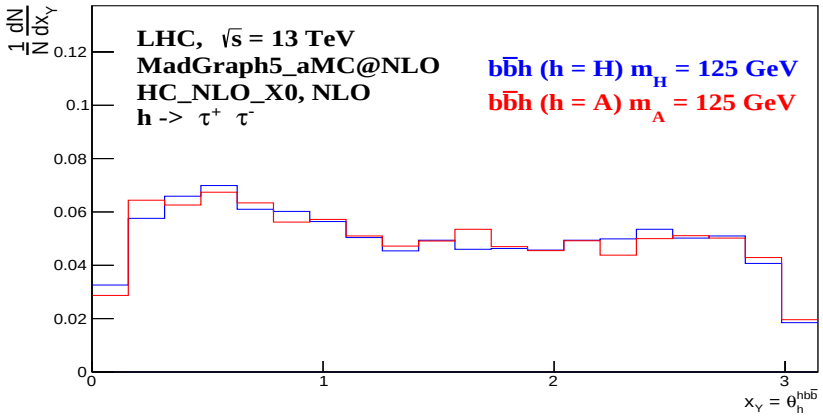

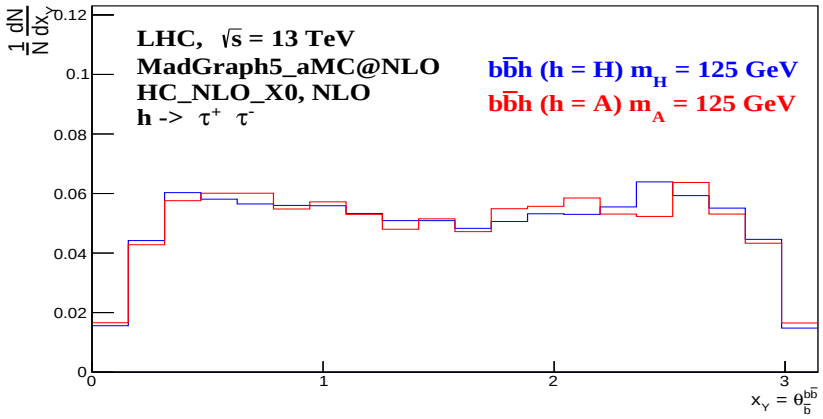

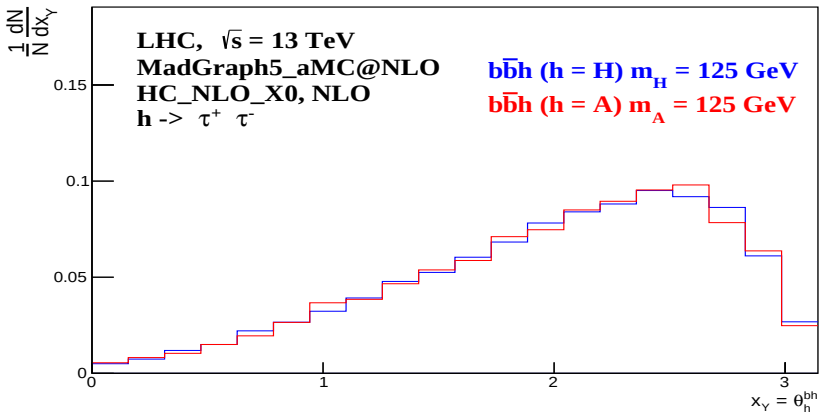

Figure 4.4: Continued.

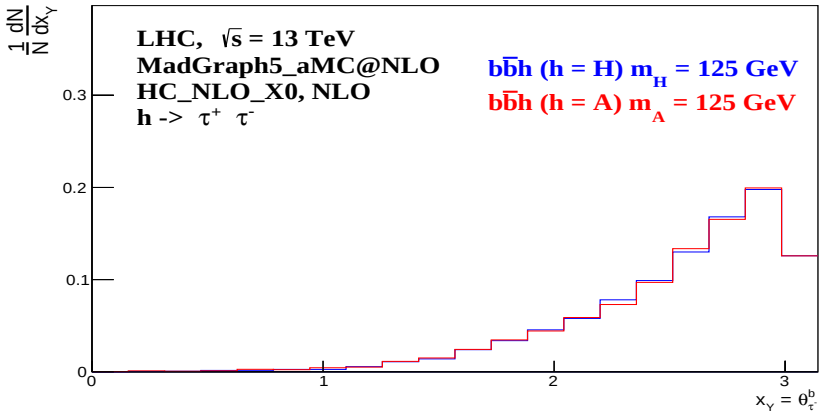

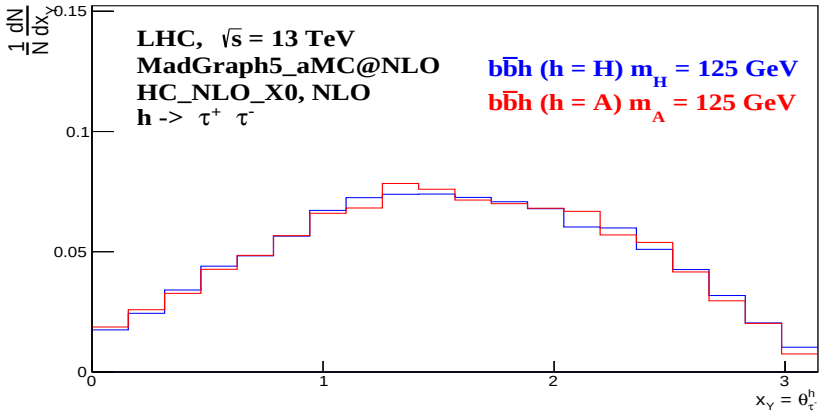

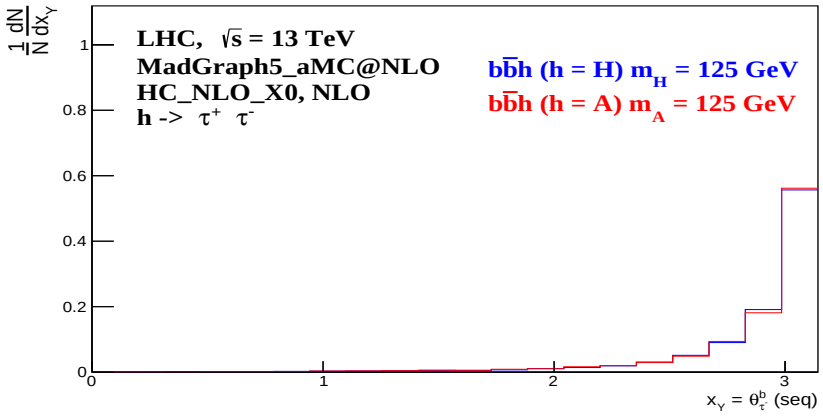

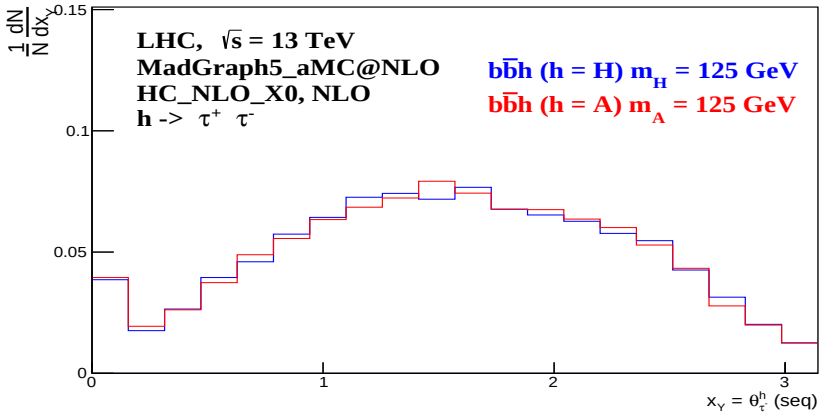

Figure 4.4: Continued.

In order to study how the differences between a CP-even and a CP-odd state change as a function of the quark mass, we have set the mass of the bottom equal to the mass of the top quark, which is similar to generating $t\bar{t}h$ processes, and we have compared two distributions, b_4 and $\sin(\theta_h^{b\bar{b}h})\sin(\theta_{\bar{b}}^{b\bar{b}})$, with the similar distributions for $t\bar{t}h$ (b_4 and $\sin(\theta_h^{t\bar{t}h})\sin(\theta_{\bar{t}}^{t\bar{t}})$) that are in [54]. This is shown in Figure 4.5.

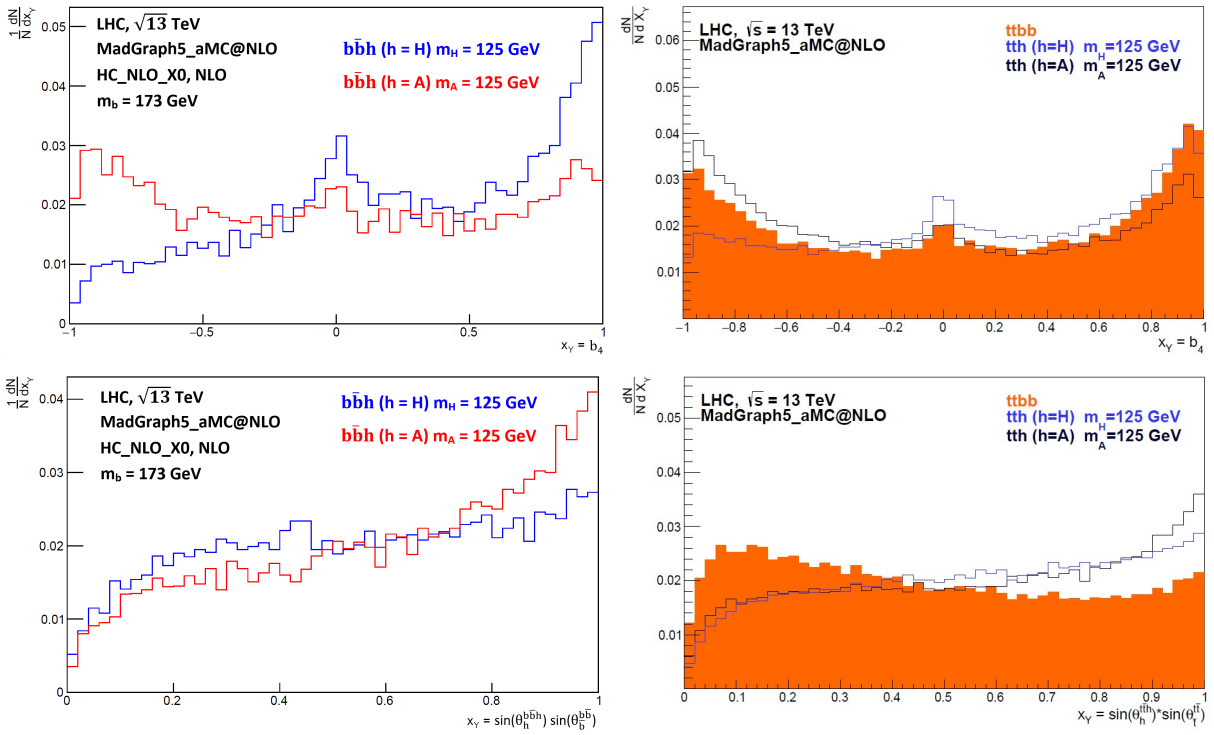

Figure 4.5: Left: distributions b_4 (top) and $\sin(\theta_h^{b\bar{b}h})\sin(\theta_{\bar{b}}^{b\bar{b}})$ (bottom) for $b\bar{b}h$ with $m_b = 173$ GeV. Right: distributions b_4 (top) and $\sin(\theta_h^{t\bar{t}h})\sin(\theta_{\bar{t}}^{t\bar{t}})$ (bottom) for $t\bar{t}h$ after event selection and reconstruction. For more details see [54].

There are two observations that are important to make about these results: first, the histograms on the left and right panels are similar, which shows that the signal was simulated in a consistent way relative to previous studies. Second, the differences observed are sensitive to the mass of the quark that is produced alongside the scalar particle. This is in agreement with the observations in [58], where it was proven by an explicit evaluation of the $f\bar{f}h$ production from the gg or $q\bar{q}$ initial states that the differences between the CP-even and CP-odd components are proportional to m_f^2 and are only significant when m_f is of the same order of magnitude as m_h. This is why only the top can be used to probe the vertex of this process.

If the Higgs mass also affects the observation of different CP-states in this process, then it is only natural to ask whether we can see any significant difference of asymmetries when its mass is smaller. With this in mind, we decided to look into $b\bar{b}$ production with a new scalar of different mass. In Figure 4.6 we show distributions for several Higgs masses which go from $m_h = 10$ GeV to $m_h = 100$ GeV, but the lack of differences is still notorious, even for very small Higgs masses. A few other observables were considered but to no avail.

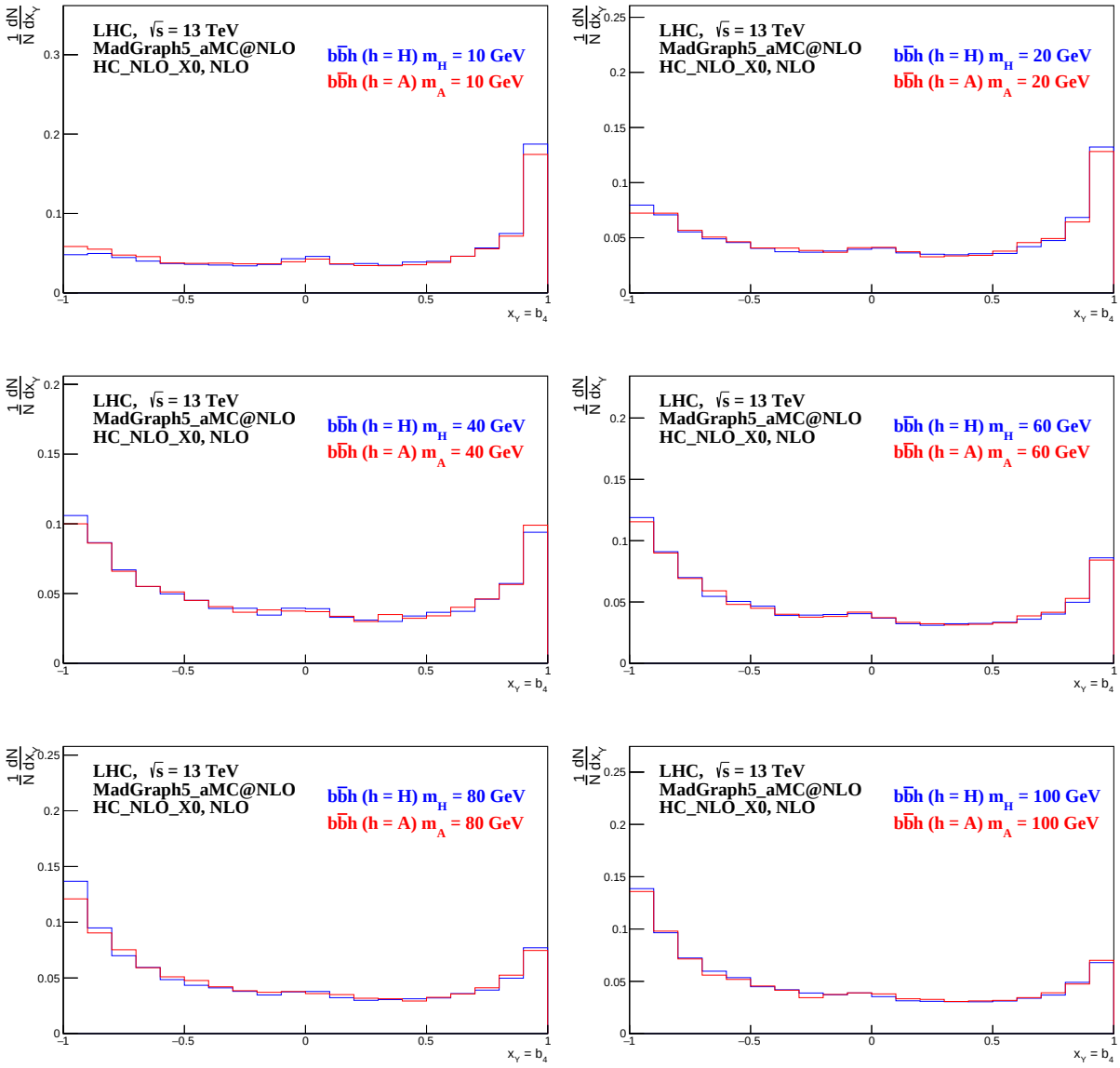

Figure 4.6: Generator level b_4 distributions for different Higgs masses.

In a last attempt to probe the couplings between the bottom quark and the Higgs, we have considered the only other process where the vertex of this interaction can be studied directly: the single bottom and Higgs associated production (bh). This process was generated in MadGraph5_aMC@NLO at LO. The relevant tree level Feynman diagrams are shown in Figure 4.7. This time three b_4-like distributions were used: b_4(h,b), b_4(j,b) and b_4(j,h), where j represents a gluon or any quark lighter than the b-quark. The b_4(i,k) notation corresponds to

$$b_4(i,k) = \frac{p_i^z p_k^z}{|\vec{p_i}||\vec{p_k}|}. \tag{4.3}$$

The results are shown in Figure 4.8, from which we again conclude that both CP-even and CP-odd signals behave in a similar way.

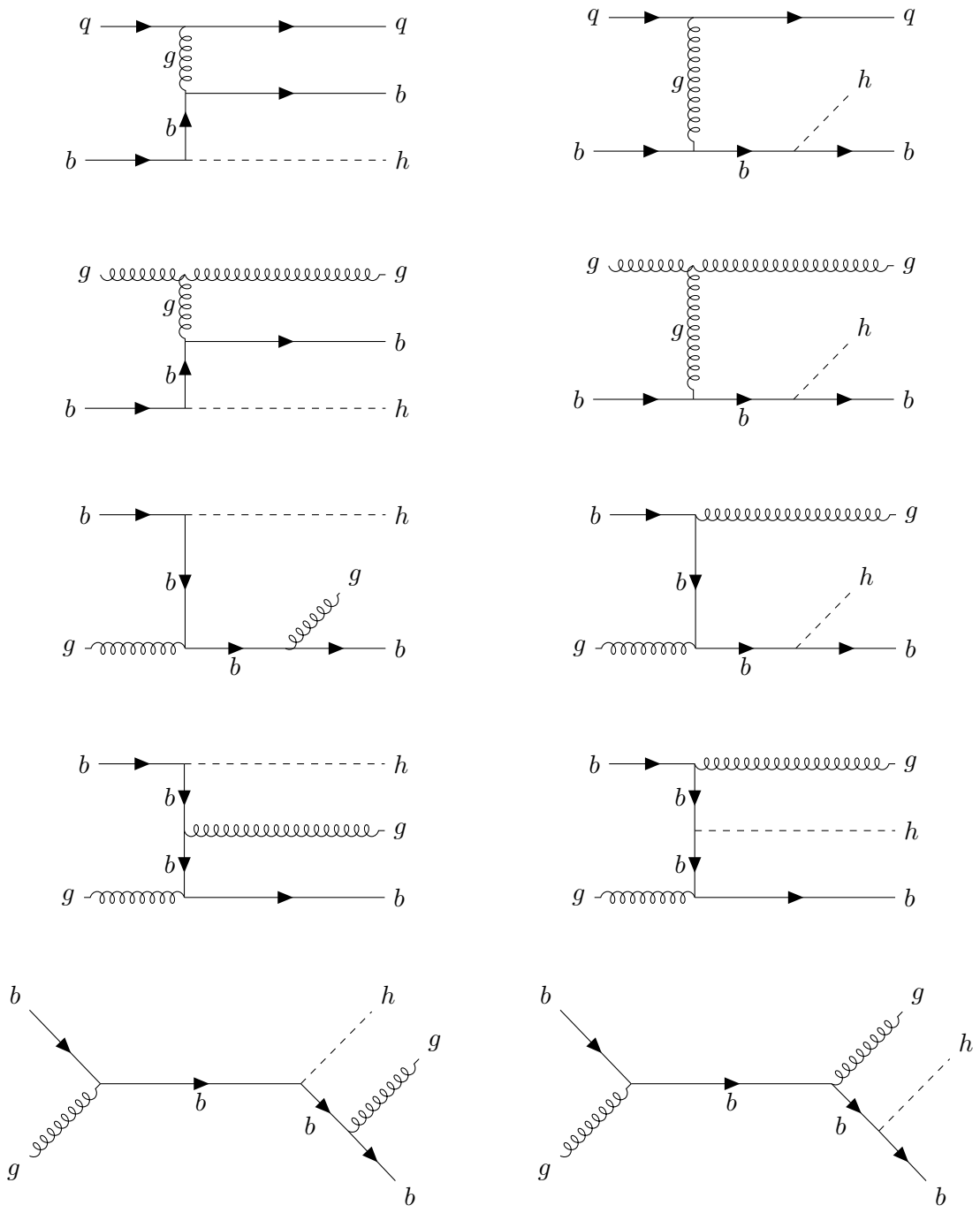

Figure 4.7: Tree level Feynman diagrams for the $gb \to gbh$ and $qb \to qbh$ processes at LO. Diagrams where the production is mediated by a Z boson or a photon were not considered.

Even though the results in this section are in general largely negative, we have managed to confirm previous findings and to show the incapability of CP probes in these channels, using these observables, even for very light Higgses. In the following sections we consider again a scalar of arbitrary mass but this time produced alongside a top pair, which as we show next is a much more interesting scenario.

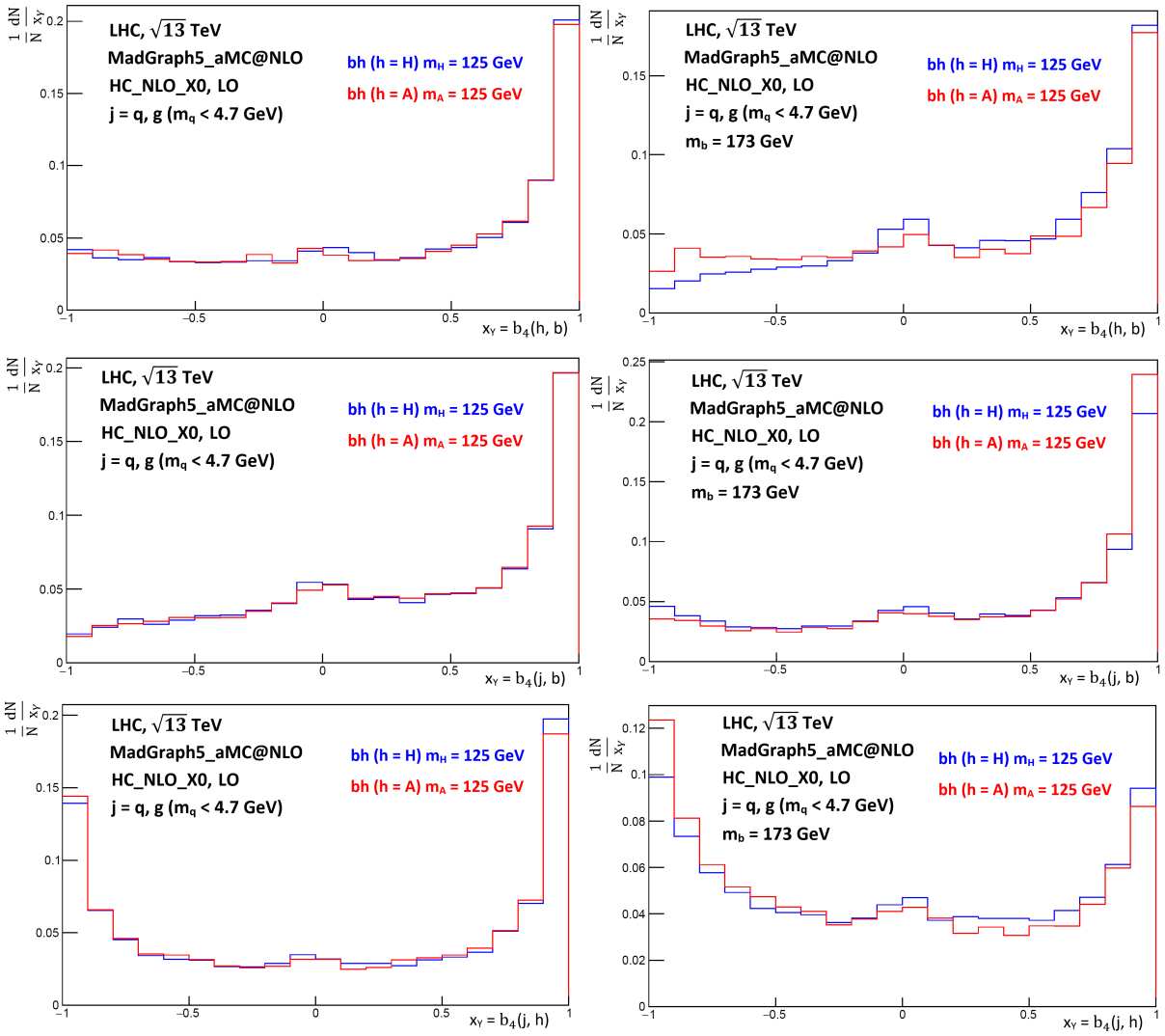

Figure 4.8: Distributions for the single bottom and Higgs associated production at parton level. On the right panels we show the same distributions with $m_b = 173$ GeV, showing that changing the mass of the quark in this case has very little influence in the results.

4.4 Generation of $t\bar{t}h$ and background events

As it was mentioned, previous works [55, 58–60] proposed several angular variables, not only to increase the sensitivity in discriminating signals from irreducible backgrounds, but also as a means to probe the CP nature of the Yukawa coupling in $t\bar{t}h$ production at the LHC. The results in [59, 60] showed that we can define a minimal set of variables to obtain the best possible sensitivity to achieve both goals. While these studies assumed a mass of 125 GeV for the Higgs boson, in this thesis we extend their use to a wider mass range, from 40 GeV to 500 GeV.

Since $t\bar{t}$ events will be the main background for $t\bar{t}h$ signal events, it is important to know the decay chain of the top quark (top production at the LHC occurs through the processes in appendix D). Due to its large decay width - $\Gamma_t = 1.35$ GeV [12] - and, consequently, short lifetime ($\tau_t \approx 0.5 \times 10^{-24}$ s), the top decays much before hadronization. This decay is mostly to a Wb pair, because $|V_{tb}| \gg |V_{t,d}|, |V_{t,s}|$ (see

appendix C) and $m_t > m_W + m_b$. Top quark pair decay can be separated into three classes [12]:

$$(a)\ t\bar{t} \to W^+bW^-\bar{b} \to q\bar{q}'bq''\bar{q}'''\bar{b}, \qquad (45.7\%) \tag{4.4}$$

$$(b)\ t\bar{t} \to W^+bW^-\bar{b} \to q\bar{q}'b\ell^-\bar{\nu}_\ell\bar{b} + \ell^+\nu_\ell bq''\bar{q}'''\bar{b}, \qquad (43.8\%) \tag{4.5}$$

$$(c)\ t\bar{t} \to W^+bW^-\bar{b} \to \ell^+\nu_\ell b\ell'^-\bar{\nu}_{\ell'}\bar{b}. \qquad (10.5\%) \tag{4.6}$$

The quarks in the final state will give rise to jets[5] due to the hadronization process. What separates these channels is their final state products which in turn depend on whether the W bosons decay hadronically or to leptons. The channels (a), (b) and (c) are referred to as fully hadronic (6 jets, two hadronic decays), semileptonic (2 leptons + 4 jets, one hadronic and one decay to leptons) and dileptonic (4 leptons + 2 b-jets, two leptonic decays), respectively. In parenthesis is their Branching Ratio (BR), which is defined as the ratio between the decay rate of each channel and the total decay rate. In principle, the W bosons can decay to any lepton, but tipically most analyses distinguish the electron (e) and muon (μ) from the tau (τ) channel, since the latter is more difficult to reconstruct. In this thesis, we have considered the dileptonic channel with electrons and muons ($e + \mu$) for the signal events. Although the two neutrinos in the final state make this channel difficult to reconstruct, the two charged leptons that come with them provide a clean experimental signature.

Signal events of $pp \to t\bar{t}h$, with $h = H, A$, were generated using MadGraph5_aMC@NLO at NLO precision with the Higgs characterization model HC_NLO_X0. Feynman diagrams at LO are shown in Figure 4.9. The CP-even/odd Higgs boson is set to decay to a pair of b-quarks. The $t\bar{t}$ system decays to a pair of b-quarks and two intermediary $W^\pm$ gauge bosons which, in turn, decay to two charged leptons and two neutrinos. The final particles, at parton level, are two oppositely charged leptons, two neutrinos and two $b\bar{b}$ quark pairs.

In addition to signal samples, background events are also generated using MadGraph5_aMC@NLO, now with the Standard Model implementation. The dominant background, $t\bar{t}b\bar{b}$, a pair of top- and b-quarks, and $t\bar{t}H^{SM}$, where H^{SM} is the SM Higgs, are generated at NLO and have the same final state products as our signal. Every other background topology is generated at tree level. The remaining backgrounds considered are:

- $t\bar{t}$+3 jets: A top-quark pair plus up-to three jets[6].
- $t\bar{t}V$+ jets: A top-quark pair, one gauge boson plus up-to one jet.
- Single top s-channel: A ($t\bar{b}$ + $\bar{t}b$) pair.
- Single top t-channel+ jets: A t or $\bar{t}$ plus up-to two jets.
- Single top Wt-channel: A $(W^+\bar{t} + W^-t)$ pair.
- W+4 jets: A $W^\pm$ boson plus up-to four jets.
- $Wb\bar{b}$+2 jets: A $W^\pm$ boson, two b-quarks and up-to two jets.
- Z+4 jets: A Z^0 boson plus up-to four jets.
- $Zb\bar{b}$+2 jets: A Z^0 boson, a pair of b-quarks plus up-to two jets.

[5]When a quark goes through the process of hadronization, it creates a large bunch of particles that are confined in a region of space that forms a narrow cone. This collective of objects that tend to travel in the same direction is called a jet.

[6]Here, jets refer to gluons and quarks (anti-quarks) lighter than the b-quark that after hadronization may result in an actual jet.

- WW+3 jets: A W^+W^- pair plus up-to three jets.
- WZ+3 jets: A $W^\pm Z^0$ pair plus up-to three jets.
- ZZ+3 jets: A Z^0 boson pair plus up-to three jets.

These are the backgrounds that can lead to events with at least 4 jets and 2 leptons of opposite charge. Each cross-section was computed directly in MadGraph5_aMC@NLO, except for the $t\bar{t}$+3 jets and $t\bar{t}b\bar{b}$ cross-sections, which were normalised to the QCD Next-to-Next-to Leading Order (NNLO) cross-section with Next-to-Next-to Leading Logarithmic (NNLL) resummation of soft gluons [68]. Also, the single top production (including all three channels) was normalized to the NNLO theoretical predictions for the single top production [69, 70]. The generated cross-sections (without cuts other than the simulation cuts) for all background topologies and for $tt\bar{h}$ events with $m_h = 40, 80, 120, 160$ and 200 GeV are shown in Table 4.1. These cross sections are not normalized to the same integrated luminosity. The integrated luminosity $\mathcal{L}$ is defined as the number of events for a given process, N, divided by its cross-section, σ:

$$\mathcal{L} = \frac{N}{\sigma}. \tag{4.7}$$

To calculate the number of events at a different luminosity, we only need to multiply the number of generated events by the weight of each event when the value of $\mathcal{L}$ changes. This weight is defined as $w = \mathcal{L}\sigma_{\text{gen}}/N_{\text{gen}}$, where σ_{gen} and N_{gen} are the generated cross-section and number of events, respectively.

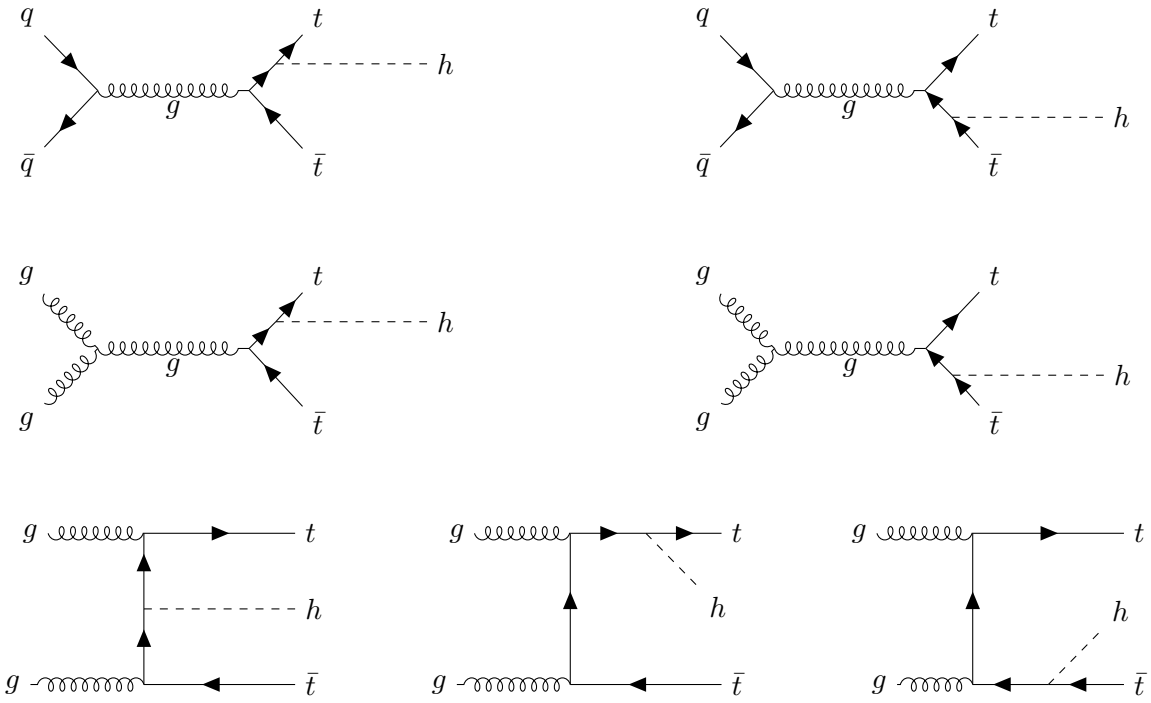

Figure 4.9: Main LO Feynman diagrams for Higgs production in association with a $t\bar{t}$ pair.

All events were generated for LHC pp collisions, with a Center of Mass energy of 13 TeV. The masses of the top quark (m_t) and the W boson (m_W) were set to 173 GeV and 80.4 GeV, respectively. For all samples, the NNPDF2.3 [71] parton distribution functions were used. Spin correlations between the decay products and the respective heavy resonance parents, $h, t, \bar{t}, W^\pm$, are preserved using MadSpin for $t\bar{t}h$ and $t\bar{t}H^{SM}$. Simulation of parton shower and hadronization was accomplished with Pythia6 [72]. Matching

Table 4.1: Expected cross-sections (in pb) with basic generator selection cuts and including decays of the top, Higgs, $W^{\pm}$ and Z, at 13 TeV, for background and (some) signal events at the LHC.

Topology	Order	Generated cross-section (pb)	Generated number of events
$t\bar{t}H$ (m_H = 40 GeV)	NLO	0.2557	99 984
$t\bar{t}A$ (m_A = 40 GeV)	NLO	0.01994	99 982
$t\bar{t}H$ (m_H = 80 GeV)	NLO	0.06864	99 979
$t\bar{t}A$ (m_A = 80 GeV)	NLO	0.01362	99 982
$t\bar{t}H$ (m_H = 120 GeV)	NLO	0.02438	99 988
$t\bar{t}A$ (m_A = 120 GeV)	NLO	0.009516	99 975
$t\bar{t}H$ (m_H = 160 GeV)	NLO	0.0105	99 980
$t\bar{t}A$ (m_A = 160 GeV)	NLO	0.006762	99 976
$t\bar{t}H$ (m_H = 200 GeV)	NLO	3.406×10^{-5}	99 980
$t\bar{t}A$ (m_A = 200 GeV)	NLO	0.004946	99 983
$t\bar{t}H^{SM}$	NLO	0.025	2 499 612
$t\bar{t}b\bar{b}$	NLO	0.79	1 599 714
$t\bar{t}$+3 jets	LO	37.89	3 624 813
$t\bar{t}V$+ jets	LO	0.0618	120 194
Single top s-channel	LO	2.1916	500 000
Single top t-channel+ jets	LO	46.863	500 000
Single top Wt-channel	LO	15.1827	500 000
W+4 jets	LO	34500	167 519
$Wb\bar{b}$+2 jets	LO	289	155 511
Z+4 jets	LO	3120	160 456
$Zb\bar{b}$+2 jets	LO	123	153 508
WW+3 jets	LO	84.2	119 409
WZ+3 jets	LO	37.9	41 849
ZZ+3 jets	LO	11	215 885
Total Background		38 268.1041	10 358 470

between the generator and the parton shower was performed using the MLM [73] scheme for LO events and the MC@NLO [74] matching for NLO events.

For a fast detector simulation of a LHC-like experiment, we used Delphes [75], using the default ATLAS parameter card. During detector simulation, jets and charged leptons are reconstructed, as well as the transverse missing energy. For jet reconstruction of the signal and background events, FastJet [76] is employed with the anti-k_t algorithm [77], cone size of $\Delta R = 0.7$ [7]. The analysis of the generated events was performed with MadAnalysis5 [78] in the expert mode [79].

4.5 Event selection

There are three instances where we apply selection cuts to the events that we will generate and reconstruct. The first one is in the actual simulation of the events, where transverse momentum (p_T) cuts are applied to jets and photons such that, in any events, these objects are kept if the following conditions

[7] $\Delta R \equiv \sqrt{\Delta\phi^2 + \Delta\eta^2}$, where ϕ is the azimuthal angle and η is the pseudo-rapidity, defined as $\eta = -\ln[\tan\frac{\theta}{2}]$. The angle θ is the angle between the three-momentum of a particle relative to the positive direction of the beam axis.

are met

$$p_{T_{\text{jet}}} \geq 10 \text{ GeV}, \qquad p_{T_{\text{photon}}} \geq 20 \text{ GeV}. \tag{4.8}$$

No cuts were applied to the transverse momentum of leptons nor to the pseudo-rapidity of jets, leptons and photons. These initial cuts were applied in the signal events. The remaining cuts are for both signal and backgrounds events.

The second instance of selection is enforced immediately before the reconstruction of our events. Only events with (at least) two charged leptons of opposite charge and four jets are eligible for reconstruction. Also, both leptons and jets were required to have $p_T \geq 20$ GeV and $|\eta| \leq 2.5$. These are the most restrictive cuts, after which only 5-20% of $t\bar{t}h$ generated events are accepted (for a range between $m_h = 40$ GeV and $m_h = 300$ GeV). For reconstruction using parton level information, it is additionally required that only events with an exact number of 12 partons can go through to reconstruction, these being two top quarks, four bottom quarks, two W gauge bosons, two charged leptons and two neutrinos. Finally, the third type of cuts is applied upon reconstruction: events where no solution for the neutrino reconstruction is found are rejected. Further details about the reconstruction process and its performance will be discussed in the next section.

4.6 Event Reconstruction

The major goal of any analysis done at the LHC is to infer the parton level information of a collision from the measured data of the detected objects. In our simulations, we have access to the parton level information. However, we need to estimate how that information would translate in terms of measured data, to determine the experimental predictions of a certain model. This means that we need to simulate what would actually be seen in an LHC detector and to match and reconstruct the objects that we observe at the detector (experimental level) with the corresponding objects at generator level.

The meaning of reconstructing an event is the following: from the available information after simulation we make the correspondence between the parton level object and the experimental object that originates from the former. That being done, we determine the four-momentum of the object at generator level. This process of reconstruction is not trivial. First, the detectors are not perfect, i.e. they deviate/smear the energy of particles, they have blind spots, and so on. Also, NLO effects may lead to the detection of more (or less) objects than what is expected. For example, two different jets can come from the same object at parton level, or two jets from different objects can recombine and form only one jet.

The first step in the reconstruction process is to select events that have a similar topology to the signal events that we want to reconstruct, in order to increase the signal to background ratio. This justifies the cuts applied to the number of jets, charged leptons, and number of partons already stated, as they match what is expected for the final state topology of our signal. The cuts on the p_T and η of these objects is motivated by the experimental limitations of the detector. The downside of this event selection is that we are possibly removing objects which would match better the parton level objects than the ones that are effectively selected. This has an impact on the purity of the sample, i.e., on how close the reconstructed events are to the generated events.

Afterwards, it is necessary to match the objects present in the detector to the generator objects. To simplify the discussion, we introduce some terminology to be used along the text. Parton level objects will from now on be referred to as GEN objects, while detector objects will be referred to as either REC or EXP objects. This distinction has to do with the fact that we have two alternatives to perform the

reconstruction:

- Reconstruction with Truth Match (TM).
- Reconstruction without Truth Match.

The difference between the two is that in reconstruction with TM, the association between GEN and detector objects is done while having access to the GEN objects. In this case, detector objects = REC objects. In reconstruction without Truth Match, we do not have access to the GEN objects. In this case, detector objects = EXP objects. In an ideal scenario, REC and EXP actually point to the same objects, but since the methodology used for the matching is different, that is not always the case.

The following assumptions are made in order to perform the reconstruction: a single GEN object can only give rise to one REC/EXP object and one REC/EXP object can only come from a single GEN object. This is what we call one-to-one correspondence. Also, it is assumed that all of the missing energy is due to neutrinos.

TM reconstruction corresponds to the best reconstruction method that we can hope to achieve. It tells us how efficient the reconstruction is when he have access to the GEN objects. We assume that the right association between GEN and detector objects is obtained for TM reconstruction. This association is correct[8] when we find a REC object with the least ΔR distance to the GEN object, considering all possible combinations. The ΔR function between two particles of indexes i and j is given by

$$\Delta R_{ij} = \sqrt{\left(\eta_i^{\text{GEN}} - \eta_j^{\text{REC}}\right)^2 + \left(\phi_i^{\text{GEN}} - \phi_j^{\text{REC}}\right)^2}. \tag{4.9}$$

Only objects with $\Delta R \leq 0.5$ ($\Delta R \leq 0.1$) for jets (leptons) can be associated. These objects are said to be well matched. In order for the reconstruction to continue we need to have six well matched objects in an event: 4 jets and two leptons. This process is called matching with TM. Afterwards, this information is used to find the momentum of the remaining particles, as we will see shortly. The matching efficiency, i.e., the number of times where we have six well matched objects is between 18-61%, taking into account all the signal samples that have been reconstructed.

For reconstruction without Truth Match, one typically needs to consider all combinations of EXP objects (jets in particular) along with some criterion to match the GEN objects (b-quarks) that come from the Higgs and the ones that come from the tops to the observed jets at detector level. Due to the large number of possible combinations, this association of jets to the b-quarks is one of the main problems of the reconstruction. Choosing a wrong assignment leads to combinatorial background, i.e., we identify that the jet comes from a b-quark, but it is the wrong bottom quark (for instance, we say that jet 1 comes from the $\bar{b}$ of the $\bar{t}$, $\bar{b}_{\bar{t}}$, when in fact it comes from the b of the Higgs, b_h).

To tackle this, we find the combination of four jets that best resembles the kinematics of the parton level b-quarks by using an association algorithm. This algorithm is applied for each of the generated samples. It relies on a multivariate data analysis method employed using the Toolkit for Multivariate Analysis (TMVA) [80]. Two samples labeled as signal and background were created from $t\bar{t}h$ signal events and used for training and testing, corresponding to the right and wrong jet combinations, respectively. For training the methods, eleven parton level variables were used as input: ΔR, $\Delta\phi$, and $\Delta\theta$ for the pairs (b_t, l^+), $(\bar{b}_{\bar{t}}, l^-)$ and $(b_h, \bar{b}_h)$, and the invariant masses of the two first pairs. Information about the

[8]The word correct here is slightly ambiguous. When we say the association is correct, we mean that we found a pair of REC and GEN objects that meets the criteria chosen for this reconstruction process. However, the REC object that we choose may have come from a different GEN object, hence in reality it may not be correct.

invariant mass of the latter pair was also included, and computed after reconstruction with TM. Because the Higgs decays to two b-quarks, NLO effects will be considerable. These effects lead to a different reconstructed Higgs mass relative to its parton counterpart, which is why we need to use the former for the reconstruction. The input variables for TMVA and their correlations are shown in Figure 4.10 and Figure 4.11, for the CP-odd case with $m_A = 40$ GeV.

For all signal samples, the best methods are Boosted Decision Trees with an adaptatie boost (BDTs) or Boosted Decision Trees with a Gradient boost (BDTGs). The latter was the method used. The jet combination chosen is the one returning the highest value of the BDTG discriminant, which maximizes signal purity in the methods implemented. The Receiver Operating Characteristic (ROC) curve and the BDT and BDTG discriminant distributions are shown in Figures 4.12 and 4.13, respectively, for $t\bar{t}A$ with $m_A = 40$ GeV.

In events where the number of jets is more than six, we only consider the six jets with the highest transverse momentum. Around 95% of all signal events are contained in this subset. Furthermore, the invariant mass of the jet combinations are required to verify $m_{l^+b_t} < 150$ GeV, $m_{l^-\bar{b}_{\bar{t}}} < 150$ GeV and 20 GeV $< m_{b_h\bar{b}_h} < 300$ GeV. The first two constraints are because typically those distributions have no events after 150 GeV for $t\bar{t}h$.

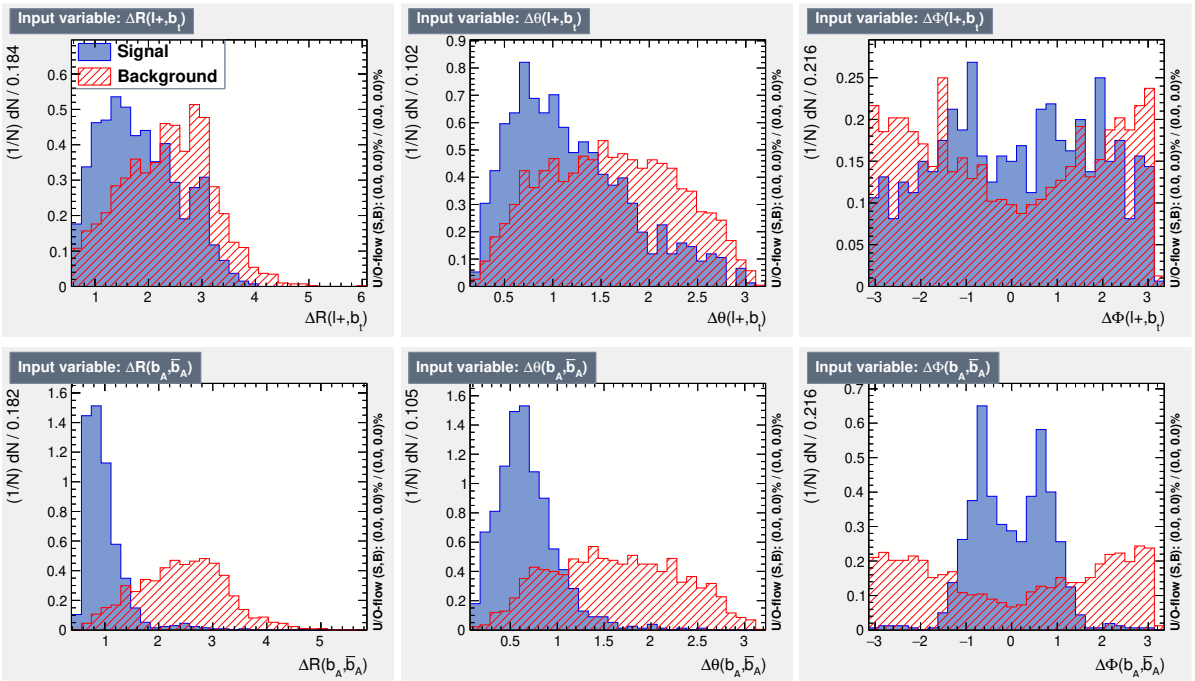

Figure 4.10: Distributions of the TMVA input variables for the signal (blue) and background (red) samples for $t\bar{t}A$ events with $m_A = 40$ GeV. The angular variables ΔR, $\Delta\theta$ and $\Delta\Phi$ for the pairs (l^+, b_t) (top) and $(b_A, \bar{b}_A)$ (bottom) are computed at generator level.

At this point, we have two leptons and four b-quarks identified. The last part consists in the reconstruction of the undetected neutrinos, and is valid for both TM and without TM reconstruction. This is

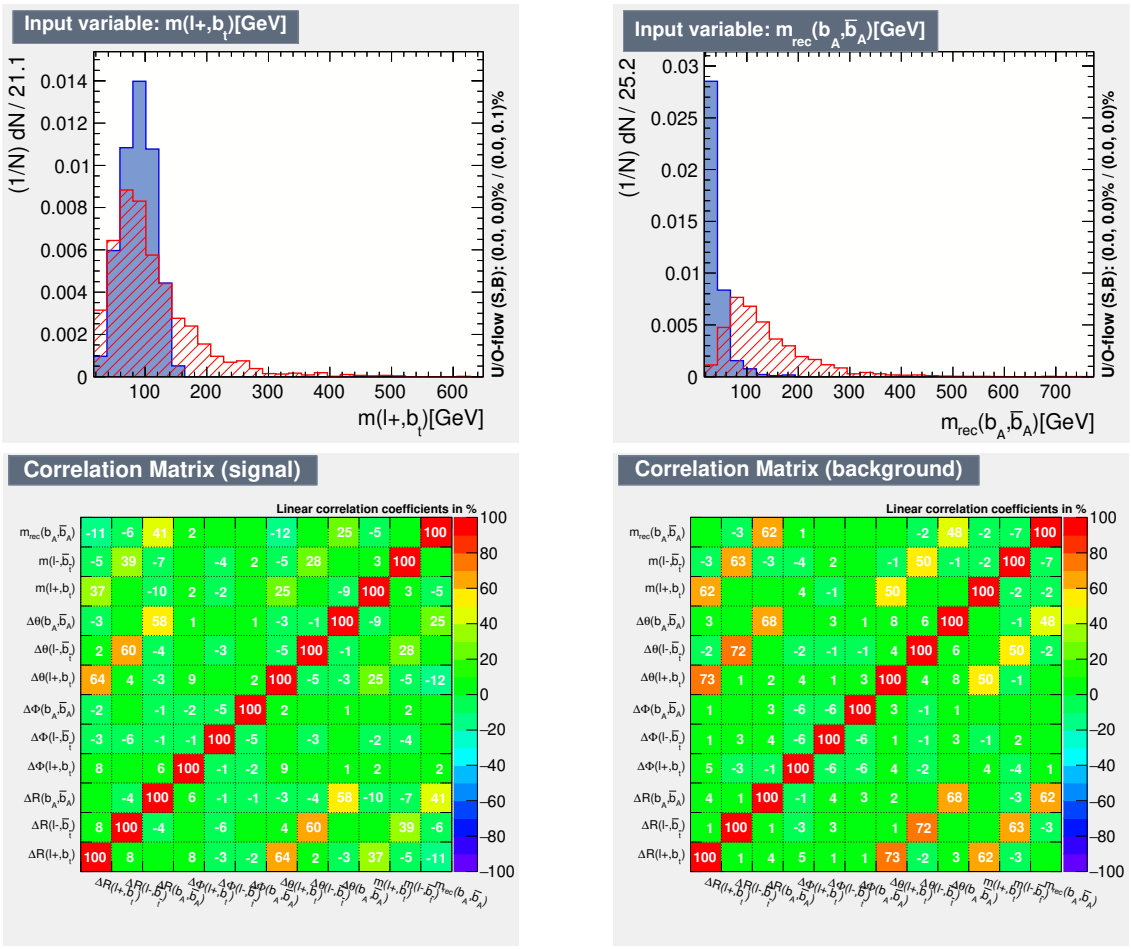

Figure 4.11: Invariant masses for the systems (l^+, b_t) at parton level (top left) and $(b_A, \bar{b}_A)$ obtained with Truth Matching (top right), for $t\bar{t}A$ events with $m_A = 40$ GeV. Below, we have the matrix correlations between the TMVA input variables for the signal (left) and background (right) samples.

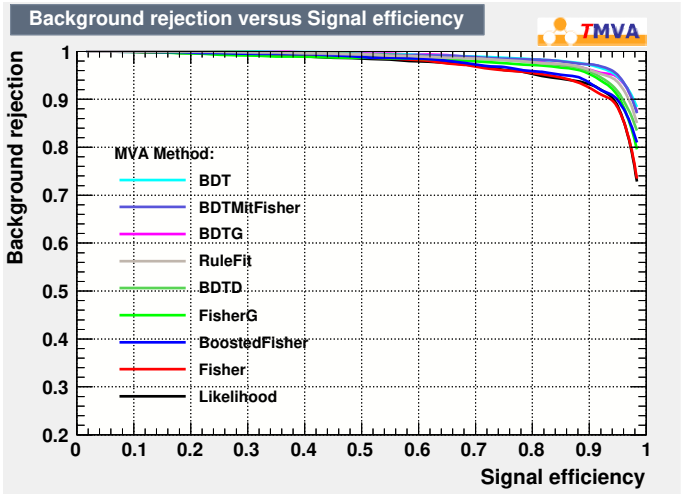

Figure 4.12: Most performant methods in terms of correct jet assignment for $t\bar{t}A$ events with $m_A = 40$ GeV. We found that typically BDTs or BDTGs are the best for all h boson masses.

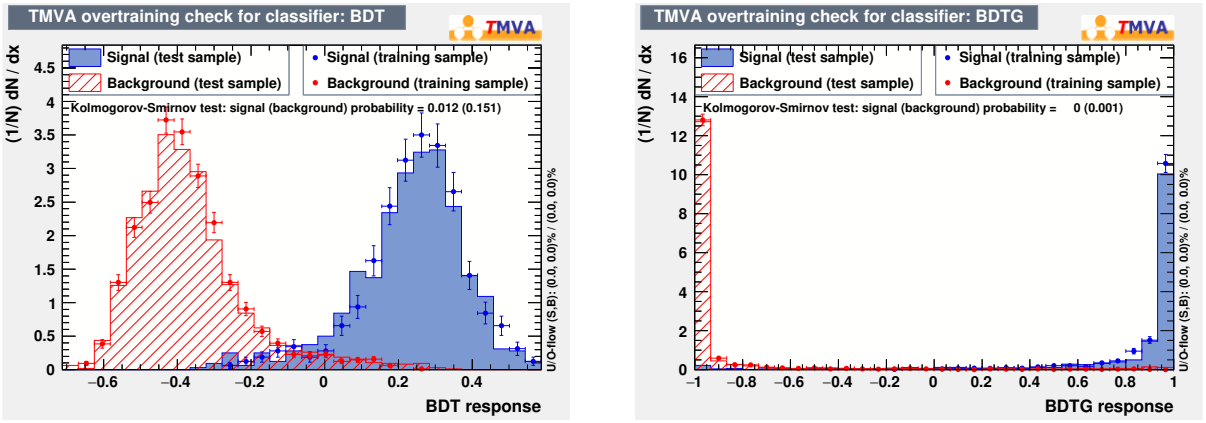

Figure 4.13: Distributions of the BDT (left) and BDTG (right) discriminants for the signal and background in training and test samples, for $t\bar{t}A$ events with $m_A = 40$ GeV.

done by using energy-momentum conservation which allows us to write the following set of equations

$$(p_{l^+} + p_\nu)^2 = m_{W^+}^2, \tag{4.10}$$
$$(p_{l^-} + p_{\bar{\nu}})^2 = m_{W^-}^2, \tag{4.11}$$
$$(p_{W^+} + p_{b_t})^2 = m_t^2, \tag{4.12}$$
$$(p_{W^-} + p_{\bar{b}_{\bar{t}}})^2 = m_{\bar{t}}^2, \tag{4.13}$$
$$p_\nu^x + p_{\bar{\nu}}^x = \not{E}^x, \tag{4.14}$$
$$p_\nu^y + p_{\bar{\nu}}^y = \not{E}^y. \tag{4.15}$$

The first four equations are relativistic on-shell conditions and the last two are due to momentum conservation, where $\not{E}^{x/y}$ are the missing transverse energy components. Its values are measured by the detector. Since we already know the momenta of the two b-quarks that come from the pair of tops, as well as the momenta of the charged leptons from the gauge bosons decay (p_{l^+} and p_{l^-}), we are left with six unknowns. They are the components of the three-momentum of the neutrino and anti-neutrino (the neutrinos masses are assumed to be zero), thus a solution can be found. The masses of the top-quarks and the $W^\pm$ bosons are randomly generated from Two-Dimensional Probability Density Functions (2D PDFs) constructed with parton level information, so to preserve possible correlations. If no solution is found, the generation of masses is repeated up-to a maximum of 500 trials. If there is still no solution, the event is discarded. Additionally, because the first four equations are quadratic, there might be several solutions instead. In that case, a likelihood function is computed for each solution from the transverse momenta PDFs of the neutrinos, top-quarks and $t\bar{t}$ system at parton level, respectively $P(p_{T_\nu})$, $P(p_{T_{\bar{\nu}}})$, $P(p_{T_t})$, $P(p_{T_{\bar{t}}})$, $P(p_{T_{t\bar{t}}})$. Furthermore, we consider the two dimensional mass PDF of the $t\bar{t}$ pair, $P(m_t, m_{\bar{t}})$, and the mass of the reconstructed Higgs, $P(m_h)$, obtained with Truth Matching. Some of the PDFs used in the reconstruction are shown in Figure 4.14 and Figure 4.15, again for the CP-odd case with $m_A = 40$ GeV. With all these pieces the likelihood reads

$$L_{t\bar{t}h} \propto \frac{1}{p_{T_\nu} p_{T_{\bar{\nu}}}} P(p_{T_\nu}) P(p_{T_{\bar{\nu}}}) P(p_{T_t}) P(p_{T_{\bar{t}}}) P(p_{T_{t\bar{t}}}) P(m_t, m_{\bar{t}}) P(m_h), \tag{4.16}$$

and the solution with the largest value of $L_{t\bar{t}h}$ is chosen. Since energy losses due to QCD radiation as well as detector effects may result in overestimating the neutrino and anti-neutrino p_T after reconstruction,

the pre-factor $1/p_{T_\nu} p_{T_{\bar{\nu}}}$ is introduced in the likelihood to preferentially pick solutions with lower neutrino and anti-neutrino p_T that better match parton level.

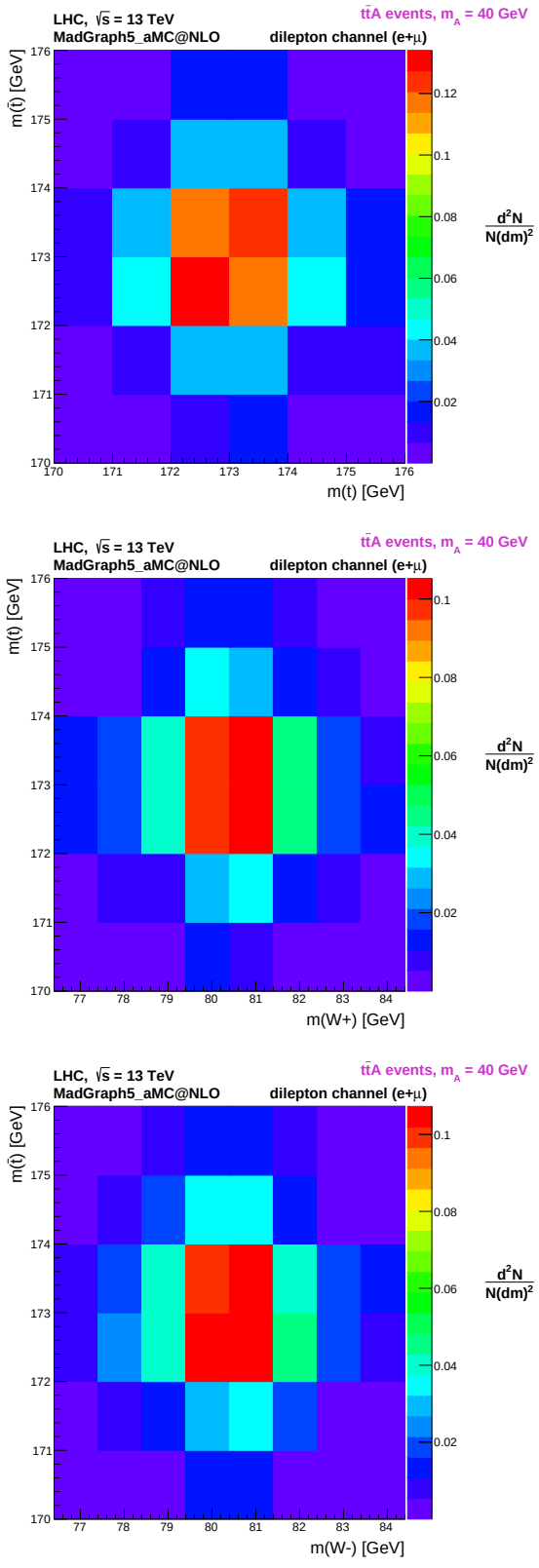

Figure 4.14: 2D PDFs at parton level for the masses of the pairs $(t, \bar{t})$ (top), (W^+, t) (middle) and $(W^-, \bar{t})$ (bottom).

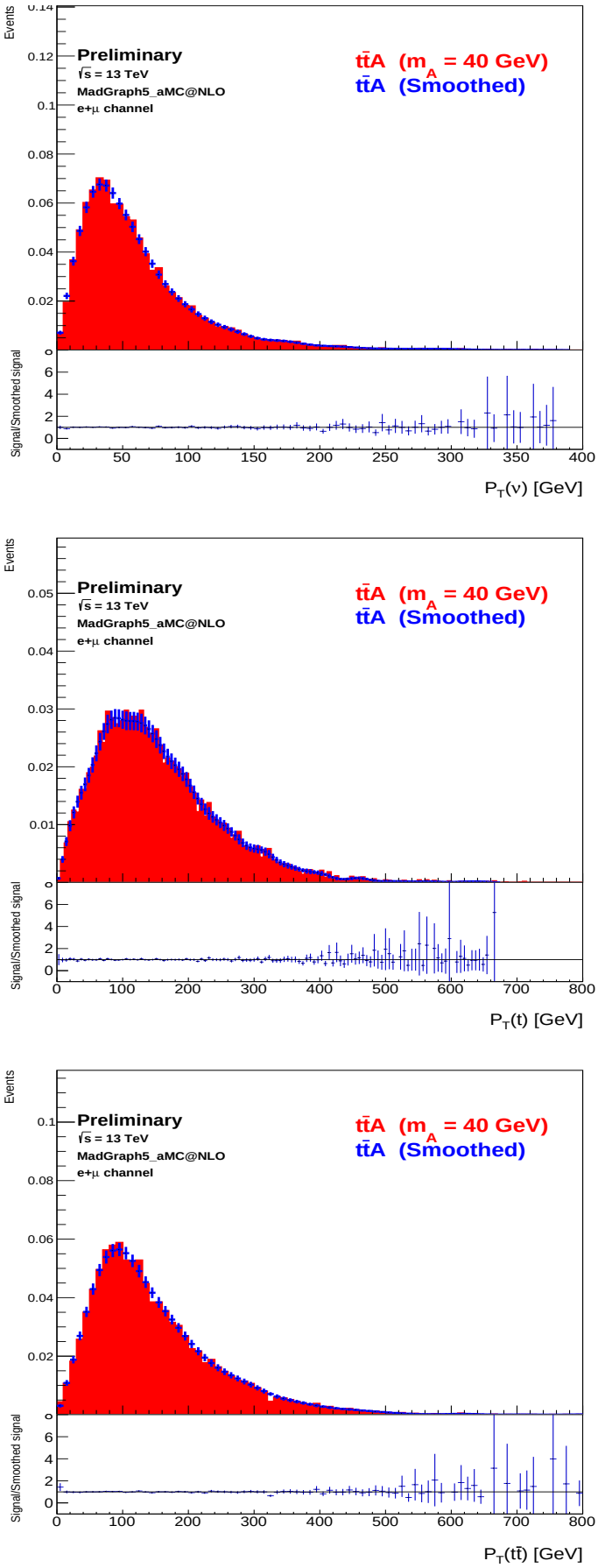

Figure 4.15: PDFs used for the likelihood (in blue) and actual distributions at parton level (in red) for the neutrino, top and $t\bar{t}$ system. Below, the ratio between these distributions is shown.

Following event selection, 66-73% of $t\bar{t}h$ signal events are successfully reconstructed with Truth Match (after matching), for a Higgs mass ranging from 40 to 300 GeV. Without Truth Match, the efficiency of the reconstruction is around 49-63% (matching included). In 29-55% of the cases, the reconstruction without Truth Match results in the same jet combination as the Truth Matched one. Given these percentages, if we start with a given number of $t\bar{t}h$ events, N_{gen}, we end up with (at least) $N_{REC} = N_{gen} \times 0.05 \times 0.18 \times 0.66$ and $N_{EXP} = N_{gen} \times 0.05 \times 0.49$, where N_{REC} and N_{EXP} are the total number of reconstructed events with and without Truth Match, respectively. The various efficiencies cited along the text about the reconstruction and selection of events are summarized in Table 4.2. Similar performance numbers for the reconstruction discussed in this thesis were found relative to the one discussed in [60].

Table 4.2: Efficiencies of the selection cuts and of the reconstruction method applied to $t\bar{t}h$ events where m_h varies between 40 GeV and 300 GeV. $N_{jets} \geq 4$ & $N_{lep} \geq 2$ already includes objects with $p_T \geq 20$ GeV and $|\eta| \leq 2.5$. The efficiencies for specific h boson masses for the first and last rows are shown in appendix E.

	Efficiency (%)
$N_{jets} \geq 4$ & $N_{lep} \geq 2$	5-20
Matching with TM	18-61
Reconstruction with TM (after matching)	66-73
Reconstruction without TM (matching included)	49-63

Figure 4.16 shows, after reconstruction without Truth Match of $t\bar{t}H$ events for $m_H = 40$ GeV, Two-Dimensional p_T distributions of the W^+ (top-left), the top quark (top-right), the $t\bar{t}$ system (bottom-left) and the Higgs boson (bottom-right). The correlation between the parton level p_T distributions at NLO with shower effects (x-axis), labeled NLO+Shower, and reconstructed ones without Truth Match (y-axis), is clearly visible. The same kind of plots are obtained for the $t\bar{t}A$ signals and are shown in Figure 4.18. The neutrino reconstructed p_T for $t\bar{t}H$ and $t\bar{t}A$ is compared with the p_T at NLO+Shower in Figure 4.17 (left) and Figure 4.19 (left), respectively. The distribution of the reconstructed Higgs boson masses is shown in Figure 4.17 (right) and Figure 4.19 (right). In spite of the wider spread of values in the neutrino p_T distribution, a direct consequence of the reconstruction of two neutrinos in each one of the events, good correlation between the NLO+Shower distribution and the reconstructed neutrino p_T is observed.

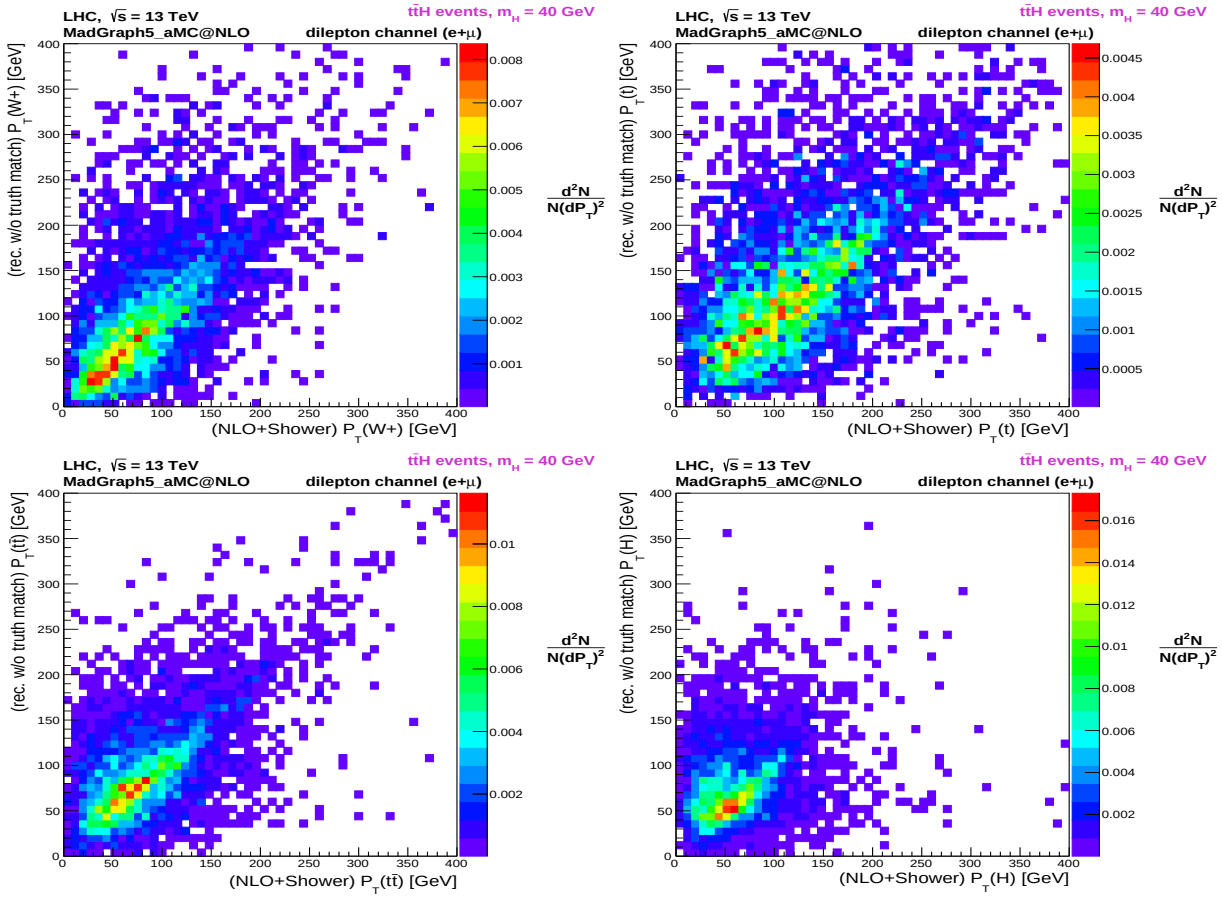

Figure 4.16: Two-Dimensional distributions of p_T in $t\bar{t}H$ events. The horizontal axes represent variables recorded at NLO+Shower, and the vertical axes represent the corresponding variables recorded at reconstruction level without Truth Match. Upper-left: distribution for W^+. A similar distribution is obtained for W^-, but is not shown here. Upper-right: distribution for t. A similar distribution is obtained for $\bar{t}$, but is not shown here. Lower-left: distribution for $t\bar{t}$. Lower-right: distribution for H. All distributions are shown for a Higgs mass of 40 GeV.

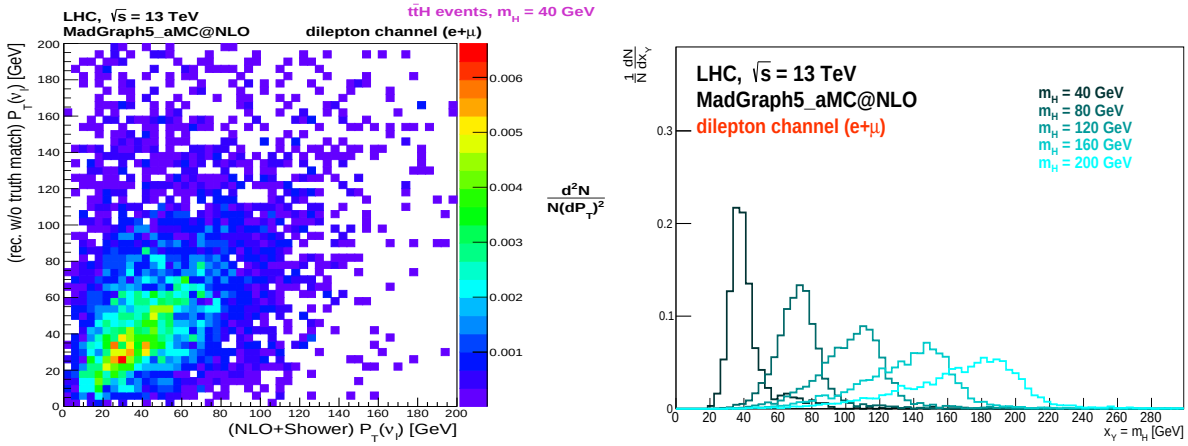

Figure 4.17: Two-Dimensional distribution of the neutrino p_T in $t\bar{t}H$ events with $m_H = 40$ GeV (left): the NLO+Shower p_T (x-axis) against the reconstructed p_T without Truth Match (y-axis) is shown. Distribution of the reconstructed Higgs boson mass with Truth Matched jets in $t\bar{t}H$ events (right).

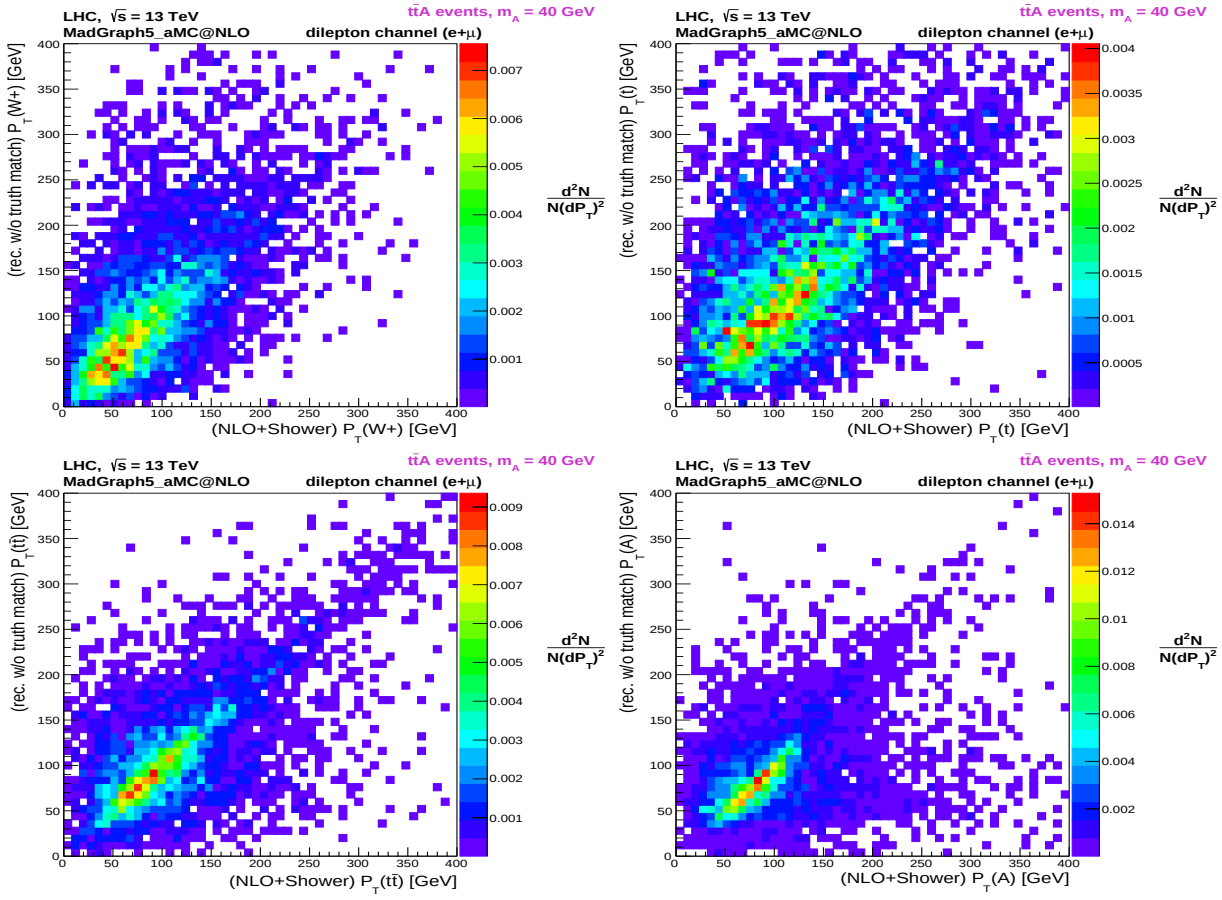

Figure 4.18: Two-Dimensional distributions of p_T in $t\bar{t}A$ events. The horizontal axes represent variables recorded at NLO+Shower, and the vertical axes represent the corresponding variables recorded at reconstruction level without Truth Match. Upper-left: distribution for W^+. A similar distribution is obtained for W^-, but is not shown here. Upper-right: distribution for t. A similar distribution is obtained for $\bar{t}$, but is not shown here. Lower-left: distribution for $t\bar{t}$. Lower-right: distribution for A. All distributions are shown for a Higgs mass of 40 GeV.

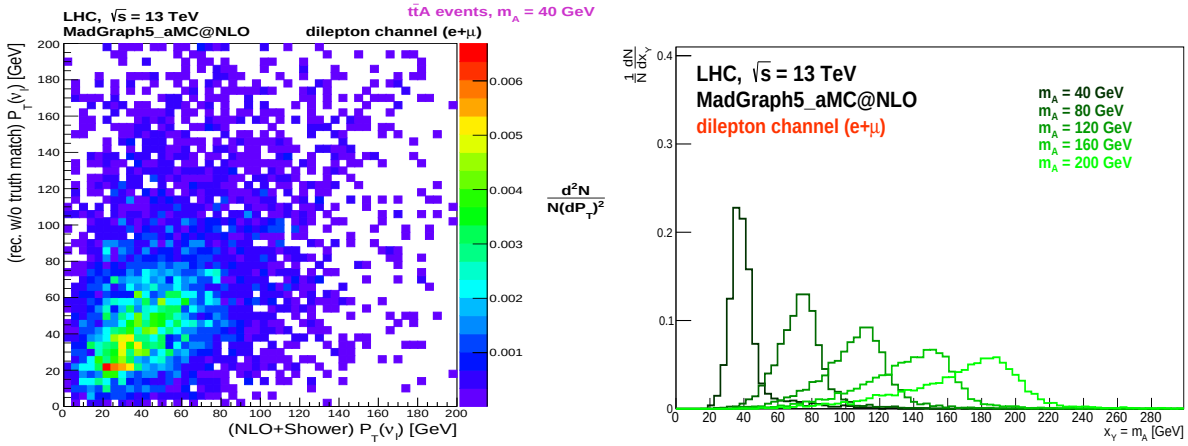

Figure 4.19: Two-Dimensional distribution of the neutrino p_T in $t\bar{t}A$ events with $m_A = 40$ GeV (left): the NLO+Shower p_T (x-axis) against the reconstructed p_T without Truth Match (y-axis) is shown. Distribution of the reconstructed Higgs boson mass with Truth Matched jets in $t\bar{t}A$ events (right).

4.7 Asymmetries in the Yukawa sector

Since the differences between distinct CP-states in $f\bar{f}h$ production depend on m_f^2, those differences should show an increase of at least 3 orders of magnitude in $t\bar{t}h$, relative to the $b\bar{b}h$. Thus, CP-discrimination between the different CP-states of the Higgs might now be possible. The variables considered to this effect are

$$b_4 = p_t^z p_{\bar{t}}^z / |\vec{p}_t||\vec{p}_{\bar{t}}|, \tag{4.17}$$

$$b_2 = (\vec{p}_t \times \hat{k}_z).(\vec{p}_{\bar{t}} \times \hat{k}_z)/|\vec{p}_t||\vec{p}_{\bar{t}}|, \tag{4.18}$$

$$\cos\left(\theta_h^{\bar{t}h}\right)\cos\left(\theta_{\ell-}^{h}\right), \tag{4.19}$$

$$\sin\left(\theta_h^{t\bar{t}h}\right)\sin\left(\theta_{b_{\bar{t}}}^{\bar{t}}\right)\text{(sequential boost)}, \tag{4.20}$$

$$\sin\left(\theta_h^{t\bar{t}h}\right)\cos\left(\theta_{b_h}^{\bar{t}}\right)\text{(sequential boost)}, \tag{4.21}$$

$$\sin\left(\theta_h^{t\bar{t}h}\right)\sin\left(\theta_{W+}^{h}\right)\text{(sequential boost)}, \tag{4.22}$$

$$\sin\left(\theta_{\bar{t}}^{t\bar{t}h}\right)\sin\left(\theta_{b_h}^{h}\right)\text{(sequential boost)}, \tag{4.23}$$

$$\sin\left(\theta_h^{t\bar{t}h}\right)\sin\left(\theta_{\bar{t}}^{t\bar{t}}\right), \tag{4.24}$$

with $0 \leq \theta \leq \pi$. In Equation 4.18, $\hat{k}_z$ is the unitary vector along the z-direction. The b_2 and b_4 variables were computed in the LAB and in the CM frame of the $t\bar{t}h$ system ($b_2^{t\bar{t}h}$ and $b_4^{t\bar{t}h}$). Figure 4.20 and Figure 4.21 show the NLO+Shower b_2 and b_4 distributions, without any cuts, for $t\bar{t}H$ and $t\bar{t}A$ events with different Higgs masses, in the LAB and CM frames, respectively. Clear differences are now visible between the scalar and pseudoscalar signals, and also between the distributions computed in the Laboratory and in the Center of Mass frame. For completeness, we also show the same distributions in Figure 4.22 and Figure 4.23, after reconstruction without TM. As we can see, the shape of these distributions is largely preserved, hence there is still a good level of discrimination[9].

To see how asymmetry differences between CP-even and CP-odd signals change with the scalar boson mass, forward-backward asymmetries associated to each of the observables under study were defined according to [59]

$$A_{FB}^{Y} = \frac{\sigma(x_Y > x'_Y) - \sigma_Y(x_Y < x'_Y)}{\sigma_Y(x_Y > x'_Y) + \sigma_Y(x_Y < x'_Y)}, \tag{4.25}$$

where $\sigma(x_Y > x'_Y)$ and $\sigma(x_Y < x'_Y)$ correspond to the total cross section with x_Y above and below a cut-off value equal to the central value of the x_Y domain, respectively. Some of those asymmetries are shown in Figure 4.24. As we can see, for large enough Higgs masses the difference between CP-even and CP-odd distributions vanishes. This was observed for all the variables that were tested. Also, the exact h boson mass for which these differences disappear depends on the variable. The maximum value of the scalar boson mass for which we can still see a visible difference is around 450 GeV.

Finally, the dependence of the total cross section for the process $pp \to \bar{t}tH$ (blue) and $pp \to \bar{t}tA$ (red) as a function of the scalar boson mass was computed at NLO in Figure 4.25. For smaller Higgs

[9] While detector simulation and reconstruction degrade the discriminating power of these observables, the most dramatic effect on the distribution shapes comes from applying the acceptance cuts, which spoils the purity of the samples.

masses, we see a significant relative difference (more than one order of magnitude) between the scalar and pseudoscalar cross sections. This difference gradually decreases as the Higgs mass increases, which is consistent with the observation that the differences between scalar and pseudoscalar distributions vanish for large enough Higgs masses.

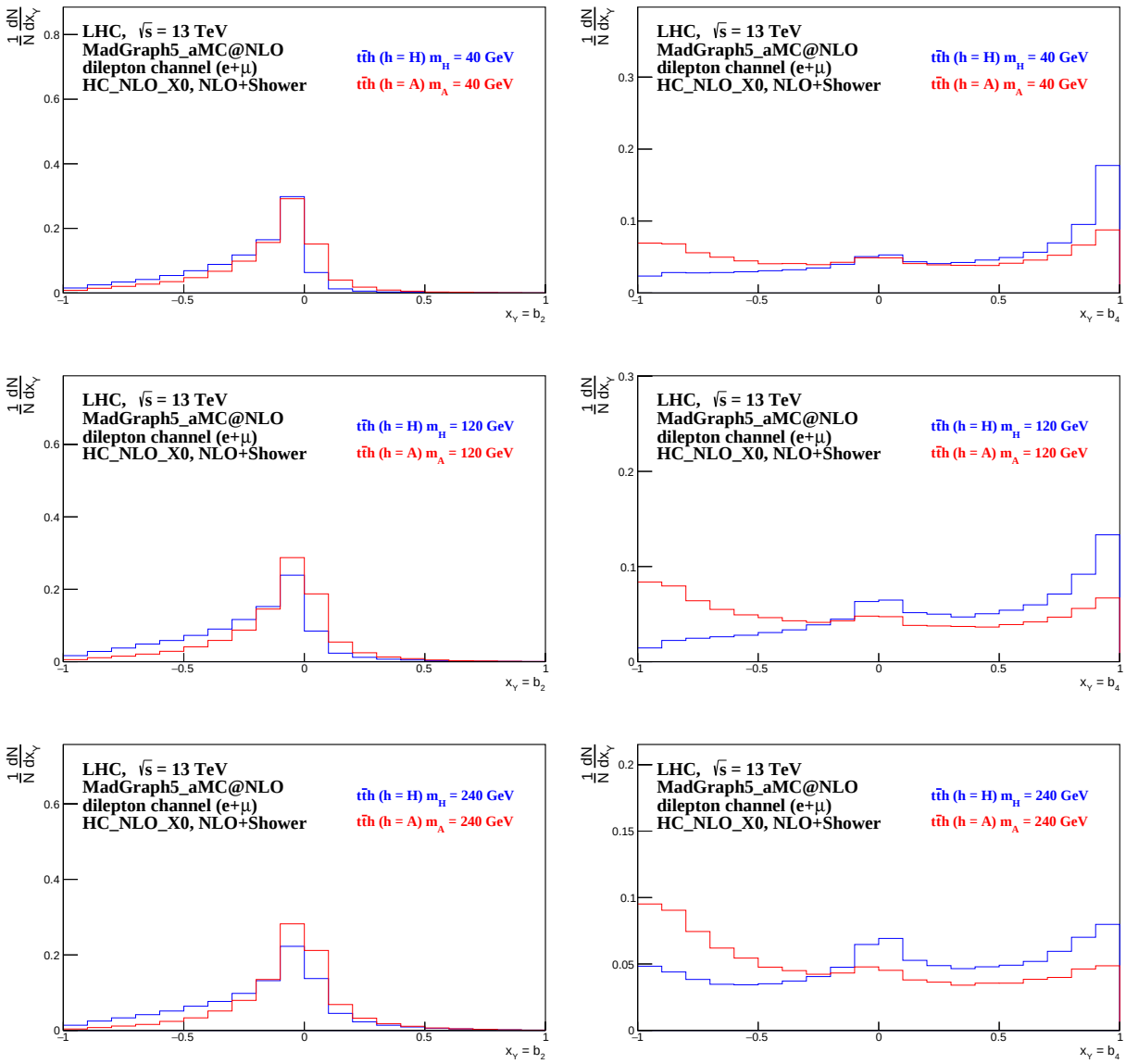

Figure 4.20: Full normalized distributions at NLO+Shower for the variables b_2 (left) and b_4 (right) in the LAB frame, without any selection cuts nor reconstruction, for both the pure scalar (blue line) and pure pseudoscalar (red line) signals with $m_h = 40$, 120 and 240 GeV.

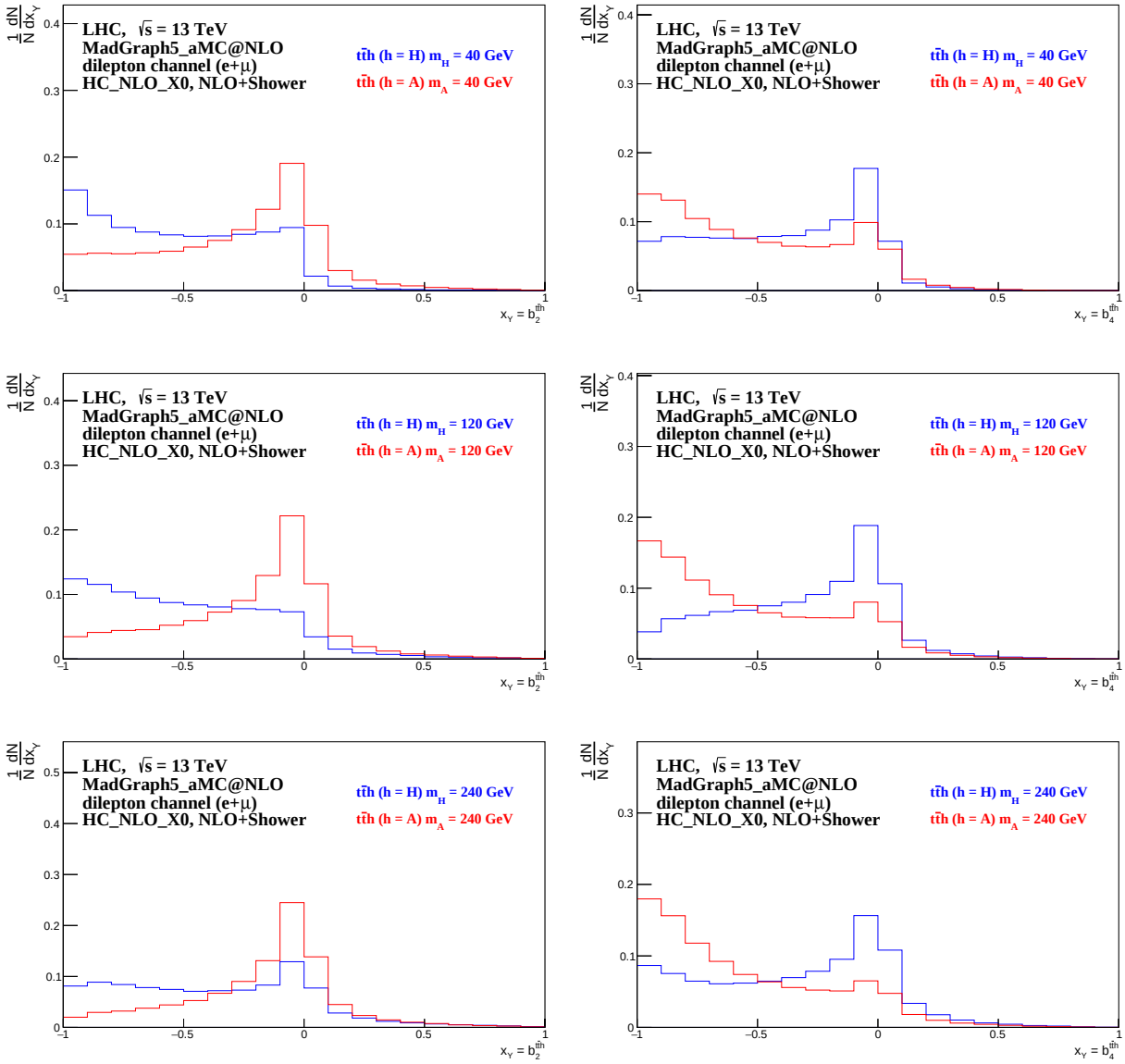

Figure 4.21: Same as in Figure 4.20, but now the b_2 and b_4 distributions are computed in the CM of the $t\bar{t}h$ system.

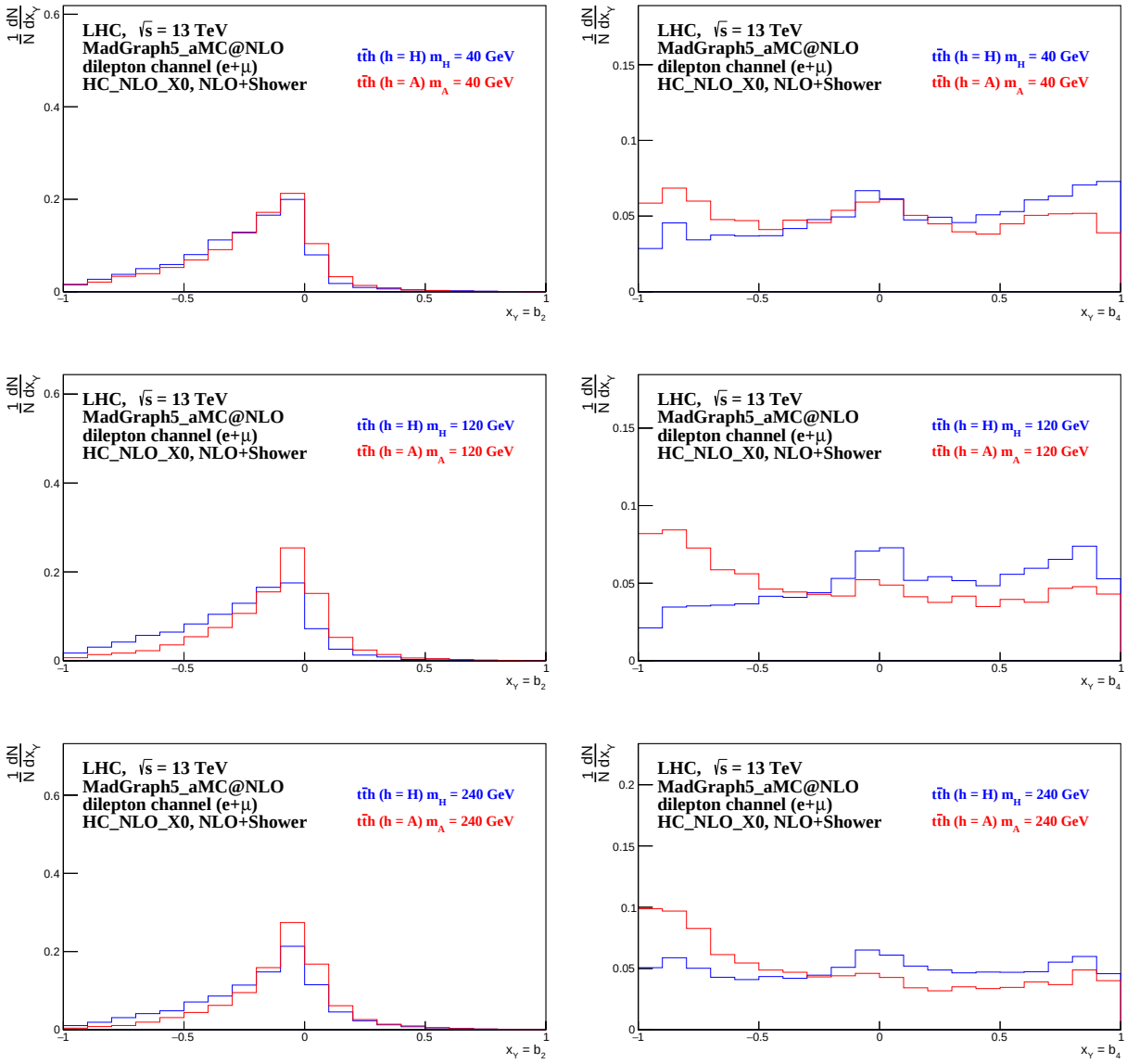

Figure 4.22: Full normalized distributions after reconstruction without TM for the variables b_2 (left) and b_4 (right) in the LAB frame, for both the pure scalar (blue line) and pure pseudoscalar (red line) signals with $m_h = 40$, 120 and 240 GeV.

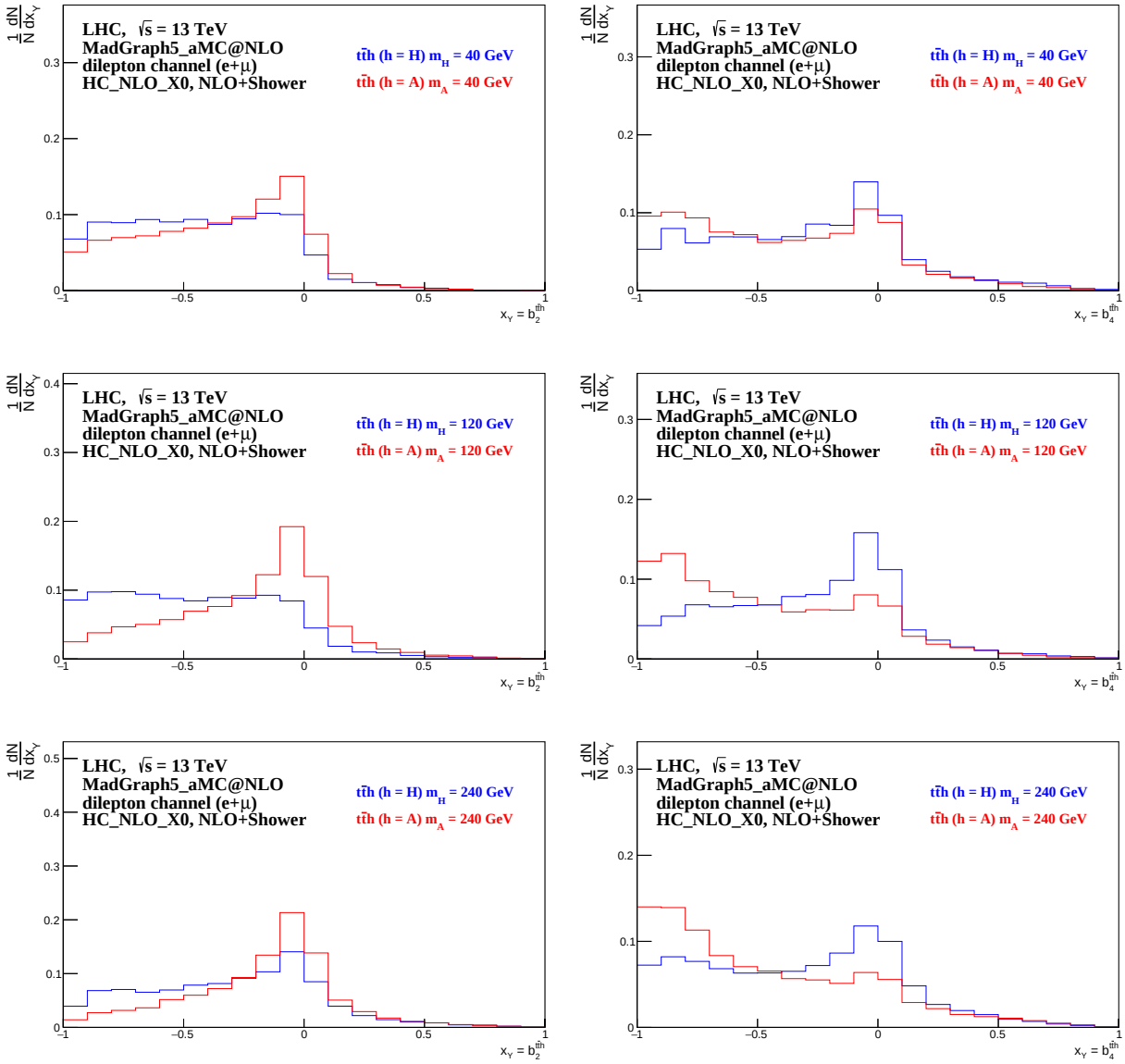

Figure 4.23: Same as in Figure 4.22, but now the b_2 and b_4 distributions are computed in the CM of the $t\bar{t}h$ system.

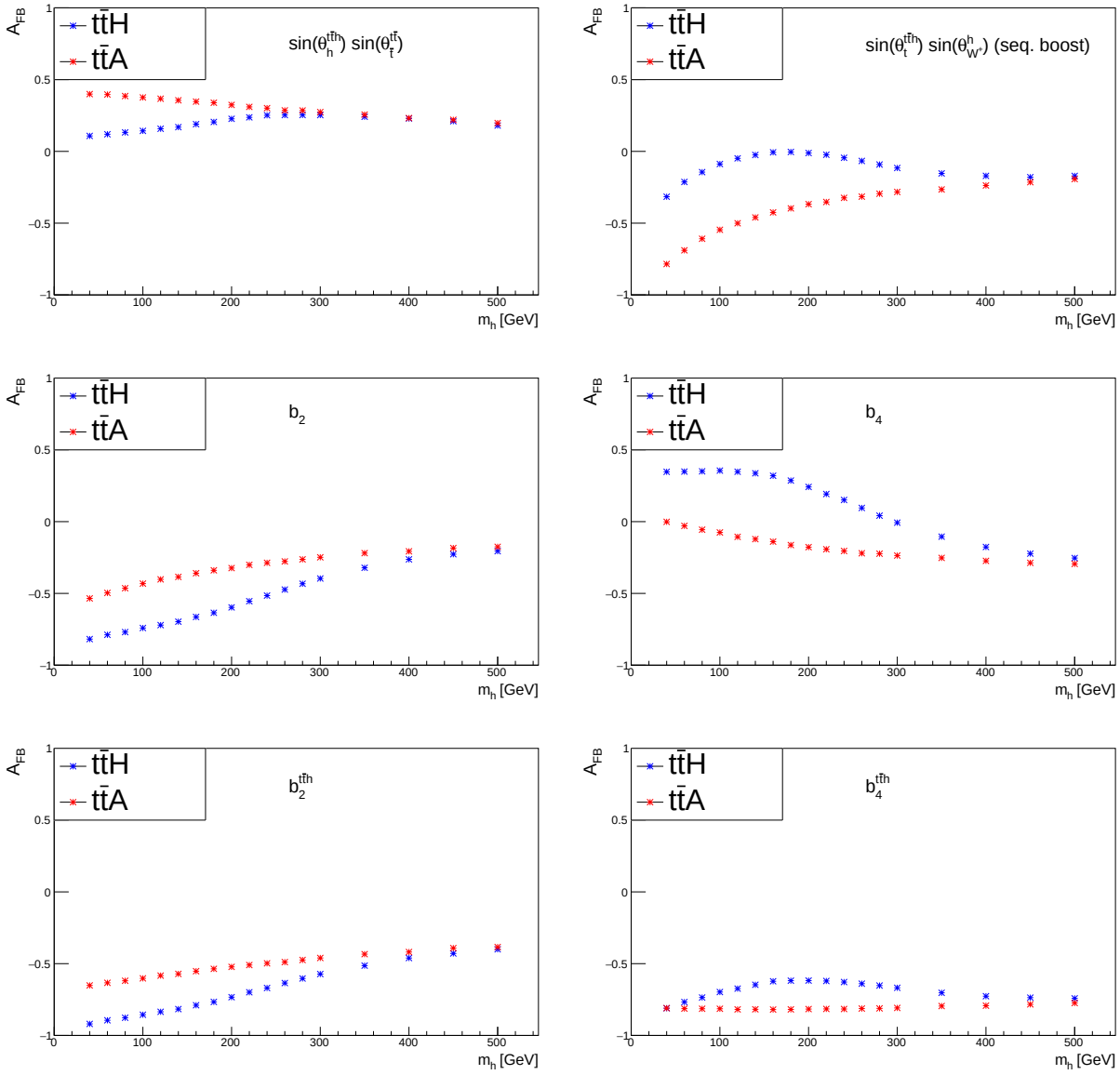

Figure 4.24: Forward-backward asymmetries as a function of the scalar boson mass, without cuts, at NLO+Shower. On top, we have two angular distributions, $\sin\theta_h^{t\bar{t}h}\ \sin\theta_{\bar{t}}^{t\bar{t}}$ (left panel) and $\sin\theta_t^{t\bar{t}h}\ \sin\theta_{W^+}^{h}$ with a sequential boost (right panel). On the middle and last rows, we show the variables b_2 (left) and b_4 (right), in the LAB and CM frame, respectively.

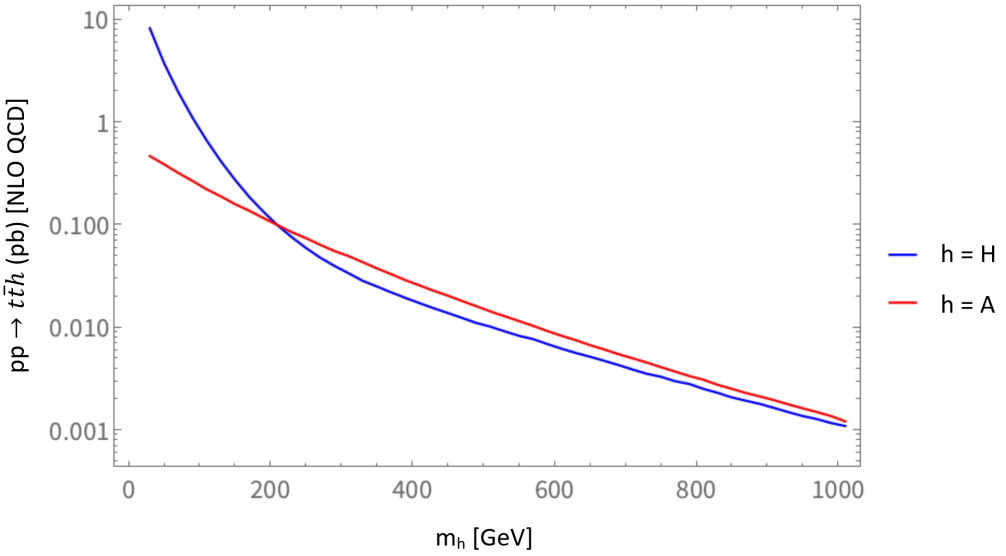

Figure 4.25: Total cross section, at NLO, for a CM energy of 13 TeV at the LHC, for the process $pp \to \bar{t}tH$ (blue) and $pp \to \bar{t}tA$ (red), as a function of the scalar boson mass, without decays of the top or the Higgs.

4.8 Background contributions

The reconstruction described in section 4.6 was applied not only to $t\bar{t}h$ events, but also to its backgrounds, in order to estimate the number of background events that we are expecting to find when looking for $t\bar{t}h$. To further reduce the background to signal ratio, additional selection criteria are applied after reconstruction, for both signal and background samples. Depletion of the $Z + 4$ jets and $Zb\bar{b} + 2$ jets backgrounds is accomplished by selecting events with a dilepton invariant mass such that $|m_{l^+l^-} - m_Z| > 10$ GeV. Most backgrounds, notably $t\bar{t} + 3$ jets, are then mitigated by selecting events with at least 3 b-tagged jets, i.e., three jets that the detector identifies as coming from a b-quark. In Figure 4.26, the expected number of events that survive all stages of selection cuts for the different SM backgrounds is shown for a luminosity of 100 fb^{-1}, and compared to the CP-even and -odd signals with $m_h = 40$ GeV, for different observables. In this figure, single top refers to the three channels of single top production. Z+jets includes $Z + 4$ jets and $Zb\bar{b} + 2$ jets, W+jets includes $W + 4$ jets and $Wb\bar{b} + 2$ jets. Diboson events are the $WW + 3$ jets, $WZ + 3$ jets and $ZZ + 3$ jets backgrounds, $t\bar{t}c\bar{c}$, $t\bar{t}+$ light jets is the $t\bar{t} + 3$ jets process and $t\bar{t}H$ (m_H = 125 GeV) is the $t\bar{t}H^{SM}$ process. In Table 4.3, we show the number of signal and total background events that survive the reconstruction and all additional cuts, when we look for $t\bar{t}H$ events with five different scalar boson masses. The numbers on this table are the ones effectively used in the calculation of the expected Confidence Levels, which will be discussed in the next section.

Table 4.3: Total number of predicted events for the total background, CP-even and CP-odd signal samples. These are the events that survive reconstruction without TM and all additional selection cuts, for a luminosity of 100 fb^{-1} at the LHC. The efficiencies for the final selection cuts ($|m_{l^+l^-} - m_Z| > 10$ GeV and at least 3 b-tagged jets) are shown in appendix E.

	N_{final} $t\bar{t}H$ m_H = 40 GeV	N_{final} $t\bar{t}H$ m_H = 80 GeV	N_{final} $t\bar{t}H$ m_H = 120 GeV	N_{final} $t\bar{t}H$ m_H = 160 GeV	N_{final} $t\bar{t}H$ m_H = 200 GeV
Total background	775	821	838	844	787
CP-even signal	68	42	27	13	0
CP-odd signal	8	13	12	10	8

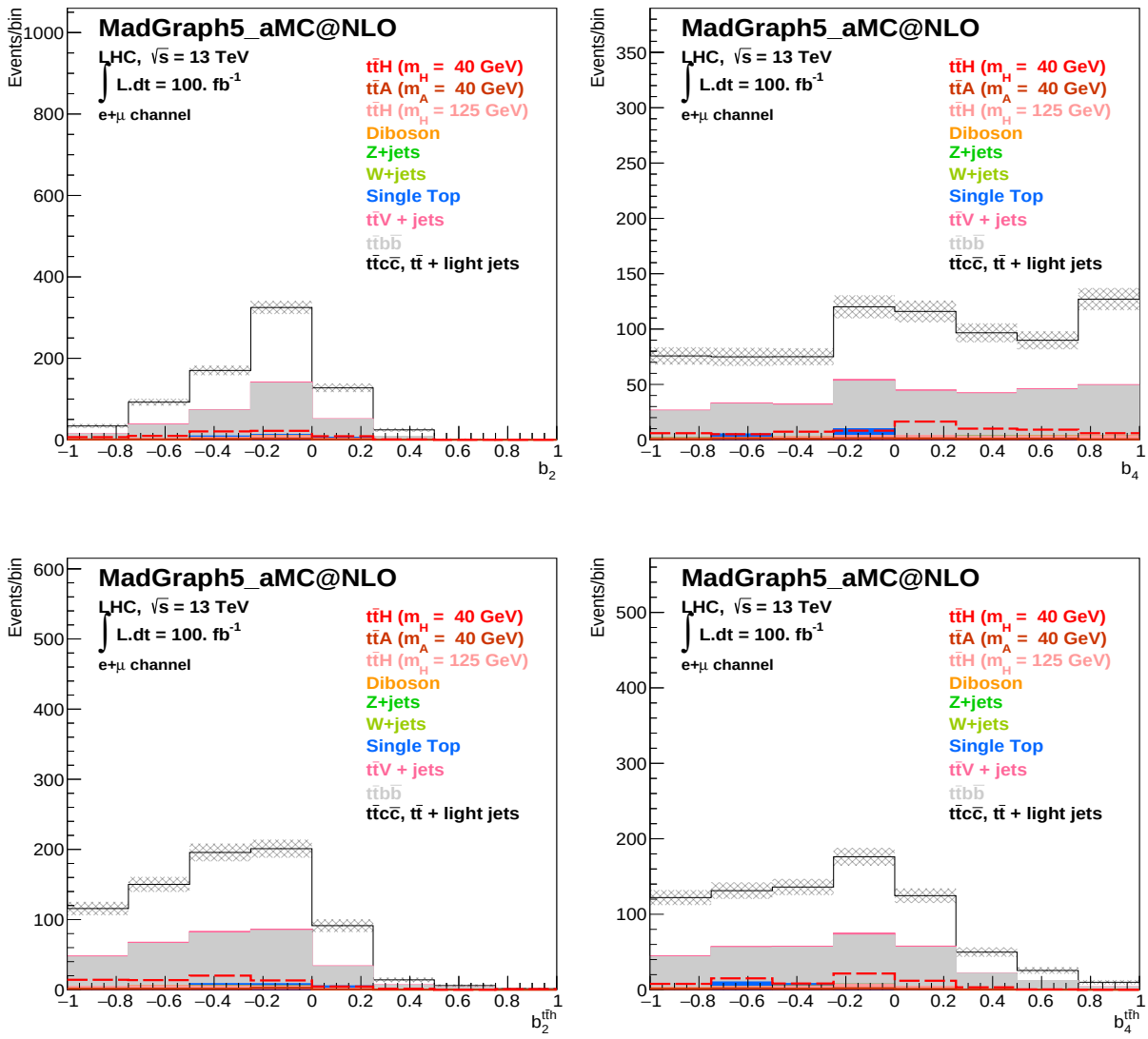

Figure 4.26: Expected number of background versus signal events with $m_h = 40$ GeV for the distributions b_2 (top left), b_4 (top right), $b_2^{t\bar{t}h}$ (bottom left) and $b_4^{t\bar{t}h}$ (bottom right), for a luminosity of 100 fb^{-1}. Reconstruction without TM and final selection cuts are considered.

4.9 Expected Confidence Levels in $t\bar{t}h$ production

In this section, Confidence Levels for $t\bar{t}h$ production in different scenarios are calculated, following the description in [81, 82]. We start by a brief explanation on how those Confidence Levels were computed, after which we show the results obtained for each of the scenarios that were studied.

The analysis of search results can be formulated in terms of a hypothesis test. Usually, the null hypothesis, H_0, is that the signal is absent (background only) and the alternative hypothesis, H_1, is that it exists. The goal is to exclude the alternative hypothesis in favor of the null hypothesis, with a certain degree of confidence.

The first step in defining an analysis of search results is to identify the observables in the experiment that we want to measure. In our case, we have considered the b_2 and b_4 variables, both in the LAB and

in the CM of the $t\bar{t}h$ system. The next step is to define a test-statistic or function of the observables and the model parameters that indicates which hypothesis is more compatible with the expected observations. The test-statistic that was chosen in this analysis is the likelihood ratio test, Q, which is defined as the ratio of probability densities of H_1 and H_0. This method is a good indicator of the compatibility between our data and our hypothesis since in the high-statistics limit the distribution of -2 ln Q converges to a χ^2 distribution.

The likelihood ratio for experiments with N_{chan} independent search channels, assuming that both the alternative and null hypotheses likelihoods are described by Poisson distributions, can be written as

$$Q = \prod_{i=1}^{N_{chan}} \frac{\frac{e^{-\lambda_{1i}}\lambda_{1i}^{n_i}}{n_i!}}{\frac{e^{-\lambda_{0i}}\lambda_{0i}^{n_i}}{n_i!}} = e^{-(\lambda_{1\text{tot}}-\lambda_{0\text{tot}})} \prod_{i=1}^{N_{chan}} \left(\frac{\lambda_{1i}}{\lambda_{0i}}\right)^{n_i}. \tag{4.26}$$

In Equation 4.26, n_i is the number of observed events in each channel assuming a certain hypothesis, and λ_{0i} and $\lambda_{0\text{tot}}$ (λ_{1i} and $\lambda_{1\text{tot}}$) are the number of predicted events per channel and in total, respectively, for the null (alternative) hypothesis. Thus, we have $\sum_{i=1}^{N_{chan}} \lambda_{0i} = \lambda_{0\text{tot}}$ and $\sum_{i=1}^{N_{chan}} \lambda_{1i} = \lambda_{1\text{tot}}$. The observed events are the ones seen in an actual experiment. In our case, they are generated randomly using the number of predicted events for a given hypothesis, i.e., the number of events after reconstruction with TM and additional cuts in that hypothesis. λ_{0i}, $\lambda_{0\text{tot}}$, λ_{1i} and $\lambda_{1\text{tot}}$ are already determined (see Figure 4.26 and Table 4.3) and fixed for a given exclusion scenario.

The logarithm of Equation 4.26 takes the form

$$\ln Q = -(\lambda_{1\text{tot}} - \lambda_{0\text{tot}}) + \sum_{i=1}^{N_{chan}} n_i \ln\left(\frac{\lambda_{1i}}{\lambda_{0i}}\right). \tag{4.27}$$

Computing the logarithm of the likelihood for H_1, we have

$$\ln L(H_1) = \ln \prod_{i=1}^{N_{chan}} \frac{e^{-\lambda_{1i}}\lambda_{1i}^{n_i}}{n_i!}. \tag{4.28}$$

With $p_i = \lambda_{1i}/\lambda_{1\text{tot}}$ and $\sum_{i=1}^{N_{chan}} n_i = n_{\text{tot}}$, we get

$$\begin{aligned} \ln L(H_1) &= \sum_{i=1}^{N_{chan}} (n_i \ln p_i + n_i \ln \lambda_{1\text{tot}} - p_i\lambda_{1\text{tot}} - \ln n_i!) \\ &= \sum_{i=1}^{N_{chan}} (n_i \ln p_i) + (n_{\text{tot}} \ln \lambda_{1\text{tot}} - \lambda_{1\text{tot}}) - \sum_{i=1}^{N_{chan}} \ln n_i!. \end{aligned} \tag{4.29}$$

The first term in the bottom line of Equation 4.29 depends on the shape of the distributions (number of events in each bin). The second and third terms, where no summation exists, depend only on the total number of observed and predicted events. Both the shape and total number of events are considered for the calculation of the Confidence Levels.

After the test-statistic is defined, the last step consists in specifying a CL above which we decide to exclude our alternative hypothesis. In particle physics, that CL is 2σ for exclusion, and 5σ for discovery. The Confidence Level is defined as a function of the test-statistic by

$$CL = P\left(Q \geq Q_{obs} | \, H_1\right), \tag{4.30}$$

where Q_{obs} is the value observed for the test-statistic assuming the null hypothesis and

$$P\left(Q \geq Q_{obs} | \, H_1\right) = \int_{Q_{obs}}^{\infty} \frac{dP(Q|H_1)}{dQ} dQ. \tag{4.31}$$

This is the probability that $Q \geq Q_{\text{obs}}$, i.e. that we observe a value of Q equal or more extreme than Q_{obs}. In Equation 4.31, $dP(Q|H_1)/dQ$ is the probability distribution function of the test-statistic according to the alternative hypothesis. If 1 - CL $\leq \alpha$, where α is the significance level of the test, we claim that for a given null hypothesis, the alternative hypothesis is excluded with a Confidence Level of CL$\times 100\%$.

Now that the CLs are defined, we will show the results for the hypotheses studied. Four different scenarios were considered:

- Scenario 1: Exclusion of the SM plus a new CP-even scalar particle, assuming the SM. In this case, H_0 is the SM only hypothesis[10], while H_1 is the SM plus a new CP-even signal hypothesis.
- Scenario 2: Exclusion of the SM plus a new CP-odd scalar particle, assuming the SM. In this case, H_0 is the SM only hypothesis, while H_1 is the SM plus a new CP-odd signal hypothesis.
- Scenario 3: Exclusion of the SM plus a new CP-odd scalar particle, assuming the SM plus a new CP-even scalar particle of the same mass. In this case, H_0 is the SM plus a new CP-even signal hypothesis, while H_1 is the SM plus a new CP-odd signal hypothesis.
- Scenario 4: SM exclusion, assuming the SM plus a new CP-even scalar particle. In this case, H_0 is the SM plus a new CP-even signal hypothesis, while H_1 is the SM only hypothesis.

For each scenario, 1.000.000 pseudo-experiments were simulated for both the null and alternative hypotheses. In each pseudo-experiment, the number of observed events is randomly generated, bin-by-bin, according to a Poisson distribution. That distribution has a mean value equal to the predicted number of events for each bin according to the assumed hypothesis. This gives us the value of n_i per bin. Furthermore, the value of $\ln Q$ is computed and used to construct $dP(Q|H_1)/dQ$ and $dP(Q|H_0)/dQ$. The latter is the probability distribution function of the test-statistic according to H_0. The value of $\ln Q_{\text{obs}}$ is taken as the median of $dP(Q|H_0)/dQ$. The values of the median $\pm 1\sigma$ of $dP(Q|H_0)/dQ$ were also determined and used to estimate the statistical uncertainty of the CLs computed. This is depicted in Figure 4.27.

Figure 4.28 to Figure 4.31 show the expected Confidence Levels, for all four scenarios, and different Higgs masses. In each plot, different observables are presented, as a function of the integrated luminosity. Only statistical uncertainties are considered. In Figure 4.28 (scenario 1), we conclude that the luminosity to achieve a certain CL increases with the scalar boson mass. For instance, $m_H = 40$ GeV requires roughly 500 fb^{-1} and 1400 fb^{-1} less luminosity to achieve CL$= 2\sigma$ when compared with $m_H = 120$ GeV and $m_H = 160$ GeV, respectively. This is consistent with the decrease of the $t\bar{t}H$ cross section with said mass (see Figure 4.25), which in this case leads to a smaller signal to background ratio and smaller CLs for larger Higgs masses. We exclude the existence of the CP-even hypothesis for the first two CP-even Higgs masses, with a Confidence Level that exceeds 2σ given the current LHC luminosity. CP-even Higgs masses above 200 GeV cannot be excluded in our analysis. Similar results are seen in Figure 4.31 (scenario 4). Exclusion of the SM-only hypothesis is possible with a 5σ CL for the three lighter h boson masses.

Figure 4.29 (scenario 2) shows that the Confidence Levels are different for the CP-odd case, compared to the CP-even case. The luminosity for CP-odd exclusion at a given CL is higher for lighter CP-odd

[10]Consisting of diboson, Z + jets, W + jets, single top, $t\bar{t}$V + jets, $t\bar{t}b\bar{b}$, $t\bar{t}c\bar{c}$, $t\bar{t}$ + light jets and $t\bar{t}H$ (m_H = 125 GeV) events.

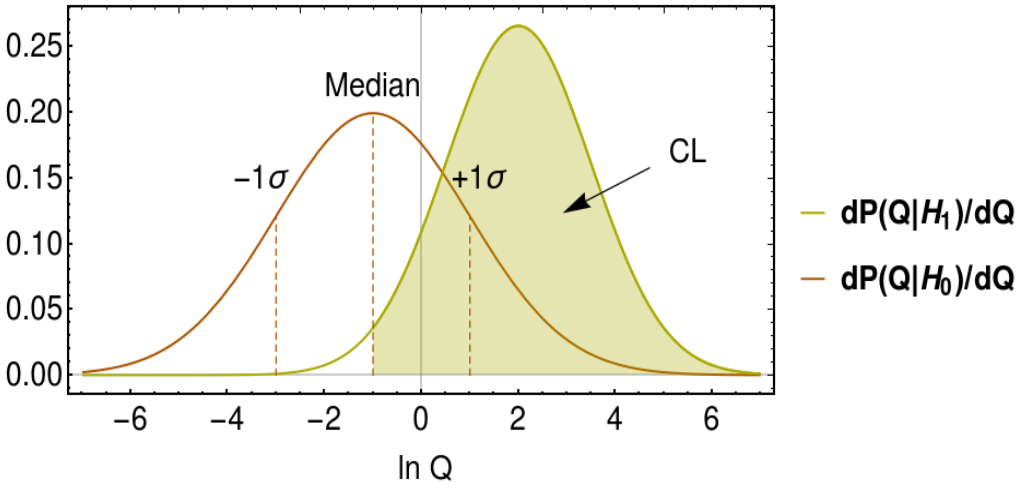

Figure 4.27: Representation of the calculation of the CLs. The distributions shown here are merely for illustration purposes, and do not correspond to the actual probability distributions.

Higgs masses. However, for $m_A > 160$ GeV, the opposite is observed since the cross section of $t\bar{t}A$ relative to $t\bar{t}H$ is much larger (see Table 4.1). For $t\bar{t}A$ events with $m_A = 40$ GeV, the CL for each luminosity is lower relative to the heavier CP-odd Higgs masses, despite its cross section being larger. This happens because the decrease of the cross section with the scalar boson mass is smoother for the CP-odd case in comparison to the CP-even case, being compensated by an increase in the number of events that go through reconstruction for larger Higgs masses[11]. This is why we have more $t\bar{t}A$ events after reconstruction for heavier CP-odd Higgs masses (see Table 4.3). Finally, in Figure 4.30 (scenario 3), we show that if a new scalar assumed to be CP-even is found, CP-odd exclusion is possible for the Higgs masses considered, except for $m_h = 160$ GeV. This happens because both hypotheses for this case have almost the same number of events distributed similarly in the variables considered, which degrades the sensitivity for exclusion.

A summary of the above conclusions is presented in Figure 4.32. Each plot shows the luminosity required to surpass a given CL (2σ for the first three scenarios, and 5σ for scenario 4). If no points are shown, that is because, even for $\mathcal{L} = 3000$ fb^{-1}, exclusion is not possible.

[11] Since a heavier Higgs tends do decay into more energetic b-quarks, the percentage of events accepted after applying the cuts on the jets p_T is normally higher for larger scalar boson masses (see appendix E). Thus, we end up with more events that may be reconstructed for $t\bar{t}A$.

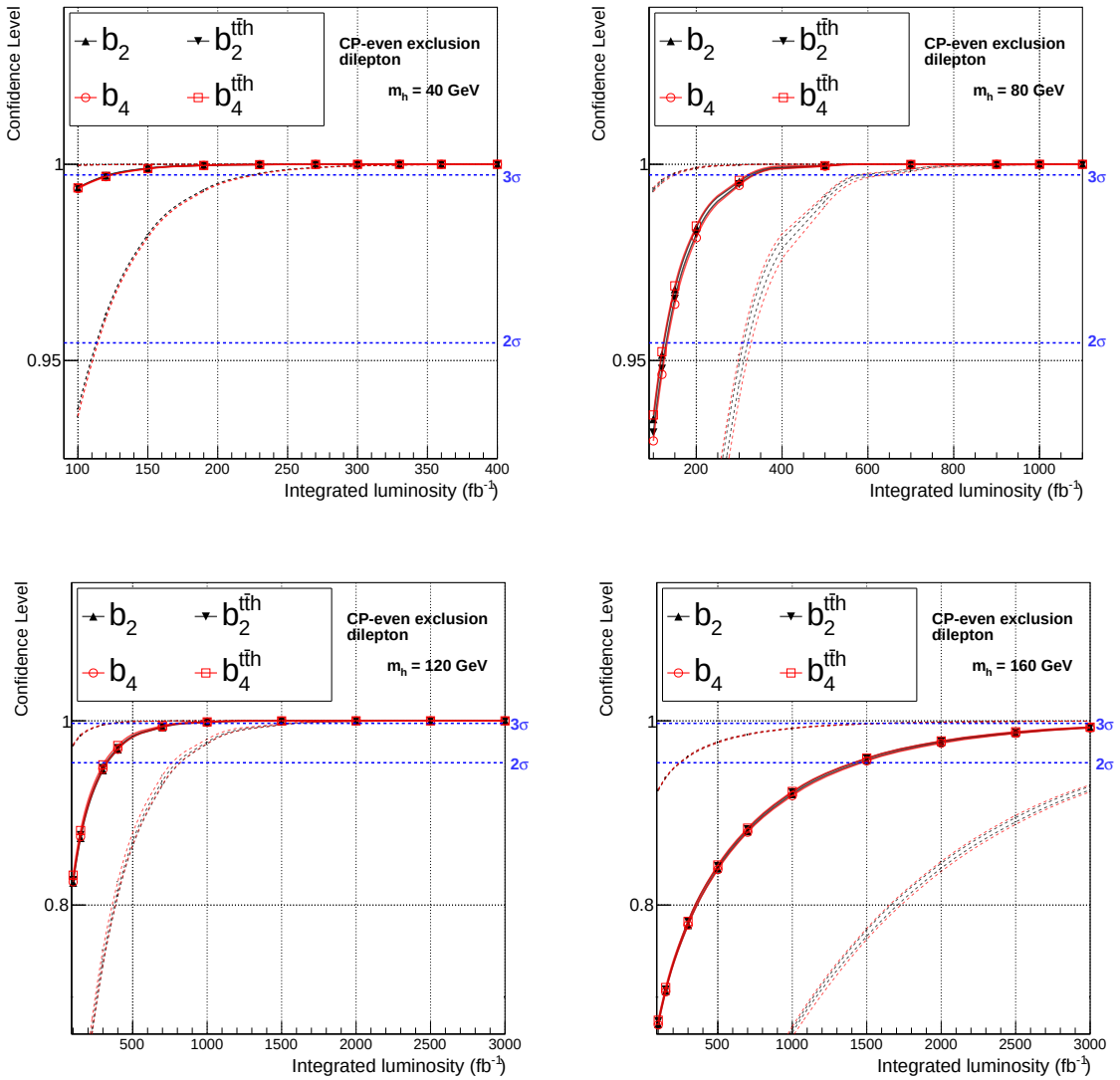

Figure 4.28: Expected CLs for CP-even exclusion assuming the SM (scenario 1), as a function of the integrated luminosity. The luminosity is increased until CL$= 1$ or $\mathcal{L} = 3000$ fb^{-1}. Each plot represents a different h boson mass. The vertical axis scale also changes, for visualization purposes. The red and black dashed lines represent the $\pm 1\sigma$ bands for the variables considered. The blue dashed lines represent the 2σ or 3σ CL lines.

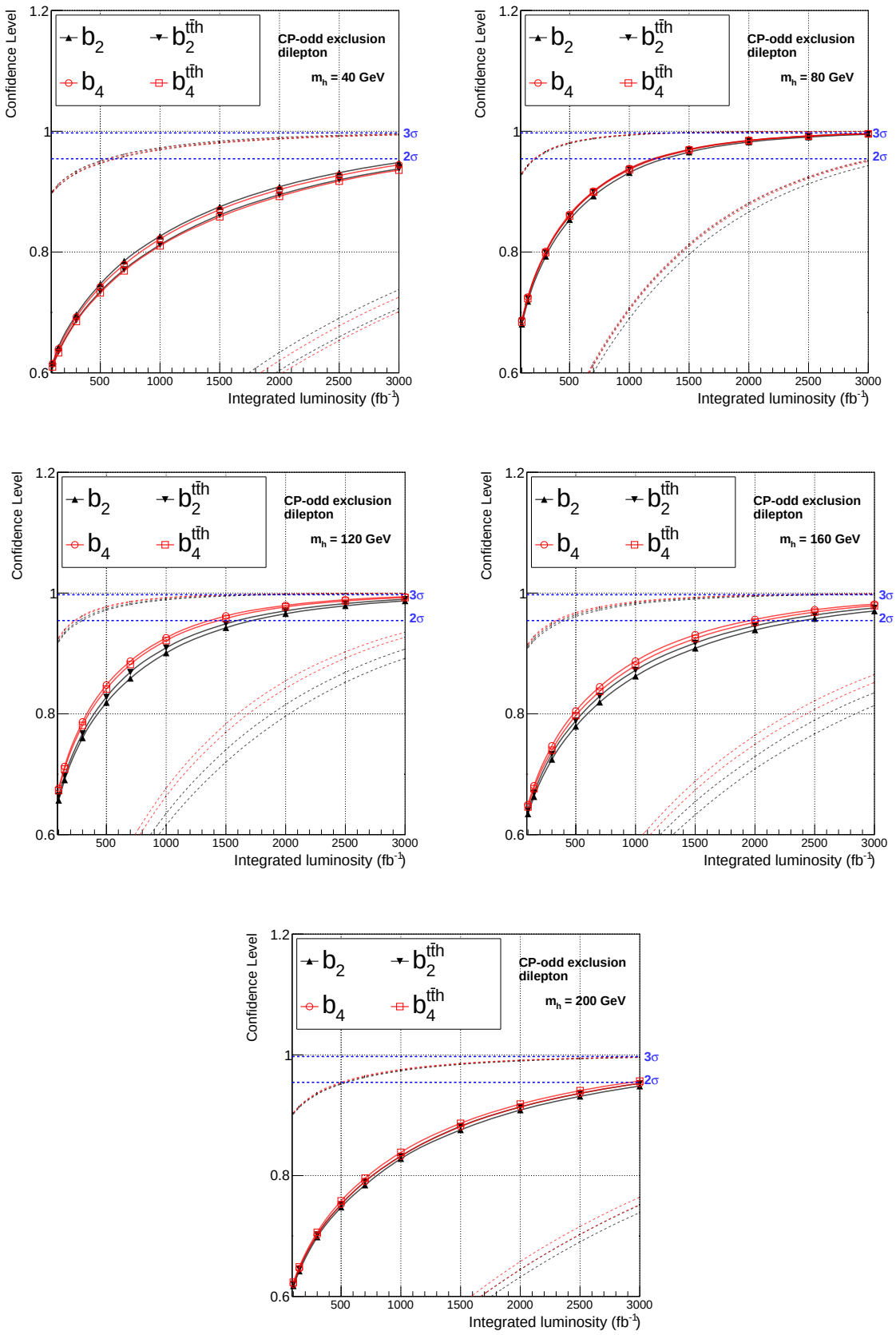

Figure 4.29: Expected CLs for CP-odd exclusion assuming the SM (scenario 2), as a function of the integrated luminosity.

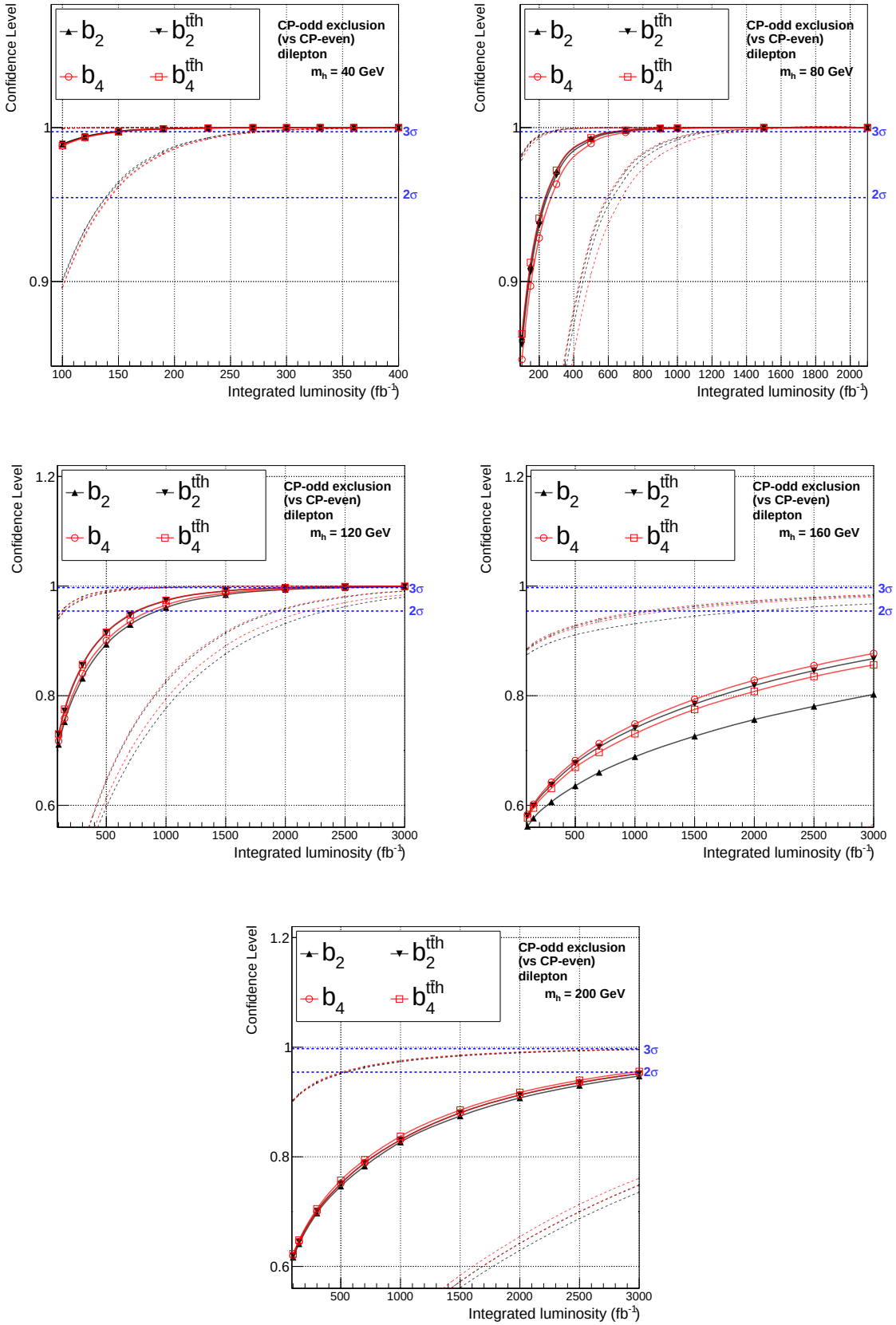

Figure 4.30: Expected CLs for CP-odd exclusion assuming the SM plus a new CP-even scalar particle (scenario 3), as a function of the integrated luminosity.

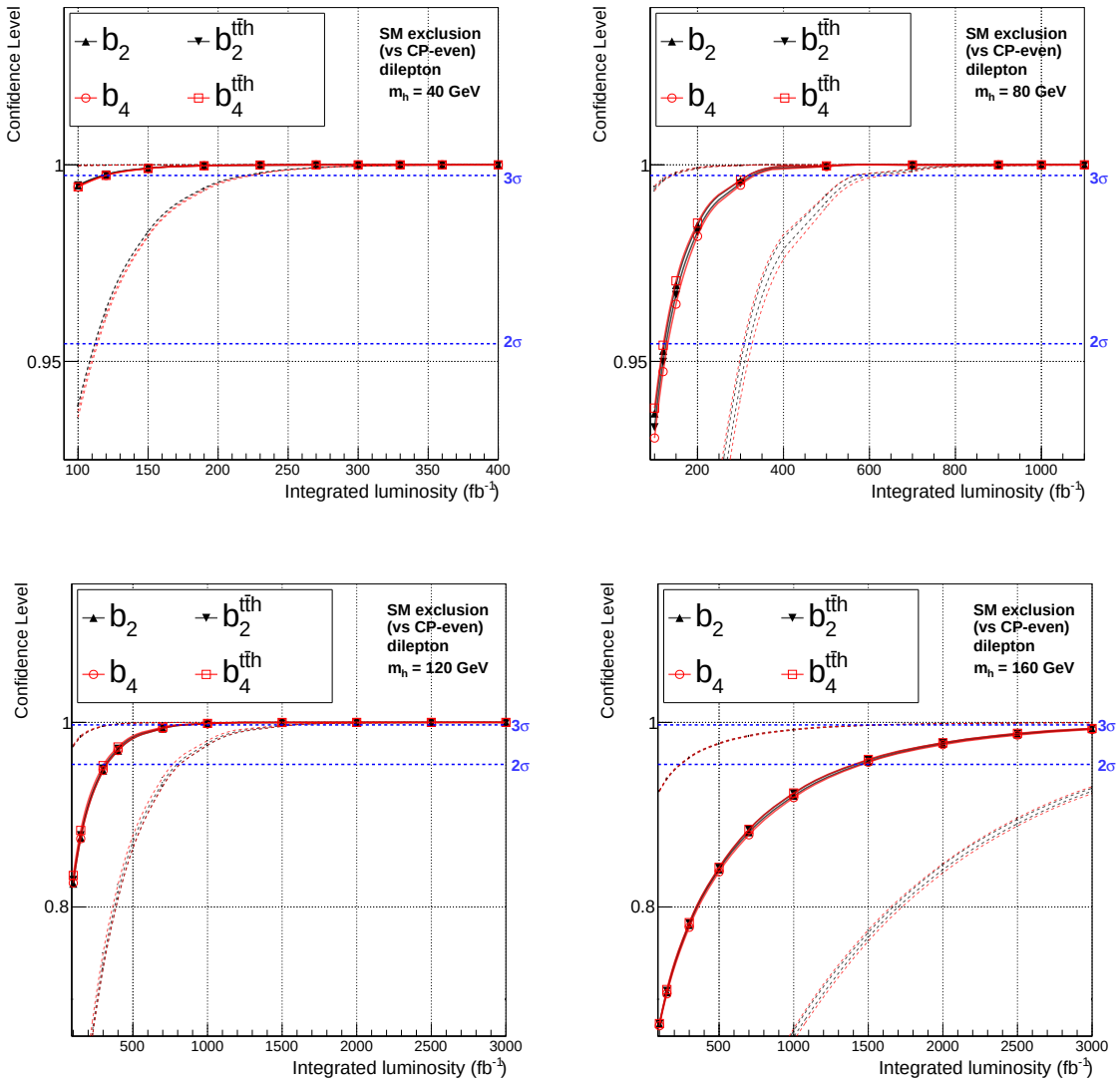

Figure 4.31: Expected CLs for SM exclusion assuming the SM plus a new CP-even scalar particle (scenario 4), as a function of the integrated luminosity.

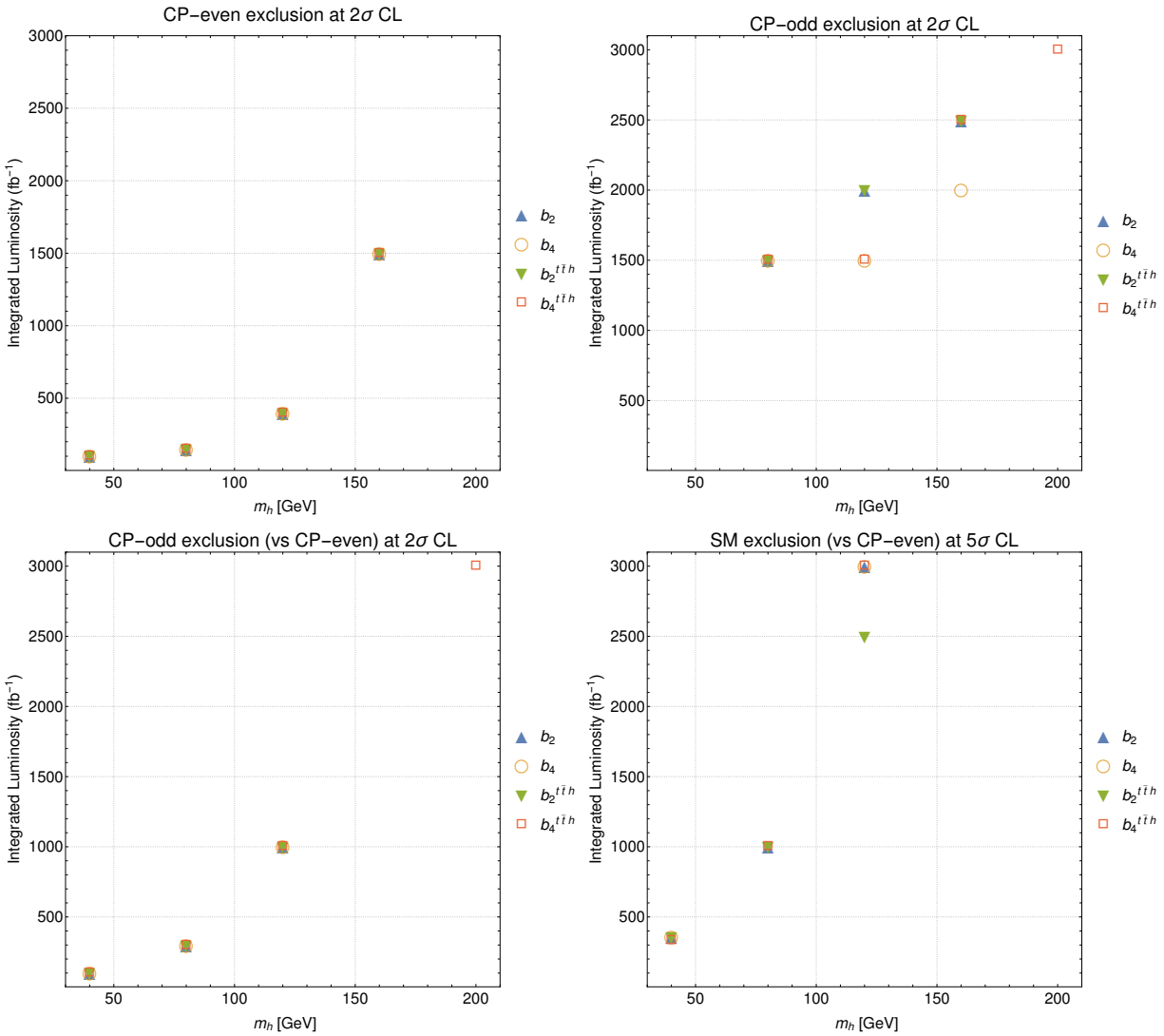

Figure 4.32: Luminosity needed to exclude scenarios 1 (top left), 2 (top right) and 3 (bottom left) at the 2σ level, and scenario 4 (bottom right) at the 5σ level, as a function of the scalar boson mass.

4.10 The C2HDM revisited

The C2HDM was introduced in section 3.4. Now, we want to understand how a measurement or an exclusion for a given Higgs mass, such as the ones presented in the last section, affects the allowed parameter space of this model.

We will consider H_2 to be the 125 GeV Higgs, while $m_{H_1} < 125$ GeV. In the C2HDM, there are four types of Yukawa models that preserve an exact $\mathbb{Z}_2$ symmetry to suppress FCNCs at tree level. In all four, the top Yukawa couplings are equal (see Table 3.3). Hence, this discussion is valid for all of them. The Yukawa Lagrangian for the top, with $H_i = H_1$, is given by

$$\mathcal{L}_{\text{Yukawa}}^{\text{top}} = -\frac{m_f}{v}\bar{t}\left[\frac{s_1 c_2}{s_\beta} - i\frac{s_2}{t_\beta}\gamma_5\right] t H_1. \tag{4.32}$$

Comparing Equation 4.32 and Equation 4.1, with $H_1 = h$, we get the following conditions:

$$\begin{cases} \kappa_{ht\bar{t}} \cos\alpha = \dfrac{s_1\, c_2}{s_\beta} \\ \kappa_{ht\bar{t}} \sin\alpha = -\dfrac{s_2}{t_\beta} \end{cases} \qquad s_\beta^2 \kappa_{ht\bar{t}}^2 = s_1^2 c_2^2 + s_2^2 c_\beta^2. \tag{4.33}$$

As no new scalar was found, both $\kappa_{ht\bar{t}}$ and α are free to vary in the range that we choose. These are the parameters that will be measured or constrained experimentally. The limits in this work were set for the pure scalar and pure pseudoscalar scenarios. For these scenarios we get, respectively,

$$\begin{cases} \sin\alpha = 0 \implies \kappa_{ht\bar{t}} = \pm\dfrac{s_1}{s_\beta} \\ \cos\alpha = 0 \implies \kappa_{ht\bar{t}} = \pm\dfrac{s_2}{t_\beta}\ (\text{if } s_1 = 0) \quad \text{or} \quad \kappa_{ht\bar{t}} = \pm\dfrac{1}{t_\beta}\ (\text{if } c_2 = 0)\,. \end{cases} \tag{4.34}$$

Thus, a limit set on $\kappa_{ht\bar{t}}$ constrains the parameters of the model. For the case $\cos\alpha = 0$ and $c_2 = 0$, $\kappa_{ht\bar{t}}$ only depends on t_β. Because t_β is already constrained to be above one by low energy physics measurements [19], we would have $\kappa_{ht\bar{t}} \leq 1$. Besides, because an exclusion for $\kappa_{ht\bar{t}} > 1$ is expected to be easier, i.e., to require less luminosity for a given CL, we are interested in the limits set for $\kappa_{ht\bar{t}} \leq 1$. For instance, if $\kappa_{ht\bar{t}} \leq 1/2$, we get for the pure pseudoscalar limit $\tan\beta \geq 2$ ($c_2 = 0$) and $s_2 \leq t_\beta/2$ ($s_1 = 0$), and for the pure scalar limit we have $s_1 \leq 1/2$ ($s_2 = 0$). In Figure 4.33 we present the luminosity needed to exclude $\kappa_{ht\bar{t}}$ at the 2σ level for the scenario of exclusion of a new CP-even scalar particle with a mass of 40 GeV (scenario 1). This is the best of all scenarios for exclusion. We can exclude $\kappa_{ht\bar{t}}$ above 0.4 by the end of the LHC run. Smaller values of $\kappa_{ht\bar{t}}$ will require to consider more $t\bar{t}h$ decay channels.

As we can see in Equation 4.33, the CP-even limit is obtained for $\sin\alpha = 0$, which is equivalent to $\sin\alpha_2 = 0$ in the C2HDM. In order to see how $\sin\alpha_2$ changes when $\sin\alpha$ is well constrained, the constraints on the parameter space in scenarios where one is either close to the CP-even or to the CP-odd limits were studied. In Figure 4.34 we present the allowed points in the C2HDM parameter space (c_1 vs. s_2), for the case where we are close to the CP-even limit. We vary the values of $\kappa_{ht\bar{t}}$, $\sin\alpha$ and $\tan\beta$ in the ranges $0.1 \leq \kappa_{ht\bar{t}} \leq 1.2$, $0.1 \leq \sin\alpha \leq 0.2$ and $1 \leq \tan\beta \leq 10$. In the left plot we see the variation with $\kappa_{ht\bar{t}}$, in the middle with $\sin\alpha$ and on the right with $\tan\beta$. In Figure 4.35 we present the limit where we are close to the CP-odd case, with $0.8 \leq \sin\alpha \leq 0.9$. Even though $\sin\alpha$ only changes by 0.1 in both cases, the allowed values for $\sin\alpha_2$ are quite dispersed, and depend on the values of both $\kappa_{ht\bar{t}}$ and

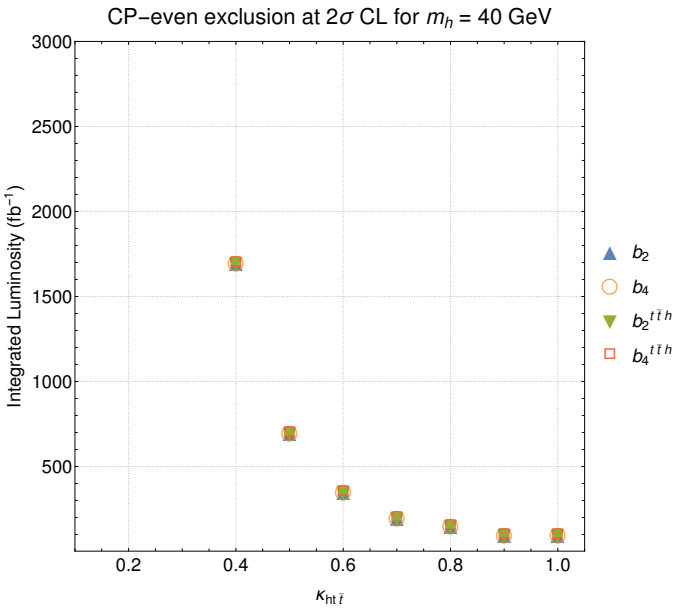

Figure 4.33: Luminosity needed to exclude $\kappa_{ht\bar{t}}$ at the 2σ level for the pure CP-even case (scenario 1) for a mass of 40 GeV.

$\tan\beta$. Thus, the allowed parameter space of the C2HDM is quite large and we need some other sources of measurement to constraint it. To be clear, no other theoretical/experimental constraints for the C2HDM were taken into consideration other than the ones already stated.

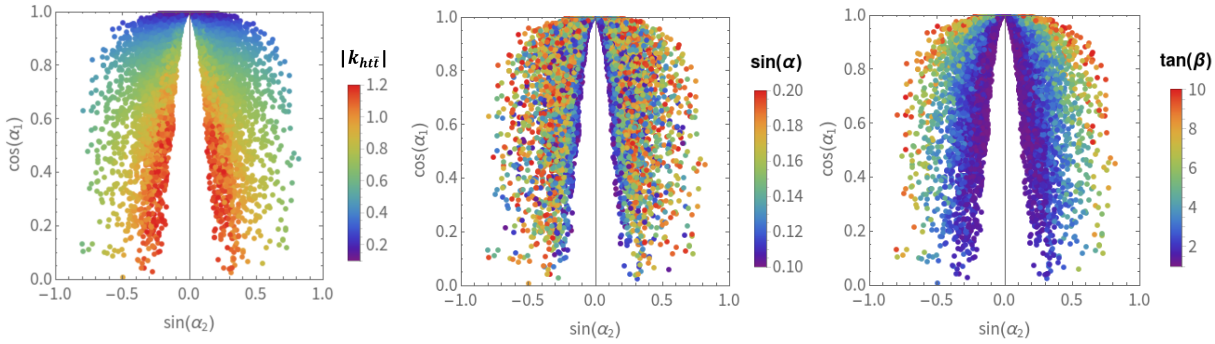

Figure 4.34: Points allowed in the plane c_1 vs. s_2 of the C2HDM for $0.1 \leq \kappa_{ht\bar{t}} \leq 1.2$ and $0.1 \leq \sin\alpha \leq 0.2$ and $1 \leq \tan\beta \leq 10$. In the left plot we see the variation with $\kappa_{ht\bar{t}}$, in the middle with $\sin\alpha$ and on the right with $\tan\beta$.

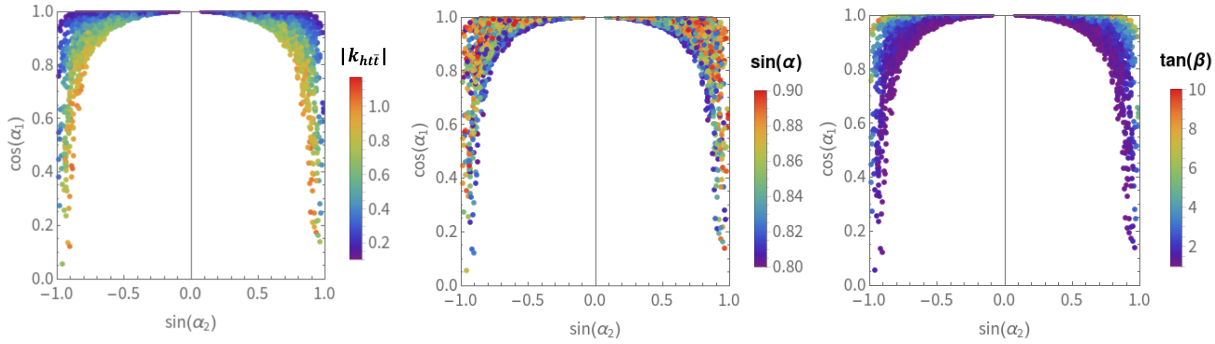

Figure 4.35: Points allowed in the plane c_1 vs. s_2 of the C2HDM for $0.1 \leq \kappa_{ht\bar{t}} \leq 1.2$ and $0.8 \leq \sin\alpha \leq 0.9$ and $1 \leq \tan\beta \leq 10$. In the left plot we see the variation with $\kappa_{ht\bar{t}}$, in the middle with $\sin\alpha$ and on the right with $\tan\beta$.

Chapter 5

Conclusion

The original motivation for this study was to examine the possibility to determine the CP-structure of the bottom quark Yukawa interaction with the discovered Higgs in $b\bar{b}h$ production. In particular, we wanted to see if a pure CP-even Higgs could be distinguished from a pure CP-odd one. We found that strategies suggested in the literature for this determination in the case of the top quark do not work for the bottom quark. This was also confirmed for very light Higgs bosons with masses of 10 GeV, and for the single bottom and Higgs associated production. The underlying reason for these observations is that the differences between CP-even and CP-odd components are proportional to m_f^2, and will only be meaningful when the fermion mass is of the same order of magnitude as m_h.

Previous works established that several kinematic distributions for $t\bar{t}h$ are indeed sensitive to the CP-components of the top Yukawa coupling. While these studies assumed $m_h = 125$ GeV, a study of its applicability to other Higgs masses was missing. In this thesis, we investigate the dilepton final states of the $t\bar{t}h$ (with $h = H, A$) for scalar boson masses up to 500 GeV. We found that for the h boson masses considered, there is still a good level of discrimination between scalar and pseudoscalar Yukawa interactions, at parton level. However, the differences between those states become smaller as the Higgs mass increases, and vanish around $m_h = 450$ GeV.

After the parton level study we proceeded to a full reconstruction of the $t\bar{t}h$ events. Confidence levels are presented for the exclusion of several scenarios as a function of the luminosity, for different Higgs masses. It is shown that the required luminosity for exclusion at a given CL increases with the scalar boson mass. Given the current LHC luminosity of 150 fb^{-1}, exclusion of a pure CP-even Higgs with masses below 80 GeV, assuming SM-like Higgs couplings, is already possible. For $m_H > 200$ GeV, that same exclusion is not possible. We also found that CP-odd exclusion, again assuming SM-like Higgs couplings, is harder than CP-even exclusion for h boson masses up to 160 GeV. For higher masses, the opposite is true. Additionally, if a new Higgs is found, we have enough sensitivity to exclude the possibility of said scalar being purely CP-odd in the explored Higgs mass range. Furthermore, we have set a lower limit for $\kappa_{ht\bar{t}}$ of $\kappa_{ht\bar{t}} = 0.4$, for exclusion of a new CP-even scalar with a mass of 40 GeV (scenario 1), at the 2σ level. For the limits where we are close to the CP-even or CP-odd cases, we saw that the allowed parameter space of the C2HDM is quite large and that other measurements to constrain it are necessary.

A natural follow up to the work developed in this thesis would be to study how the confidence levels change as a function of the CP-phase. Another possibility is to combine several $t\bar{t}h$ decay channels, which should further improve the results obtained.

Bibliography

[1] Ellis, John (2002). "Physics gets physical (correspondence)". Nature. 415 (6875): 957. Bibcode:2002Natur.415..957E. doi:10.1038/415957b. PMID 11875539.

[2] Newton, Isaac, Philosophiae Naturalis Principia Mathematica ("Mathematical Principles of Natural Philosophy"), London, 1687; Cambridge, 1713; London, 1726.

[3] Maxwell, James Clerk (1865). "A dynamical theory of the electromagnetic field". Philosophical Transactions of the Royal Society of London. 155: 459–512. doi:10.1098/rstl.1865.0008.

[4] Einstein, Albert (1916). "Die Grundlage der allgemeinen Relativitätstheorie" [The Foundation of the General Theory of Relativity] (PDF). Annalen der Physik (in German). 354 (7): 769–822. Bibcode:1916AnP...354..769E. doi:10.1002/andp.19163540702.

[5] Pati, J.; Salam, A. (1974). "Lepton Number as the Fourth Color". Physical Review D. 10 (1): 275–89. Bibcode:1974PhRvD..10..275P. doi:10.1103/PhysRevD.10.275.

[6] S. L. Glashow, "Partial-symmetries of weak interactions," Nuclear Physics 22 no. 4, (1961) 579 – 588. http://www.sciencedirect.com/science/article/pii/0029558261904692.

[7] S. Weinberg, "A Model of Leptons," Phys. Rev. Lett. 19 (Nov, 1967) 1264–1266. http://link.aps.org/doi/10.1103/PhysRevLett.19.1264.

[8] A. Salam, "Weak and Electromagnetic Interactions," Conf. Proc. C680519 (1968) 367–377.

[9] G. Aad et al. [ATLAS Collaboration], Phys. Lett. B 716 (2012) 1, arXiv:1207.7214 [hep-ex].

[10] S. Chatrchyan et al. [CMS Collaboration], Phys. Lett. B 716 (2012) 30, arXiv:1207.7235 [hep-ex].

[11] P.W. Higgs, Phys. Rev. Lett. 13 (1964) 508; ibid. Phys. Rev. 145 (1966) 1156; F. Englert and R. Brout, Phys. Rev. Lett. 13 (1964) 321; G.S. Guralnik, C.R. Hagen and T. Kibble, Phys. Rev. Lett. 13 (1965) 585.

[12] M. Tanabashi et al. (Particle Data Group), Phys. Rev. D 98, 030001 (2018) and 2019 update.

[13] S. Bifani, S. Descotes-Genon, A. Romero Vidal, and M.-H. Schune, "Review of Lepton Universality tests in B decays," J. Phys. G46 no. 2, (2019) 023001, arXiv:1809.06229 [hep-ex].

[14] V. Khachatryan et al. [CMS Collaboration], Phys. Rev. D 92 (1) 012004 (2015), arXiv:1411.3441 [hep-ex].

[15] V. Khachatryan et al. [CMS Collaboration], Phys. Lett. B 759, 672 (2016), arXiv:1602.04305 [hep-ex].

[16] G. Aad et al. [ATLAS Collaboration], Eur. Phys. J. C 75 (10) 476 (2015), Erratum: [Eur. Phys. J. C 76 (3) 152 (2016)], arXiv:1506.05669 [hep-ex].

[17] A. D. Sakharov, "Violation of CP Invariance, c Asymmetry, and Baryon Asymmetry of the Universe," Pisma Zh. Eksp. Teor. Fiz. 5 (1967) 32–35. [Usp. Fiz. Nauk161,61(1991)].

[18] M. Persic and P. Salucci, "The baryon content of the Universe," Monthly Notices of the Royal Astronomical Society 258 no. 1, (1992) 14P–18P, http://mnras.oxfordjournals.org/content/258/1/14P.full.pdf+html. http://mnras.oxfordjournals.org/content/258/1/14P.abstract.

[19] D. Fontes, M. Mühlleitner, J. C. Romão, R. Santos, J. P. Silva, and J. Wittbrodt, The C2HDM revisited, JHEP 1802, 073 (2018) [arXiv:1711.09419 [hep-ph]].

[20] M. Thomson, "Modern Particle Physics", Cambridge University Press, (2013).

[21] L. O'Raifeartaigh and N. Straumann, Gauge Theory: Historical Origins and Some Modern Developments. Rev. Mod. Phys. 72, 1-23 (2000).

[22] M. E. Peskin and D. V. Schroeder, An Introduction to quantum field theory. Advanced book program. Westview Press Reading (Mass.), 1995.

[23] https://journals.aps.org/pr/pdf/10.1103/PhysRev.105.1413.

[24] Drewes, Marco (2013). "The phenomenology of right handed neutrinos". International Journal of Modern Physics E. 22 (8): 1330019–593. arXiv:1303.6912. Bibcode:2013IJMPE..2230019D. doi:10.1142/S0218301313300191.

[25] CMS Collaboration, D. Pedrini, "Search for the flavour-changing neutral current decay $D^0 \to \mu^+\mu^-$ in pp collisions at $\sqrt{s} = 7$ TeV with CMS," in Proceedings, 5th International Workshop on Charm Physics (Charm 2012). 2012. arXiv:1208.5908 [hep-ex].

[26] ATLAS, CDF, CMS, D0 Collaboration, E. Yazgan, "Flavor changing neutral currents in top quark production and decay," in 6th International Workshop on Top Quark Physics (TOP2013) Durbach, Germany, September 14-19, 2013, pp. 285–294. 2014. arXiv:1312.5435 [hep-ex].

[27] Y. Nambu, Spontaneous symmetry breaking in particle physics: a case of cross fertilization, The Nobel Foundation (2008).

[28] J. Goldstone, Field Theories with Superconductor Solutions, Nuovo Cim. 19 (1961) 154–164. doi:10.1007/BF02812722.

[29] J. Goldstone, A. Salam, S. Weinberg, Broken Symmetries, Phys. Rev. 127 (1962) 965–970. doi:10.1103/PhysRev.127.965.

[30] J. F. Gunion, H. E. Haber, G. L. Kane, and S. Dawson, "The Higgs Hunter's Guide," Front. Phys. 80 (2000) 1–448.

[31] I. P. Ivanov, Building and testing models with extended Higgs sectors, Prog. Part. Nucl. Phys. 95, 160 (2017) [arXiv:1702.03776 [hep-ph]].

[32] Weinberg, Steven (1973). "General Theory of Broken Local Symmetries". Physical Review D. 7 (4): 1068–1082. Bibcode:1973PhRvD...7.1068W. doi:10.1103/PhysRevD.7.1068.

[33] R.N. Mohapatraet al., Rep. Prog. Phys. 70, 1757 (2007).

[34] G. C. Branco, L. Lavoura, J. P. Silva, CP Violation, Int. Ser. Monogr. Phys. 103 (1999) 1–536.

[35] M. Kobayashi and T. Maskawa, "CP Violation in the Renormalizable Theory of Weak Interaction," Prog. Theor. Phys. 49 (1973) 652–657.

[36] Christenson, J. H.; Cronin, J. W.; Fitch, V. L.; Turlay, R. (1964). "Evidence for the 2π Decay of the K_2^0 Meson System". Physical Review Letters. 13 (4): 138. Bibcode:1964PhRvL..13..138C. doi:10.1103/PhysRevLett.13.138.

[37] J. F. Gunion, H. E. Haber, Higgs Bosons in Supersymmetric Models. 1., Nucl. Phys. B 272 (1986) 1, [Erratum: Nucl. Phys. B 402, 567 (1993)]. doi:10.1016/0550-3213(86)90340-8, 10. 1016/0550-3213(93)90653-7.

[38] T. D. Lee, A Theory of Spontaneous T Violation, Phys. Rev. D 8 (1973) 1226–1239, [,516(1973)]. doi:10.1103/PhysRevD.8.1226.

[39] M. Trodden, "Electroweak baryogenesis," Rev. Mod. Phys. 71 (1999) 1463–1500, arXiv:hep-ph/9803479 [hep-ph].

[40] Planck Collaboration, P. A. R. Ade et al., "Planck 2013 results. I. Overview of products and scientific results," Astron. Astrophys. 571 (2014) A1, arXiv:1303.5062 [astro-ph.CO].

[41] A. Belyaev, G. Cacciapaglia, I. P. Ivanov, F. Rojas-Abatte, and M. Thomas, Anatomy of the Inert Two Higgs Doublet Model in the light of the LHC and non-LHC Dark Matter Searches, Phys. Rev. D 97 (2018), no. 3 035011, [1612.00511].

[42] G. C. Branco, P. M. Ferreira, L. Lavoura, M. N. Rebelo, M. Sher, and J. P. Silva, "Theory and phenomenology of two-Higgs-doublet models," Phys. Rept. 516 (2012) 1–102, arXiv:1106.0034 [hep-ph].

[43] M. Maniatis, A. von Manteuffel, O. Nachtmann, and F. Nagel, Eur. Phys. J. C 48 (2006) 805 [hep-ph/0605184].

[44] P. M. Ferreira, R. Santos and A. Barroso, Phys. Lett. B603 (2004) 219; Erratum, Phys. Lett. B629 (2005) 114.

[45] A. Barroso, P. M. Ferreira, and R. Santos, Phys. Lett. B632, 684 (2006), hep-ph/0507224.

[46] M. Krause, On the Renormalization of the Two-Higgs-Doublet Model, Master's thesis, KIT, Karlsruhe, ITP, 2016.

[47] F. J. Botella and J. P. Silva, Phys. Rev. D 51, 3870 (1995).

[48] A. Pich, P. Tuzon, Yukawa Alignment in the Two-Higgs-Doublet Model, Phys. Rev. D 80 (2009) 091702. arXiv:0908.1554, doi:10.1103/PhysRevD.80.091702.

[49] I. F. Ginzburg, M. Krawczyk, and P. Osland, Two Higgs doublet models with CP violation, in Linear colliders. Proceedings, International Workshop on physics and experiments with future electron-positron linear colliders, LCWS 2002, Seogwipo, Jeju Island, Korea, August 26-30, 2002, pp. 703–706, 2002, hep-ph/0211371, [,703(2002)].

[50] A. Barroso, P. M. Ferreira, R. Santos, and J. P. Silva, Phys. Rev. D86, 015022 (2012), 1205.4247.

[51] D. Fontes et al., JHEP 1506, 060 (2015), arXiv:1502.01720 [hep-ph].

[52] D. Fontes, M. Mühlleitner, J. C. Romão, R. Santos, J. P. Silva and J. Wittbrodt, Couplings of the C2HDM: http://porthos.tecnico.ulisboa.pt/arXiv/C2HDM/, October, 2017.

[53] P. S. Bhupal Dev, A. Djouadi, R. M. Godbole, M. M. Mühlleitner and S. D. Rindani, Phys. Rev. Lett. 100, 051801 (2008) [arXiv:0707.2878 [hep-ph]].

[54] D. Azevedo, A. Onofre, F. Filthaut and R. Gonçalo, Phys. Rev. D98, no. 3, 033004 (2018) [arXiv:1711.05292 [hep-ph]].

[55] F. Boudjema, D. Guadagnoli, R. M. Godbole, K. A. Mohan, Laboratory-frame observables for probing the top-higgs boson interaction, Phys. Rev. D 92 (2015) 015019. doi:10.1103/PhysRevD.92.015019.

[56] A. M. Sirunyan et al. [CMS Collaboration], arXiv:1804.02610 [hep-ex].

[57] M. Aaboud et al. [ATLAS Collaboration], arXiv:1806.00425 [hep-ex].

[58] J. F. Gunion and X. G. He, Phys. Rev. Lett. 76, 4468 (1996), doi:10.1103/PhysRevLett.76.4468 [hep-ph/9602226].

[59] S. P. Amor dos Santos et al., Phys. Rev. D 92 034021 (2015), arXiv:1503.07787 [hep-ph].

[60] S. P. Amor dos Santos et al., Phys. Rev. D 96 (2017), arXiv:1704.03565 [hep-ph].

[61] A. Ferroglia, M. C. N. Fiolhais, E. Gouveia, and A. Onofre, Phys. Rev. D100, 075034 (2019), 1909.00490.

[62] A. V. Gritsan, R. Rntsch, M. Schulze and M. Xiao, Phys. Rev. D 94, no. 5, 055023 (2016) [arXiv:1606.03107 [hep-ph]].

[63] T. Ghosh, R. Godbole, X. Tata, Phys. Rev. D 100, 015026 (2019), arXiv:1904.09895 [hep-ph].

[64] J. Alwall et al., JHEP 1407 (2014).

[65] P. Artoisenet et al., JHEP 1311 (2013), arXiv:1306.6464 [hep-ph].

[66] D. Azevedo (2017). Probing the CP nature of the Higgs' couplings in ttH events at the LHC (Master's thesis, Faculdade de Ciências da Universidade do Porto).
Retrieved from https://hdl.handle.net/10216/104395.

[67] P. Artoisenet et al., JHEP 1303, 015 (2013), arXiv:1212.3460 [hep-ph].

[68] M. Czakon, P. Fiedler and A. Mitov, Phys. Rev. Lett. 110, 252004 (2013) arXiv:1303.6254 [hep-ph].

[69] N. Kidonakis, Phys. Rev. D 81, 054028 (2010) [arXiv:1001.5034 [hep-ph]].

[70] N. Kidonakis, Phys. Rev. D 83, 091503 (2011) [arXiv:1103.2792 [hep-ph]].

[71] R. D. Ball et al., Nucl. Phys. B867, 244 (2013), 1207.1303.

[72] T. Sjöstrand, S. Mrenna and P. Z. Skands, JHEP 0605, 026 (2006), hep-ph/0603175.

[73] J. Alwall et al., Eur. Phys. J. C 53 (2008) 473 doi:10.1140/epjc/s10052-007-0490-5 [arXiv:0706.2569 [hep-ph]].

[74] S. Frixione and B. R. Webber, JHEP 0206 (2002) 029 doi:10.1088/1126-6708/2002/06/029 [hep-ph/0204244].

[75] J. de Favereau et al. [DELPHES 3 Collaboration], JHEP 1402, 057 (2014), arXiv:1307.6346 [hep-ex].

[76] M. Cacciari, G. P. Salam, and G. Soyez, Eur. Phys. J. C72, 1896 (2012), 1111.6097.

[77] M. Cacciari, G. P. Salam, and G. Soyez, JHEP 04, 063 (2008), 0802.1189.

[78] E. Conte, B. Fuks and G. Serret, Comput. Phys. Com- mun. 184, 222 (2013), arXiv:1206.1599 [hep-ph].

[79] E. Conte et al., Eur. Phys. J. C 74, 3103 (2014), arXiv:1405.3982 [hep-ph].

[80] A. Hoecker, P. Speckmayer, J. Stelzer, J. Therhaag, E. von Toerne, and H. Voss, "TMVA: Toolkit for Multivariate Data Analysis," PoS A CAT 040 (2007) [physics/0703039].

[81] A. L. Read, J. Phys. G28, 2693 (2002), [,11(2002)].

[82] T. Junk, Nucl. Instrum. Meth. A434, 435 (1999), hep-ex/9902006.

[83] N. Cabibbo, "Unitary symmetry and leptonic decays," Phys. Rev. Lett. 10 (Jun, 1963) 531–533. http://link.aps.org/doi/10.1103/PhysRevLett.10.531.

Appendix A

Natural units

In particle physics it is common to use a system of units known as natural units where $c = \hbar = 1$ [20]. The main advantage of this choice is that it simplifies mathematical expressions as there is no longer the need to carry around powers of $\hbar$ and c. On the other hand, all quantities are now expressed in terms of energy units, usually powers of GeV (see Table A.1), which makes dimensional analysis impossible unless the dimensions of the quantity in question are already known.

As a consequence of using units where $c = 1$, both time and space have the same dimension. The Compton wavelength[1] is given by $\lambda = 2\pi\hbar/mc$, therefore in these units length has dimensions of inverse mass or equivalently inverse energy, which we represent by saying $[L] = M^{-1}$. The partial derivative ∂_μ has dimensions of inverse of length, therefore $[\partial_\mu] = M$. Since the action S, which is defined as $S = \int_{-\infty}^{+\infty} dt\, dx\, dy\, dz\, \mathcal{L}$, is dimensionless, because it has the same units as $\hbar$, this forces the Lagrangian dimension to be M^4. From this, we can determine the dimension of the fields and other objects that come in the Lagrangian.

Table A.1: Relation between S.I. and natural units.

Quantity	**S.I.**	$\hbar = c = 1$
Energy	kg m^2 s^{-2}	GeV
Momentum	kg m s^{-1}	GeV
Mass	kg	GeV
Time	s	GeV^{-1}
Length	m	GeV^{-1}
Area	m^2	GeV^{-2}

[1] The Compton wavelength of a particle is equal to the wavelength of a photon whose energy is the same as the rest energy of that particle.

Appendix B

Some terminology on group theory and the SU(n) group

The generators are the vectors of a Lie algebra[1] that are the elements of its basis. The commutator of two generators G_a and G_b is given by

$$[G_a, G_b] = i \sum_c f_{abc} G_c, \tag{B.1}$$

where f_{abc} are the structure constants of the algebra.

In physics, the group SU(n) is of particular importance. It is a Lie group which, in the fundamental representation[2], is composed of $n \times n$ complex unitary matrices U with determinant $+1$. Such matrices contain $2n^2$ real Degrees of Freedom, but the unitarity constraints

$$\sum_{k=1, i \neq j}^{n} U_{ik} U_{jk}^{*} = 0 \tag{B.2}$$

and

$$\sum_{k=1}^{n} |U_{ik}|^2 = 1 \tag{B.3}$$

reduce this number in half. Since the determinant must be $+1$, the total number of Degrees of Freedom becomes $n^2 - 1$.

The SU(2) group has three generators which are hermitian 2×2 matrices with zero trace in the fundamental representation. They are the Pauli matrices divided by two. The Pauli matrices are equal to

$$\tau_1 = \begin{pmatrix} 0 & 1 \\ 1 & 0 \end{pmatrix}, \tau_2 = \begin{pmatrix} 0 & -i \\ i & 0 \end{pmatrix}, \tau_3 = \begin{pmatrix} 1 & 0 \\ 0 & -1 \end{pmatrix}, \tag{B.4}$$

and the structure constants are ϵ_{abc} (with $\epsilon_{123} = 1$), which is the fully antisymmetric tensor.

In SU(2), all its representations are equivalent to its complex conjugates. This is because there exists a

[1] Vector space defined by having the operation $[A, B] = C$, which is called a Lie parenthesis. A, B and C are vectors belonging to this vector space.

[2] A Lie group is a continuous group whose elements ℓ around the identity element of the group are written as the exponential of a vector of a Lie algebra: $\ell = \exp\left(i \sum_a \theta_a G_a\right)$. In the fundamental representation, $\mathrm{tr}\,(G_a G_b) = \frac{1}{2}\delta_{ab}$.

matrix X such that $U^* = X^{-1}UX$, therefore if u is an $SU(2)$ vector, i.e., $u \to Uu$, then Xu^* is also an SU(2) vector, since $Xu^* \to UXu^*$.

The SU(3) group has 8 generators, which are the Gell-Mann matrices divided by two in the fundamental representation. The Gell-Mann matrices are given by

$$\lambda_1 = \begin{pmatrix} 0 & 1 & 0 \\ 1 & 0 & 0 \\ 0 & 0 & 0 \end{pmatrix}, \quad \lambda_2 = \begin{pmatrix} 0 & -i & 0 \\ i & 0 & 0 \\ 0 & 0 & 0 \end{pmatrix},$$

$$\lambda_4 = \begin{pmatrix} 0 & 0 & 1 \\ 0 & 0 & 0 \\ 1 & 0 & 0 \end{pmatrix}, \quad \lambda_5 = \begin{pmatrix} 0 & 0 & -i \\ 0 & 0 & 0 \\ i & 0 & 0 \end{pmatrix}, \tag{B.5}$$

$$\lambda_6 = \begin{pmatrix} 0 & 0 & 0 \\ 0 & 0 & 1 \\ 0 & 1 & 0 \end{pmatrix}, \quad \lambda_7 = \begin{pmatrix} 0 & 0 & 0 \\ 0 & 0 & -i \\ 0 & i & 0 \end{pmatrix},$$

$$\lambda_3 = \begin{pmatrix} 1 & 0 & 0 \\ 0 & -1 & 0 \\ 0 & 0 & 0 \end{pmatrix}, \quad \lambda_8 = \frac{1}{\sqrt{3}} \begin{pmatrix} 1 & 0 & 0 \\ 0 & 1 & 0 \\ 0 & 0 & -2 \end{pmatrix}.$$

The structure constants are given by

$$f_{123} = 1, \tag{B.6}$$

$$f_{147} = f_{165} = f_{246} = f_{257} = f_{345} = f_{376} = \frac{1}{2}, \tag{B.7}$$

$$f_{458} = f_{678} = \frac{\sqrt{3}}{2}. \tag{B.8}$$

Appendix C

The CKM matrix

The CKM matrix is a 3×3 unitary and in general complex matrix that arises from the mismatch between weak eigenstates and mass eigenstates in the quark sector [12, 35, 83]. A unitary square matrix of dimension n has n^2 real Degrees of Freedom. The standard parametrization of this type of matrices involves $n(n-1)/2$ rotation angles and $n(n+1)/2$ phases. If that matrix is the CKM matrix, then $2n-1$ of those phases are independent and therefore physically irrelevant because they can be cast away by rephasing the quark fields [34].

If we have a 2×2 CKM matrix, we can parametrize it using one angle and three phases, but the three of them can be removed. For a 3×3 matrix, we have 3 angles (Euler angles) and six phases, of which 5 are independent. The remaining phase that cannot be canceled out is the source of CP-violation in the SM.

Experimentally, the most accessible quantities of the CKM matrix are the moduli of its elements. For example, the amplitude for the β decay $d \to u$ is suppressed by V_{ud} and its cross-section will be proportional to $|V_{ud}|^2$, then, by measuring it, we are able to determine $|V_{ud}|$. These numbers are always smaller than unity since unitarity implies [34]

$$|V_{ud}|^2 + |V_{us}|^2 + |V_{ub}|^2 = 1, \tag{C.1}$$
$$|V_{cd}|^2 + |V_{cs}|^2 + |V_{cb}|^2 = 1, \tag{C.2}$$
$$|V_{td}|^2 + |V_{ts}|^2 + |V_{tb}|^2 = 1, \tag{C.3}$$
$$|V_{ud}|^2 + |V_{cd}|^2 + |V_{td}|^2 = 1, \tag{C.4}$$
$$|V_{us}|^2 + |V_{cs}|^2 + |V_{ts}|^2 = 1, \tag{C.5}$$
$$|V_{ub}|^2 + |V_{cb}|^2 + |V_{tb}|^2 = 1. \tag{C.6}$$

The experimental values of the magnitudes of the CKM matrix elements are [12]

$$\begin{bmatrix} |V_{ud}| & |V_{us}| & |V_{ub}| \\ |V_{cd}| & |V_{cs}| & |V_{cb}| \\ |V_{td}| & |V_{ts}| & |V_{tb}| \end{bmatrix} = \begin{bmatrix} 0.97420 \pm 0.00021 & 0.2243 \pm 0.0005 & 0.00394 \pm 0.00036 \\ 0.218 \pm 0.004 & 0.997 \pm 0.017 & 0.0422 \pm 0.0008 \\ 0.0081 \pm 0.0005 & 0.0394 \pm 0.0023 & 1.019 \pm 0.025 \end{bmatrix}. \tag{C.7}$$

Appendix D

Top production at the LHC

In hadron colliders, tops are mainly produced in pairs through the processes $\bar{q}q \to \bar{t}t$ and $gg \to \bar{t}t$ (at $\sqrt{s} = 14$ TeV, about 90% of the production is from the latter process [12]). Figure D.1 and Figure D.2 show the LO Feynman diagrams for the top quark pair production and its cross section as a function of the CM energy, respectively.

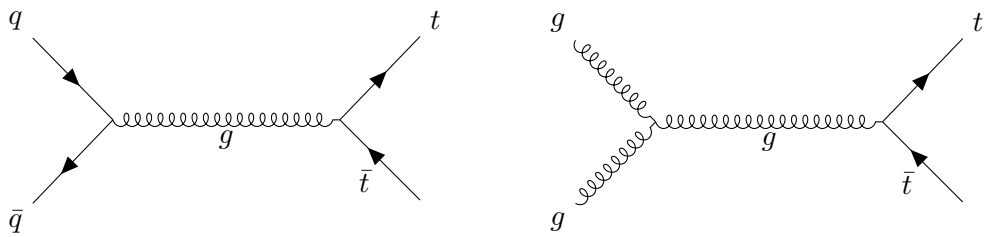

Figure D.1: Top quark pair production Feynman diagrams at LO.

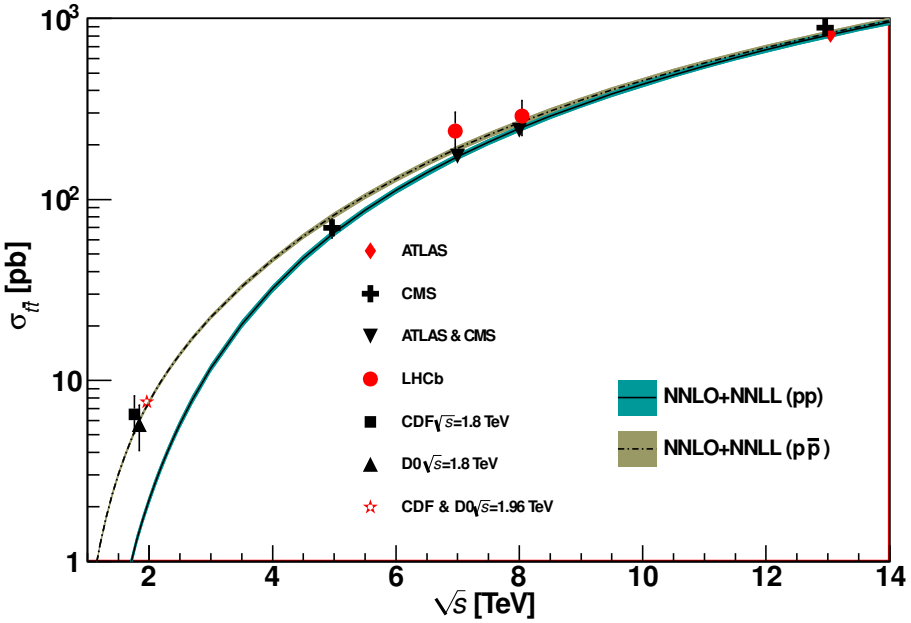

Figure D.2: Experimental and theoretical $t\bar{t}$ cross sections for $m_t = 172.5$ GeV. Image from [12].

Besides top pair production, single top production is also expected, although the cross section of this process is smaller. The relevant channels are the s- and t-channels, $\bar{q}'q \to \bar{b}t$ and $qb \to q't$, respectively, and the Wt associated production, $bg \to W^-t$ and $\bar{b}g \to W^+\bar{t}$. The Feynman diagrams are displayed in Figure D.3. The cross sections for the top and anti-top quark are different in all these processes. The cross section of all three channels that contribute to single top-quark production are shown in Figure D.4, as a function of the CM energy.

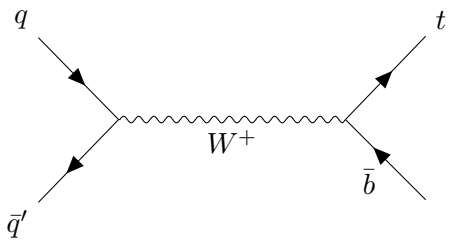

(a) s-channel.

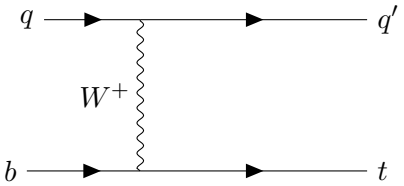

(b) t-channel.

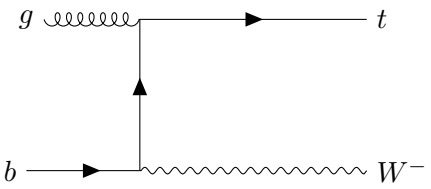

(c) Wt t-channel.

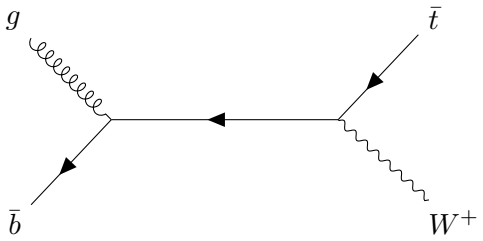

(d) Wt s-channel.

Figure D.3: Single top production Feynman diagrams at LO.

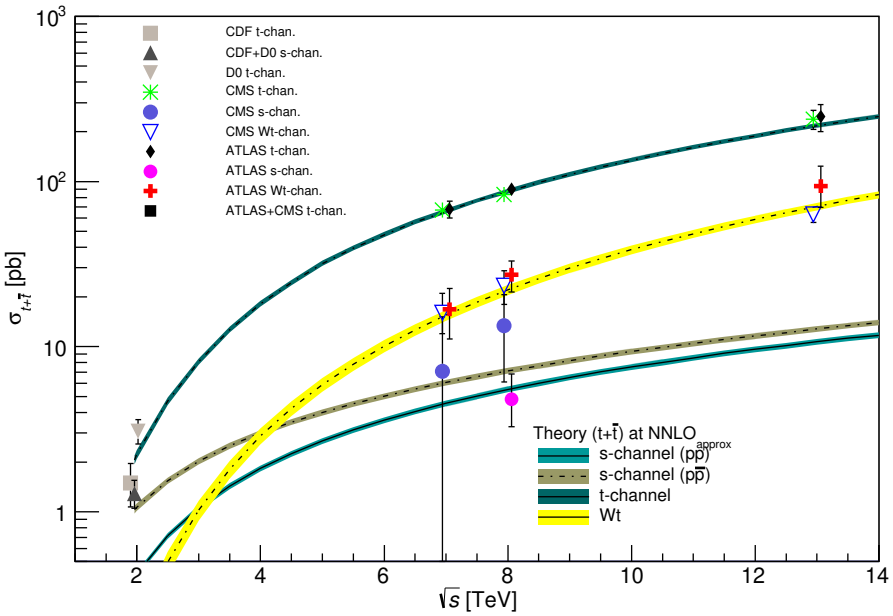

Figure D.4: Experimental and theoretical single top cross sections for $m_t = 172.5$ GeV. Image from [12].

Appendix E

Efficiencies in $t\bar{t}h$ reconstruction

In Table E.1 the signal efficiencies as a function of different Higgs masses (for both scalar and pseudoscalar) are shown after the pre-selection ($N_{jets} \geq 4$ and $N_{lep} \geq 2$), reconstruction without Truth Match and final selection cuts ($|m_{l^+l^-} - m_Z| > 10$ GeV and $N_b \geq 3$). It should be stressed that no optimization of the reconstruction was intended, which could improve the results shown. That stays largely outside the scope of this thesis, since it would make more sense to perform such an optimization when using real data from LHC experiments.

Table E.1: Efficiencies (in %), rounded to the nearest unit, as a function of the selection cuts and reconstruction for $t\bar{t}h$ events. $N_b \geq 3$ means at least 3 b-tagged jets.

m_h (GeV)	$N_{jets} \geq 4$ $N_{lep} \geq 2$		Reconstruction without Truth Match		$\lvert m_{l^+l^-} - m_Z \rvert > 10$ GeV $N_b \geq 3$	
	$h = H$	$h = A$	$h = H$	$h = A$	$h = H$	$h = A$
40	9	12	57	54	5	7
80	13	15	63	62	7	10
120	16	17	61	62	11	12
160	17	19	61	62	12	13
200	18	19	60	61	14	14

More information on the details about reconstruction without Truth Match is given in section 4.6. It should be noted that the numbers of the efficiencies corresponding to the reconstruction without Truth Match (the third column of Table E.1) are normalized in respect to the percentage of events that survive pre-selection (the second column of Table E.1). This sort of representation (Table E.1) offers a correct perception of the efficiencies resulting from the method used to reconstruct the $t\bar{t}h$ system. The final selection numbers (fourth column of Table E.1) are also normalized to the numbers in the previous column. Therefore, to retrieve the full efficiency, including event pre-selection, reconstruction and final-selection, one needs only to multiply the total number of events (see Table 4.1) by the numbers in each column of Table E.1. All statistical uncertainties of the efficiencies are smaller than 0.2% at the pre-selection level.